Titre: Title:	Two-phase flow pattern identification using hidden Markov model
Auteur: Author:	Ali Mahvash Mohammadi
Date:	2006
Type:	Mémoire ou thèse / Dissertation or Thesis
Référence: Citation:	Mahvash Mohammadi, A. (2006). Two-phase flow pattern identification using hidden Markov model [Mémoire de maîtrise, École Polytechnique de Montréal]. PolyPublie. https://publications.polymtl.ca/7847/

UNIVERSITÉ DE MONTRÉAL

TWO-PHASE FLOW PATTERN IDENTIFICATION USING HIDDEN MARKOV MODEL

ALI MAHVASH MOHAMMADI
DÉPARTEMENT DE GÉNIE MÉCANIQUE
ÉCOLE POLYTECHNIQUE DE MONTRÉAL

MÉMOIRE PRÉSENTÉ EN VUE DE L'OBTENTION
DU DIPLÔME DE MAÎTRISE ÈS SCIENCES APPLIQUÉES
(GÉNIE MÉCANIQUE)
OCTOBRE 2006

Your file Votre référence
ISBN: 978-0-494-25556-8
Our file Notre référence
ISBN: 978-0-494-25556-8

UNIVERSITÉ DE MONTRÉAL

ÉCOLE POLYTECHNIQUE DE MONTRÉAL

Ce mémoire intitulé:

TWO-PHASE FLOW PATTERN IDENTIFICATION USING HIDDEN MARKOV MODEL

présenté par: MAHVASH MOHAMMADI Ali

en vue de l'obtention du diplôme de: Maîtrise ès sciences appliquées

a été dûment accepté par le jury d'examen constitué de:

M. ADJENGUE Luc-Désiré, Ph.D., président

Mme ROSS Annie, Ph.D., membre et directeur de recherche

M. MUREITHI Njuki-William, Ph.D., membre

Dedicated to my parents

Acknowledgements

The author is so grateful to his research advisor, Professor Annie Ross, for her guidance, encouragement, and helpful comments. Working with her was a very pleasant experience. Sincere appreciation goes to the members of jury, Professor Luc D. Adjengue and Professor Njuki W. Mureithi for their valuable comments and suggestions. The author expresses his sincere gratitude to Professor Michel J. Pettigrew, Chair holder of the BWC/AECL/NSERC Chair of Fluid-Structure Interaction under which the experiments and data acquisitions were carried out, and thanks research associate Thierry Lafrance, and technician Bénédict Besner for the technical support.

Résumé

Les applications industrielles telles que les systèmes de conversion d'énergie, la filtration, les procédés de brumisation, les réseaux de gaz naturel et le refroidissement de réacteur nucléaire comportent des écoulements diphasiques. Le taux de transfert de chaleur et de masse, la perte de pression, la perte de quantité de mouvement, le taux de rétromélange (*back-mixing*) et les vibrations des conduits peuvent varier considérablement avec les configurations d'écoulement. Par conséquent, il est très important d'identifier ces configurations. Les premières méthodes d'identification expérimentale étaient principalement basées sur des observations directes et étaient très subjectives. Afin d'augmenter l'objectivité, des méthodes indirectes ont été élaborées. De plus, des critères théoriques ont été établis pour définir les conditions de transition entre les régimes d'écoulement. Cependant, en raison de la nature complexe de l'écoulement diphasique, l'analyse théorique ne peut pas décrire le système entièrement.

Dans ce projet, une nouvelle méthode est développée pour identifier les régimes d'écoulement ascendant diphasique dans un tube vertical, par l'étude des signaux de phase recueillis par un système de sonde à fibre optique. Les régimes d'écoulement sont détectés en analysant la configuration du signal par le modèle de Markov caché (HMM). Le HMM a été de plus en plus employé depuis les années 1960 dans la reconnaissance de la parole et dans plusieurs autres domaines. Il s'avère un outil très puissant pour comparer deux signaux ou plus, ce qui est une clef pour résoudre plusieurs problèmes concrets. Dans l'emploi du HMM pour l'identification des configurations d'écoulements diphasiques, des données correspondant aux conditions d'écoulement diphasiques à régime clairement connu (c.-à-d., états loin des régions de transition) sont utilisées comme référence pour comparer les conditions dont le régime est inconnu (c.-à-d., conditions près des régions de transition). Pour chaque régime, trois conditions de référence ont été choisies en utilisant la carte fournie par Taitel *et al.* (1980) ainsi que les photos des diverses conditions. La vraisemblance de chaque configuration d'écoulement a été calculée pour chaque condition d'essai. Une carte d'écoulement diphasique a été

extraite à partir des résultats numériques en utilisant la vraisemblance maximum et la vraisemblance totale maximum. Dans l'approche de la vraisemblance maximum, le régime pour un test donné a été déterminé en sélectionnant la grande vraisemblance obtenue parmi toutes les conditions de référence. Dans l'approche la vraisemblance totale maximum, la somme de vraisemblances des conditions de référence d'un même régime a été employée pour la comparaison. Ensuite, toutes les conditions ont été classées par catégories et transcrites sur la carte de Taitel. Les frontières de transition entre les régimes ont été tracées.

Les signaux de taux de vide ont été obtenus pour soixante conditions d'écoulement diphasique ascendant dans une section d'essai soit : sept vitesses homogènes (0.5 m/s à 5 m/s) et neuf taux de vides (10% à 90%). Le tube de polycarbonate faisait 2 mètres de longueur et 19 millimètres de diamètre intérieur. Les débits de gaz et de liquide ont été contrôlés et compensés en fonction de la pression mesurée à l'entrée du tube.

Des signaux de taux de vide ont été obtenus à l'aide d'une sonde à fibre optique située au centre du tube et d'un terminal de National Instruments. Pour chaque condition simulée dans la section d'essai, le signal a été échantillonné sur une minute à une fréquence de 99 kHz. En outre, pour chaque essai, dix photos ont été prises à l'aide d'un appareil photo numérique "Nikon".

Les signaux étaient prétraités en quatre étapes : débruitage, réduction des échantillons, extraction de traits caractéristiques et dérivation des vecteurs caractéristiques. Durant le débruitage, les données brutes ont été converties en données binaires représentant le passage successif des deux phases. Afin d'obtenir la même échelle spatiale pour toutes les conditions, les données ont été réduites (*downsampling*) avec des taux différents en fonction des vitesses homogènes. Le spectre fréquentiel, la méthode autorégressive (AR) et une approche novatrice basée sur la durée de passage des phases liquide et gazeuse ont été examinés pour l'extraction des traits caractéristiques. Lors de la dérivation des vecteurs, une longueur définie de données a été divisée en segments décalés les uns par rapport aux autres. Ensuite les segments ont été divisés en vecteurs avec un chevauchement de 50%.

Pour le cas des traits caractéristiques tirés des spectres fréquentiels, le procédé de HMM n'a pas été complété en raison des problèmes de soupassement de capacité (*underflow*) ou de divergence. Par conséquent, il n'y avait aucun résultat disponible pour cette évaluation. Pour le cas de la méthode autorégressive (AR), les coefficients de réflexion du modèle AR d'ordre 10 ont été employés comme traits. Les frontières obtenues avaient une forme régulière ; cependant, il y avait quelques désaccords avec la carte de Taitel et les photos.

Les frontières obtenues en extrayant les traits caractéristiques basés sur le temps de passage étaient lisses, autant en utilisant les vraisemblances individuelles que les vraisemblances totales. En outre, par rapport aux autres méthodes, les résultats de cette méthode coïncidaient le mieux avec la carte de Taitel, en particulier avec l'approche de vraisemblance totale. De plus, elles concordaient bien avec les photos. Par conséquent, cette méthode a été sélectionnée pour l'extraction des traits caractéristiques.

Afin de vérifier l'effet des paramètres des HMM, des nombres d'états différents ont été essayés. Pour la plupart des cas, les frontières basées sur les vraisemblances individuelles n'étaient pas lisses et il y avait un caractère arbitraire. D'ailleurs, aucune corrélation n'a pu être notée entre l'augmentation du nombre d'états et la différence dans la forme des frontières. D'autre part, les frontières résultant de la vraisemblance totale étaient non seulement lisses, mais également, aucun changement notable n'a pu être observé pendant les changements du nombre d'états. Par conséquent, il a été conclu que la vraisemblance totale est une approche plus fiable et plus juste. En outre, l'utilisation de différentes conditions de référence a été considérée. Les résultats ont montré qu'il y avait quelques variations dans les frontières obtenues.

Afin d'étudier la confiance accordée aux résultats, la « confiance » a été définie comme étant : la différence entre les deux plus grandes valeurs de vraisemblance obtenues pour une condition de test donnée. On observe que les conditions ayant un niveau de confiance élevé sont généralement situées loin des frontières de transition obtenues. Près des frontières de transition, la confiance est faible. Par ailleurs, la plupart des conditions dans la région à bulles finement dispersées ont un faible niveau de

confiance, ce qui peut être lié aux faiblesses du système de mesure par sonde optique dans ce régime d'écoulement. En conclusion, il y a une corrélation acceptable entre les vraisemblances obtenues et la signification physique des mesures.

En conclusion, il a été montré que l'utilisation des HMM a un bon potentiel pour l'identification des régimes d'écoulement diphasiques. Aussi, la qualité de l'identification est sensiblement influencée par la méthode d'extraction des traits caractéristiques. Cette recherche doit être considérée comme une brèche donnant sur maintes recherches futures dans ce domaine.

Abstract

Two-phase flows are very often seen in industrial applications such as energy conversion systems, filtration, spray processes, natural gas networks and nuclear reactor cooling. Changes in pressure loss, heat and mass transfer rates, momentum loss, rates of back mixing, and vibration of pipes all vary greatly with two-phase flow patterns. Therefore, it is quite important to identify the flow patterns. The early experimental methods for detecting flow regimes were mostly based on direct observation, and were greatly subjective. In order to increase the objectiveness, indirect methods of observations were elaborated, based on the statistical analysis of the fluctuating characteristics of the flow. Further, criteria for flow regime transition were defined on a theoretical basis. However, due to the complex nature of two-phase flow, theoretical analyses have not been able to describe the system perfectly.

In this project, a new method is developed for identifying two-phase flow regimes in a vertical channel, from the void fraction signals gathered by an optical fiber probe system. Flow regimes are detected from signal patterns, using hidden Markov model (HMM). HMM has been increasingly used from the 1960's in speech recognition and numerous other fields. HMM is a very strong tool for comparing two or more signals, which is a key to solve several problems in practice. In the present work, for two-phase flow pattern identifications, HMM was applied as follows: the data corresponding to two-phase flow conditions with clearly known regime (i.e. conditions far away from transition regions) are used as references to detect and classify the conditions with unclear regime (i.e. conditions close to transition regions). Reference conditions were selected using the map provided by Taitel *et al.* (1980), together with photos taken during the experiments. For each regime, three reference conditions were selected. Flow pattern likelihoods were calculated for each test condition. Two-phase flow maps were extracted from the numerical results, using the maximum likelihood and total maximum likelihood. In the maximum likelihood approach, the regime for a given test condition was determined by selecting the highest likelihood value among all reference conditions.

In total maximum likelihood approach, the sum of likelihood values of reference conditions of the same regime was used for comparison. Then all the conditions were categorized and reflected on Taitel's map and the transition boundaries were depicted.

Void fraction signals were collected from sixty conditions of air-water two-phase upward flow. Seven different homogenous velocities (0.5 m/s to 5 m/s) and nine void fractions (10% to 90%) were simulated in a test section. The polycarbonate tube was 2 meters long and 19 mm in diameter. Air and water flowrates were monitored and compensated based on the pressure measured at the tube entrance.

Void fraction signals were collected using a single step index multimode optical fiber probe located at the center of the tube, and a National Instruments data acquisition board. For each condition simulated in the test section, one minute worth of data was sampled at a frequency of 99 kHz. In addition, for each test, flow patterns were captured using a Nikon digital camera.

The void fraction signals were preprocessed in four steps: de-noising, down-sampling, feature extraction and feature vector derivation. De-noising consisted in converting the collected data to binary signals representing the successive passage of liquid and gas phases. In order to attain the same spatial frequency for all conditions, the de-noised data were down-sampled with respect to the homogeneous velocities. The auto-power spectrum, autoregressive (AR) method and an inventive method based on the passage time of the liquid and gas phases were tried and examined as feature extraction. In vector derivation, a finite length of data was divided into segments separated with an offset. Then the segments were divided into vectors with 50% overlap. Feature vectors were used for HMM training and for the identification procedure.

For features extracted from the auto power spectrum, the HMM procedure was not carried out completely due to either underflow or divergence problems. Therefore, no result was available for this method. For the case of autoregressive (AR) method, the reflection coefficients of the AR model of order 10 were used as features. The transition boundaries obtained by this method had a regular shape; however, in comparison with Taitel's map and photos, there were some disagreements.

The boundaries obtained by implementing the passage time based features were smooth regardless of the likelihood approach used. In addition, among all methods tested, this type of features yielded the best correspondence to the Taitel's map and was in a good agreement with the photos, especially when the total likelihood approach was applied. Therefore, this method was picked for feature extraction.

Furthermore, in order to assess the effects of HMM parameters, HMMs with different number of states were tried. The boundaries depicted based on the maximum likelihood approach were tortuous in most cases, and there were some arbitrariness. Moreover, no certain correlation could be noticed between the number of states and difference in the shape of the boundaries. On the other hand, the boundaries resulting from the maximum total likelihood approach not only were smooth, but also no significant change could be seen as the number of states changed. Therefore, it was concluded that the maximum total likelihood approach is more reliable and has better performance. Furthermore, the results of using different reference conditions were considered. As the results showed, there were a few variations in the obtained boundaries.

In order to study the confidence of the results, the 'confidence difference' was defined as: the difference between the two largest likelihood values of a given condition. As observed, the conditions with high confidence were mostly those located away from the resulting transition boundaries. Close to the boundaries, the confidence was low, reinforcing the conclusion that the regions near the boundaries actually are transition regions. Moreover, most conditions in the finely dispersed region had a low confidence difference, which was related to weaknesses of the optical probe measuring system. It was also concluded that there is an acceptable correlation between the likelihood values and physical significance of the measurements.

Finally, it was concluded that hidden Markov modeling has a good potential in identifying two-phase flow regimes. It was also shown that the performance of this method is significantly affected by choosing different feature extraction methods. This research can be considered as a leading trial to so many follow-ups that can be practiced in this field.

Condensé en Français

Quand deux fluides différents coulent simultanément dans un même conduit, ce phénomène s'appelle l'écoulement diphasique. Les fluides peuvent être deux substances différentes, ou deux phases de la même substance. Dans ce mémoire, les fluides utilisés sont une phase liquide (eau) et une phase gazeuse (air). Les applications industrielles telles que des systèmes de conversion d'énergie, la filtration, la lubrification, les procédés de brumisation, les réseaux de gaz naturel et le refroidissement de réacteur nucléaire comportent souvent des écoulements diphasiques.

À la différence de l'écoulement monophasique pour lequel il y a deux régimes d'écoulement, laminaire et turbulent, plusieurs régimes différents existent pour l'écoulement diphasique. Dans l'étude de l'écoulement diphasique, un régime d'écoulement indique comment les phases sont distribuées et mélangées en raison de la nature physique du système. Ces régimes d'écoulement se présentent sous différentes configurations, qu'on appelle configurations d'écoulement et en conséquence, les régimes d'écoulement sont parfois confondus avec les configurations d'écoulement. Le régime d'écoulement diphasique dépend du type de combinaison fluide-fluide, du débit et de sa direction, de la forme, la taille et l'orientation du conduit. En cas d'écoulement gaz-liquide ascendant dans un conduit vertical, des régimes d'écoulement sont classés selon les catégories suivantes : régime à bulles, à bulles finement dispersées, à bouchons, agité et annulaire. Les bulles et le régime à bulles finement dispersées se produisent à de faibles débits de gaz où la phase gazeuse est à peu près uniformément distribuée sous forme de bulles séparées dans un continuum de phase liquide. Dans le régime à bouchons, la majeure partie du gaz apparaît dans les bulles, également connues sous le nom de bulles de Taylor, qui ont un diamètre presque égal au diamètre du conduit. L'écoulement agité est un écoulement fortement désordonné qui se produit aux débits élevés de gaz en raison d'instabilités à l'intérieur d'un bouchon. L'écoulement agité peut être interprété comme un écoulement à bouchons, mais plus irrégulier et plus désordonné. L'écoulement annulaire se produit à des débits plus élevés de gaz. Il y a un continuum de phase gazeuse au centre du tube. La phase liquide est répartie entre un

film liquide contre la paroi du tube et une dispersion des gouttelettes au sein du continuum gazeux.

Le taux de transfert de chaleur et de masse, la perte de pression, la perte de quantité de mouvement, le taux de rétromélange et les mouvements oscillants des conduits changent considérablement avec les régimes d'écoulement. Par conséquent, il est très important et nécessaire d'identifier ces régimes et de discerner leur corrélation avec les propriétés d'écoulement. Ces corrélations sont souvent présentées sous la forme de cartes de régime d'écoulement.

Beaucoup de travaux expérimentaux et théoriques ont été effectués dans ce domaine et en conséquence, il y a plusieurs méthodes de classification et plusieurs cartes d'écoulement. Les premiers travaux expérimentaux ont été principalement basés sur des observations directes. La photographie à haute vitesse, l'image de l'atténuation des rayons X, la sonde de contact électrique et la mesure de densité des rayons gamma multi-faisceau comptent parmi les méthodes dans lesquels les régimes d'écoulement sont détectés par des observations directes. Bien que ces méthodes soient peu coûteuses et, dans la plupart des cas, faciles à réaliser, ce sont des méthodes très subjectives.

Afin d'augmenter l'objectivité du classement, des méthodes indirectes ont été élaborées. Les méthodes d'observation indirectes traitent les caractéristiques de fluctuation de l'écoulement diphasique pour détecter le régime. Ces caractéristiques de fluctuation peuvent être observées dans la pression locale, dans la proportion instantanée de gaz et de liquide dans le mélange, etc. Il a été montré qu'il y a concordance entre les régimes d'écoulement et la fluctuation de l'écoulement diphasique. Ainsi, des modèles mathématiques et statistiques sont employés pour analyser les caractéristiques de fluctuation du régime d'écoulement. Des exemples de ces méthodes sont l'analyse de fluctuation de pression, l'analyse de bruit de neutrons, l'analyse de bruit du disque de traînée, et les méthodes d'impédance électrique.

Les méthodes expérimentales parviennent assez bien à détecter des régimes d'écoulement éloignes des états de transition. Pour les conditions proches de la transition, détecter le régime d'écoulement est particulièrement difficile et la plupart des

travaux ont été effectués sur une base théorique. Dans ces méthodes, des mécanismes de transition dans l'écoulement diphasique sont analysés par les modèles théoriques. Ensuite, pour chaque transition possible entre les régimes, un critère est choisi à partir duquel des cartes de régime d'écoulement sont tracées. La carte basée sur le travail de Taitel *et al.* (1980) est dérivée d'un modèle théorique. De plus, en raison de la nature complexe de l'écoulement diphasique, l'analyse théorique ne peut pas décrire le système entièrement. Par conséquent, une technique est exigée pour détecter et décrire le régime d'écoulement dans des conditions proches des transitions de régime.

Dans ce projet, une nouvelle méthode est développée pour identifier les régimes d'écoulement ascendant diphasique dans un tube vertical, par l'étude des signaux de phase recueillis par un système de sonde à fibre optique. L'idée fondamentale de cette méthode est de détecter des régimes d'écoulement en analysant la configuration du signal. Comme mentionné, il y a une corrélation entre les caractéristiques de fluctuation de l'écoulement diphasique et les régimes d'écoulement. Par ailleurs, les signaux de phase permettent l'interprétation de la fluctuation. Par conséquent, les configurations d'écoulement peuvent être détectées en analysant et en distinguant ces configurations de signal. Afin d'analyser les formes de signal d'une façon objective, le modèle de Markov caché (HMM pour *Hidden Markov Model*) est employé comme un outil de reconnaissance des formes.

Le HMM est un processus doublement stochastique, qui a une riche structure mathématique. Il s'est avéré être un puissant détecteur de formes, avec une grande exactitude sur des applications critiques. Le HMM a été employé dans la reconnaissance de la parole depuis des années 60 et, dans des décennies récentes, il est devenu plus populaire et il a été appliqué dans d'autres domaines.

Le HMM est une amélioration du processus de Markov. Un processus de Markov est un processus aléatoire dont les probabilités futures sont déterminées par ses valeurs les plus récentes, selon l'ordre du processus. Il peut être considéré comme un système qui, à chaque instant, est dans un état distinct choisi parmi un ensemble de N états, $S_1, S_2, ..., S_N$, et chaque état peut changer pendant une différence discrète de temps. Ce

changement peut s'effectuer à partir d'un état à un autre ou à partir d'un état à lui-même. Dans un modèle de Markov, les états correspondent aux effets physiques du processus, qui peuvent être observés. Ce modèle est trop restrictif pour être applicable à bon nombre de problèmes d'intérêt. Par conséquent, le concept des modèles de Markov a été rehaussé pour inclure le cas où les observations sont des fonctions de probabilités d'états. Dans ce cas, le modèle résultant est un processus doublement stochastique avec un processus stochastique fondamental qui n'est pas observable (il est caché), mais qui peut seulement être observé par un autre ensemble de processus stochastiques qui produisent la séquence des observations.

Les éléments d'un HMM sont : N, le nombre d'états cachés pour lesquels dans une certaine application il n'y a aucune signification claire, $A = \{a_{ij}\}$, la matrice des probabilités de transition d'états, M, le nombre de symboles d'observation, $B = \{b_j(k)\}$, la distribution de la probabilité des symboles d'observation où k indique le symbole d'observation, et finalement π, la distribution d'état initiale. Ces paramètres peuvent être présentés sous une forme courte, soit le modèle $\lambda = (A, B, \pi)$. En outre, il y a deux possibilités d'application du HMM. Quand les observations sont discrètes, le modèle correspondant est nommé modèle caché discret de Markov (DHMM pour *Discrete HMM*) ; en cas d'observations continues, on le dénote en tant que modèle caché continu de Markov (CHMM pour *Continuous HMM*).

Etant donné une séquence d'observation (O), les valeurs appropriées de N, M, A, B et π peuvent être estimées. De plus, un HMM précédemment déterminé permet de calculer la probabilité d'observer une séquence d'observation donnée. C'est-à-dire si les paramètres d'un HMM ont déjà été estimés en utilisant une séquence d'observation, alors la probabilité d'observer n'importe quelle autre séquence d'observation par ce modèle peut être calculée. Ce dispositif permet au HMM d'être un outil très puissant pour comparer deux signaux ou plus, ce qui est une clef pour résoudre plusieurs problèmes dans la pratique. Il faut d'abord que des conditions possibles d'un système soient simulées et qu'une bibliothèque de HMMs des conditions simulés soit ainsi créée. Alors, n'importe quelle condition inconnue peut être identifiée en comparant sa séquence

d'observation au HMMs dans la bibliothèque. Par exemple, cette bibliothèque peut être une bibliothèque de différents défauts d'un système mécanique ou des régimes possibles d'un système diphasique.

Comme décrit, le processus d'emploi du HMM est réalisé en deux étapes principales. La première étape est l'apprentissage, c'est-à-dire la construction du HMM d'un signal ou l'ajustement des paramètres du modèle $\lambda = (A, B, \pi)$ qui maximisent la probabilité d'observer ce signal $P(O \mid \lambda)$. La deuxième étape est l'identification, ou calcul de la probabilité d'observer un signal, pour un HMM donné. L'identification revient à déterminer la probabilité d'observer une séquence d'observation d'un signal inconnu $O = O_1 O_2 ... O_T$, pour un modèle donné $\lambda = (A, B, \pi)$, c.-à-d. $P(O \mid \lambda)$.

Dans l'emploi du HMM pour l'identification d'écoulements diphasiques, des données correspondant aux conditions d'écoulement diphasiques à régime clairement connu (c.-à-d., états loin des régions de transition) sont utilisées pour détecter les conditions avec le régime inconnu (c.-à-d., conditions près des régions de transition). En d'autres termes, les HMM sont créés en utilisant des observations (signaux de taux de vide) des conditions connues et ensuite les HMM préformés servent à calculer la probabilité d'observer les conditions inconnues.

Afin d'obtenir les signaux de taux de vide requis dans l'exécution du HMM, soixante conditions d'écoulement diphasique ascendant ont été testées dans une section d'essai soit : sept vitesses homogènes différentes (0.5 m/s à 5 m/s) et neuf taux de vides différents (10% à 90%). Dans la section d'essai, de l'air et de l'eau ont été introduits dans un mélangeur et le mélange des deux phases entre par l'extrémité inférieure d'un tube transparent pour produire un écoulement air-eau ascendant. Le tube transparent est fait de polycarbonate et il a 2 mètres de longueur et 19 millimètres de diamètre intérieur. Le conduit a été monté verticalement à l'aide de deux brides aux deux extrémités du tube. Le mélangeur est composé de deux connecteurs de conduit qui sont installés de telle manière que l'air entre avec un angle de 45 degrés et l'eau avec un angle de 90 degrés. À l'intérieur du mélangeur, un diffuseur aide l'eau et l'air à se mélanger sous de façon

uniforme. Le mélangeur a été équipé d'un baromètre pour mesurer la pression du mélange à l'entrée du tube transparent.

L'air a été fourni au mélangeur à partir du réseau d'air comprimé dans le laboratoire. Le débit d'air a été commandé avec un régulateur et une valve et il a été mesuré par un débitmètre massique électronique d'Omega (FMA-A2322). Le débitmètre a une exactitude de 1% de la pleine échelle. L'eau a été fournie à partir d'un réservoir au mélangeur à l'aide de deux pompes en série. Une des pompes a été utilisée pour de faibles débits et l'autre pour des débits plus forts. Deux débitmètres différents ont été employés pour mesurer des forts et des faibles débits d'eau. Pour les débits inférieurs, un débitmètre magnétique de Rosemount (9711TSA30FU5N0) avec une exactitude de 0.5% de l'écoulement réel a été employé, et pour des débits plus élevés, un débitmètre à turbine de Blue-White (FHXX10M2) avec une exactitude de 1% de FS. Le débit était commandé à l'aide d'une valve.

Des signaux de taux de vide ont été obtenus à l'aide d'une sonde à fibre optique située au centre du tube et ont été transmis à un PC par un terminal de National Instruments. Ensuite, le logiciel de LabVIEW a été employé pour traiter les signaux et pour les enregistrer dans des fichiers texte. Pour chaque condition simulée dans la section d'essai, une minute des signaux a été échantillonnée à une fréquence de 99 kHz. En outre, pour chaque essai, dix photos ont été prises à l'aide d'un appareil photo numérique de "Nikon E4500" à la vitesse de 1/2000s et d'une distance d'environ 35 centimètres du tube.

Puisque l'emploi des signaux bruts comme observations n'est pas efficace dans le procédé d'exécution de HMM, les signaux étaient prétraités en quatre étapes : débruitage, réduction des échantillons, l'extraction de traits caractéristiques et la dérivation des vecteurs caractéristiques.

Les signaux recueillis sont composés essentiellement de deux valeurs arbitraires de signes opposés et de bruit. Les quantités de signe positif représentent la phase gazeuse et les quantités de signe négatif représentent la phase liquide. Au moyen d'un programme simple, la valeur zéro a été utilisée comme seuil pour distinguer la phase et les données

parasitées ont été converties en données composées uniquement des valeurs -1 et 1 ; 1 était la notation pour la phase gazeuse et -1 pour l'écoulement liquide. Après le débruitage des données, les données ont été réduites (*downsampling*) avec des taux différents en fonction des vitesses homogènes. En effet, puisque les signaux des conditions à différentes vitesses homogènes ont été enregistrés à la même fréquence, cette réduction a permis d'uniformiser les données sur une échelle spatiale.

Afin d'avoir les meilleurs résultats, au lieu d'utiliser directement les données débruitées, les caractéristiques spécifiques des signaux ont été extraites et utilisées. Après le débruitage et la réduction, les données étaient une collection de -1 et de 1. Par conséquent, la prochaine étape du prétraitement était d'extraire des traits caractéristiques d'une telle collection, ce qui comportait un bon degré de difficulté. Plusieurs approches ont été essayées et examinées.

La dérivation du spectre fréquentiel des données était l'une des approches examinées. Toutefois, puisque des spectres très différents pouvaient être obtenus pour des données correspondant à un même régime, il était prévisible que les méthodes basées sur la fréquence ne soient pas un choix approprié.

Une autre approche était l'utilisation des coefficients de réflexion autorégressifs. Des modèles autorégressifs sont créés avec l'idée que la valeur actuelle d'une série chronologique x_t peut être expliquée en fonction de p valeurs passées, $x_{t-1}, x_{t-2}, ..., x_{t-p}$ où p détermine l'ordre du modèle autorégressif. Un modèle autorégressif d'ordre p peut être écrit comme :

$$x_t = \phi_1 x_{t-1} + \phi_2 x_{t-2} + ... + \phi_p x_{t-p} + w_t$$

où $\phi_1, \phi_2, ..., \phi_p$ sont les constantes appelées des coefficients autorégressifs et w_t est un bruit blanc. Quand les valeurs présentes et passées d'un signal sont déterminées, pour un bruit blanc donné, les coefficients de réflexion peuvent être obtenus et employés comme traits caractéristiques.

La dernière approche était une approche novatrice basée sur la durée de passage des phases liquide et gazeuse. Aussi longtemps que de liquide s'écoule contre la sonde, la valeur du signal capté est 1. Quand la phase change du liquide au gaz, il y aura un changement de la valeur de signal de 1 à -1. L'approche peut être expliquée comme suit : La longueur du passage d'une masse de liquide à travers la sonde est enregistrée avec un signe positif. L'index du changement de phase est aussi noté. De même, la longueur du passage d'une masse de gaz est enregistrée comme un nombre négatif. Alors ces nombres peuvent être écrits respectivement, en fonction de leur changement de phase.

La dernière étape du prétraitement, qui peut être faite après ou avant l'extraction des traits caractéristiques selon l'approche choisie, est la dérivation des vecteurs de caractéristiques. Dans cette étape, une longueur définie de données a d'abord été choisie. Ce choix doit être fait de manière à ce que les données choisies soient assez longues pour couvrir de divers comportements de la source de signal. Par la suite, les données choisies ont été divisées en quelques segments, décalés les uns par rapport aux autres. Chaque segment a été divisé en vecteurs avec un chevauchement de 50%.

Une fois les signaux filtrés et les vecteurs caractéristiques extraits, le modèle caché de Markov peut être mis en application. Pour faire l'apprentissage du HMM, des conditions d'écoulement ont été choisies comme référence pour représenter chaque régime d'écoulement. Les traits caractéristiques correspondant à ces conditions ont été utilisés aux fins d'apprentissage. Pour choisir les conditions de référence, la carte fournie par Taitel *et al.* (1980) ainsi que les photos des diverses conditions ont été employées pour sélectionner des conditions situées loin des transitions. Selon cette carte, pour des tubes de petit diamètre (19 mm y compris), le régime à bulles n'existe pas. Par conséquent, les modèles existants sont les écoulements à bulles finement dispersées, à bouchons, agité et annulaire. De plus, puisque le régime annulaire est facilement identifiable, il n'a pas été étudié dans ce projet. Par conséquent, les conditions d'écoulement diphasiques utilisées comme conditions de référence pour la formation des HMM étaient choisies parmi trois régimes différents. Pour chaque régime, trois points de référence ont été choisis et en conséquence, il y avait neuf points de référence. Alors les traits caractéristiques extraits

à partir des données des conditions choisies ont été modélisés avec un HMM par l'étape de formation. Enfin, une cote logarithmique de vraisemblance de chacune des autres conditions mesurées a été calculée en utilisant les HMM préalablement formés. Ces cotes ont été employées pour classer les conditions de test dans l'un ou l'autre des trois régimes. Ensuite, les résultats des différentes méthodes d'extraction des traits caractéristiques ont été comparés.

Pour le cas des traits caractéristiques tirés des spectres fréquentiels, les données ont été divisées en vecteurs et le spectre fréquentiel de chaque vecteur a été dérivé en utilisant la fonction de FFT (transformée de Fourier rapide). Alors une plage de fréquence couvrant la plupart de fréquences excitées dans toutes les conditions a été choisie et employé comme trait du procédé de CHMM. Malheureusement, en raison des problèmes de soupassement de capacité ou de divergence dans l'étape d'apprentissage de plusieurs conditions, le procédé de HMM n'a pas été complété. Par conséquent, il n'y avait aucun résultat disponible pour cette évaluation.

Une autre méthode d'extraction employée est la méthode autorégressive (AR). Comme dans la méthode de spectre fréquentiel, la dérivation des vecteurs a été faite avant l'extraction des traits caractéristiques. Les coefficients de réflexion du modèle autorégressif d'ordre 10 ont été employés comme traits. Pour extraire la carte d'écoulement diphasique à partir des résultats numériques deux approches différentes ont été essayées. Une approche était de trouver la vraisemblance maximum de chaque point de test en comparaison avec les neuf points de référence : le régime d'écoulement identifié pour chaque point est celui du point de référence qui produisait la vraisemblance maximum. Une autre approche était d'additionner les trois vraisemblances pour chaque régime de référence, puis de trouver la valeur totale maximum parmi ces trois sommes et de l'identifier comme régime régissant. Les frontières obtenues avaient une forme lisse ; cependant, en comparaison avec la carte de Taitel et les photos, il y avait quelques désaccords.

À la différence des méthodes précédentes, dans la méthode basée sur le temps de passage, la dérivation des vecteurs caractéristiques a été faite après l'extraction des

traits. À nouveau, les deux approches ci-dessus ont été employées pour obtenir des résultats numériques. De plus, pour chaque approche, des HMM avec différents nombres d'états ont été essayés. Les frontières résultantes obtenues en extrayant les traits caractéristiques basés sur le temps de passage étaient lisses autant en utilisant les vraisemblances individuelles que les vraisemblances totales. En outre, par rapport aux autres méthodes, le résultat de cette méthode correspondaient mieux à la carte de Taitel, en particulier avec l'approche de vraisemblance totale. Bien que les frontières obtenues aient des dissimilitudes avec la carte de Taitel, elles étaient en bonne concordance avec les photos. Par conséquent, cette méthode a été sélectionnée pour l'extraction des traits caractéristiques.

Afin de vérifier l'effet de changement des paramètres de HMM, les HMM avec des nombres différents d'états (N=2, 3, 5 et 7) ont été essayés. Les frontières basées sur les résultats de l'approche de vraisemblances individuelles pour les cas de N=2, N=5 et de N=7 n'étaient pas lisses et il y avait un caractère arbitraire, en comparaison avec le cas N=3. D'ailleurs, aucune concordance n'a pu être notée entre l'augmentation du nombre d'états et la différence dans la forme des frontières. D'autre part, les frontières résultant de l'approche de vraisemblances totales étaient non seulement lisses mais également aucun changement notable n'a pu être observé pendant que le nombre d'états changeait. Par conséquent, il a été conclu que l'approche de vraisemblances totales est plus fiable et plus juste.

En outre, l'utilisation de différents points de référence a été considérée. Il faut noter que ce changement a été testé pour les régimes à bouchons et agités seulement. Les résultats ont montré qu'il y avait quelques variations dans les frontières obtenues dues au choix de différents points de référence. Seule la frontière entre le régime à bulles finement dispersées et le régime à bouchons a subi un léger changement. La frontière entre le régime à bouchons et le régime agité n'a subi aucun changement notable.

Afin d'étudier la confiance accordée aux résultats, la « confiance » a été définie comme étant : la différence entre les deux plus grandes valeurs de vraisemblance obtenues pour une condition de test donnée (c.-à-d. valeurs dans une rangée des tables

de vraisemblance). On observe que les conditions ayant un niveau de confiance élevé sont généralement situées loin des frontières de transition obtenues en utilisant les HMMs. Près des frontières de transition, la confiance est faible, ce qui constitue une certaine assurance qu'il s'agit bel et bien de zones de transition. Par ailleurs, la plupart des conditions dans la région à bulles finement dispersées ont un faible niveau de confiance, ce qui peut être lié aux faiblesses du système de mesure par sonde optique dans ce régime d'écoulement. En conclusion, il y a une corrélation acceptable entre les valeurs de probabilité et la signification physique des mesures.

Dans cette recherche, la praticabilité de HMM pour l'identification des régimes d'écoulement diphasique a été évaluée. Il a été montré que cette méthode a un bon potentiel. Aussi, l'exécution de cette méthode est sensiblement influencée par la méthode d'extraction des traits caractéristiques. Cette recherche doit être considérée comme une brèche qui permettra a maintes recherches futures d'être effectuées dans ce domaine.

Contents

Dedication ..... **iv**
Acknowledgements ..... **v**
Résumé ..... **vi**
Abstract ..... **x**
Condensé en Français ..... **xiii**
Contents ..... **xxiv**
List of figures ..... **xxvii**
List of tables ..... **xxix**
List of symbols ..... **xxx**
List of appendices ..... **xxxiv**
Introduction **1**

Chapter 1 An Introduction to Two-Phase Flow and Literature Review **4**
1.1 Introduction 4
1.2 Flow Pattern Classification 5
1.3 Different Methods in Flow Regime Detection 6
1.3.1 Direct Observation Techniques 6
1.3.2 Indirect Techniques 8
1.4 Flow Regime Transition Mechanisms in Vertical Flow 12
1.4.1 Bubble to Slug Transition 12
1.4.2 Slug to Churn Transition 13
1.4.3 Transition to Annular Flow 15
1.5 Conclusion 15

Chapter 2 Hidden Markov Model, Theory and Applications **16**
2.1 Introduction 16
2.2 Markov Models 18

2.3 Extension to Hidden Markov Models 19
2.4 Elements of An HMM 20
2.5 Continuous Hidden Markov Model (CHMM) 22
2.6 Procedure for using HMM in Practice 23
2.7 Identification 24
2.8 Forward Variables 26
2.9 Training 28
2.10 Backward Variables 28
2.11 Baum-Welch Algorithm 30
2.12 Multiple Observation Sequence 35
2.13 Initial Estimation 36
2.13.1 Clustering 37
2.13.2 Best State Sequence 38
2.13.3 Segmental k-mean Clustering 40
2.14 Scaled Forward-Backward Variables 41
2.15 Conclusion 44

Chapter 3 Experimental and Data Acquisition Procedure 45
3.1 Test Section 45
3.1.1 Tube and Mixer 45
3.1.2 Air Supply 46
3.1.3 Water Supply 47
3.2 Adjustment Procedure 47
3.2.1 Notations and Definitions 48
3.2.2 Homogeneous Model 50
3.2.3 Gas Flow Rate Correction 51
3.3 Measurement System 52
3.3.1 Optical Probe System 52
3.3.2 Data Acquisition System 54

3.3.3 Void Fraction Verification 54

Chapter 4 Modeling Two-Phase Flow Regimes using Continuous Hidden Markov Model 56

4.1 Data Preprocessing 57

4.1.1 De-noising Signals 57

4.1.2 Down Sampling 58

4.1.3 Feature Extraction 59

4.1.4 Feature Vector Derivation 62

4.2 Procedure of Implementing the CHMM 63

4.2.1 Training 64

4.2.2 Identification 66

Chapter 5 Results and Analysis 67

5.1 Condition Selection 68

5.2 Comparison between Different Method of Feature Extraction 70

5.2.1 Power Spectral Density Method 70

5.2.2 Autoregressive Method 74

5.2.3 Passage Time Based Feature Extraction 78

5.2.3.1 Method Verification 78

5.2.3.1 The Effect of Changing CHMM Parameters 80

5.2.3.2 The Effect of Selecting Different Reference Conditions 83

5.3 Confidence Evaluation 86

5.4 Conclusion 89

Conclusion 91

Bibliography 93

Appendices 105

List of figures

Figure 2-1 An example of a doubly stochastic process..... 20
Figure 3-1 Experimental setup 46
Figure 3-2 Optical probe system 52
Figure 3-3 Step index multimode fiber 53
Figure 4-1 An example of de-noising data: (a) measured signal and (b) de-noised signal 58
Figure 4-2 Comparison of two tests with same velocity and different void fraction: (a) schematic of the two-phase flows, (b) resulting de-noised, down-sampled data.....60
Figure 4-3 feature extraction based on the passage length of each phase: (a) de-noised, down-sampled data, and (b) resulting feature 62
Figure 4-4 Feature vector derivation 63
Figure 4-5 Procedure of implementing CHMM in identifying two-phase flow regimes 64
Figure 4-6 Training procedure.....65
Figure 4-7 Identification procedure.....66
Figure 5-1 Test point on the map of Taitel et al. (1980) 69
Figure 5-2 Reference conditions on Taitel's map.....70
Figure 5-3 Power specta and photos of three different conditions with same regime: (a) α =10%, Uhom=0.5m/s (b) α =20%, Uhom=0.5m/s (c) α =30%, Uhom=0.5m/s .. 71
Figure 5-4 Spectrogram of two-phase flow at 0.5 m/s and 10%. 73
Figure 5-5 Resulting map of using AR feature extraction method 77
Figure 5-6 Resulting map of using passage time feature extraction method (N=3)..... 79
Figure 5-7 Resulting map of using passage time feature extraction method (N=5)..... 81
Figure 5-8 Resulting map of using passage time feature extraction method (N=7)..... 82
Figure 5-9 New reference conditions on Taitel's map..... 84
Figure 5-10 Resulting map of using passage time feature extraction method with

different reference conditions (N=3)..... 85
Figure 5-11 Confidence regions for period based method with a 3 states HMM on Taitel's map. 88
Figure 5-12 An interval of the raw time signal (recorded at 99 kHz) of condition number 46. 89
Figure B-1 Photographs of two-phase flow conditions, simulated in test section..... 109

List of tables

Table 3-1 Measuring Instruments 47
Table 3-2 Test numbers, and two-phase flow conditions simulated in test section 48
Table 3-3 Results of void fraction verification test 55
Table 4-1 Down sampling ratios for different mixture velocities 59
Table 5-1 Parameters of vector derivation and CHMM 72
Table 5-2 Parameters of vector derivation and CHMM 74
Table 5-3 Log-likelihood results of using AR 75
Table 5-4 Parameters of vector derivation and CHMM 79
Table 5-5 Parameters of vector derivation and CHMM 81
Table 5-6 Parameters of vector derivation and CHMM 82
Table 5-7 Parameters of vector derivation and CHMM 85
Table C-1 Log-likelihood results from the Autoregressive method. 113
Table C-2 Log-likelihood results from the passage time based method (N=2). 114
Table C-3 Log-likelihood results from the passage time based method (N=3). 115
Table C-4 Log-likelihood results from the passage time based method (N=5). 116
Table C-5 Log-likelihood results from the passage time based method (N=7). 117
Table C-6 Log-likelihood results from the passage time based method, using different reference conditions (N=3). 118
Table C-7 Numerical likelihood values and confidence difference values for passage time (N=3). 119

List of symbols

A	States transition probability distribution	
A	Sectional area	m^2
a_{ij}	Probability of transition from state i to state j	
$\overline{a}_{ij}$	Reestimated state transition probability	
AR	Autoregressive	
ARMA	Autoregressive moving average	
argmax	Argument maximum	
B	Observation symbol probability distribution (emission matrix)	
$b_i(m)$	Probability of observing symbol m in state i	
$b_i(\vec{o}_t)$	Probability of observing observation vector in state i	
$\overline{b}_j(m)$	Reestimated observation symbol probability	
c	Mixture coefficient	
c_t	Scaling coefficient	
$\overline{c}$	Reestimated mixture coefficient	
CHMM	Continuous hidden Markov model	
ECT	Electrical capacitance tomography	
ERT	Electrical resistance tomography	
FFT	Fast Fourier transform	
FS	Full scale	
HFCF	High frequency contribution fraction	
HMM	Hidden Markov model	
K	Number of observation in an observation sequence	
LOFT	Loss of fluid test	
LPM	Litter per minute	
M	Number of observation symbols per any state	

max	Maximum	
MSVM	Multi-class support vector machine	
N	Number of states	
n	Dimensionality of observation vector	
O	Observation sequence	
$\bar{O}$	Observation vector sequence	
$\bar{o}$	Observation vector	
o_t	Observation	
P	Probability	
P_{std}	Standard pressure	Pa
P_{mixer}	Pressure measured at the entrance of the tube	Pa
p	Order of the autoregressive	
PDF	Probability density function	
PSD	Power spectral density	
PSDF	Power spectrum distribution function	
Q	Sequence of states	
$Q_{g(theory)}$	Theoretical gas flow rate	m^3/s
Q_{total}	Total flow rate	m^3/s
$Q_{g(corrected)}$	Corrected gas flow rate	m^3/s
$Q_{g(measured)}$	Measured gas flow rate	m^3/s
Q_g	Gas flow rate	m^3/s
Q_l	Liquid flow rate	m^3/s
q_t	Actual state	
$q_t^{k^*}$	Best state at time t	
r_t	Cluster in which observation at time t belongs	
S	Set of states	

S	Slip ratio	
S_n	State	
s_n	nth state	
s_n	Cluster group	
SLPM	Standard Litter per minute	
SVM	Support vector machine	
t	Time	
T	Number of observations in the sequence	
U	Covariance matrix	
U_{ls}	Liquid superficial velocity	m/s
U_{gs}	Gas superficial velocity	m/s
U_{hom}	Homogeneous velocity	m/s
U_l	Average liquid velocity	m/s
U_g	Average gas velocity	m/s
$\overline{U}$	Reestimated covariance matrix	
V	Set of observation symbols	
V_l	Liquid volume	m^3
V_g	Gas volume	m^3
w_t	White noise	
x_t	Time series	
x_{nm}	mth mixture in nth state	
x_{nm}	Cluster	
α	Void fraction	
$\alpha_t(i)$	Forward variable	
β	Volumetric quality	

$\beta_t(i)$	Backward variable
$\gamma_t(i)$	Probability of being in state i at time t, given the observation sequence, and the model
$\gamma_t(i,k)$	Probability of being in state i and observing the kth mixture at time t, given observation vector sequence and model
$\Delta(y)$	Dirac delta function
$\delta_t^k(i)$	Maximum probability of observation sequence along a single path until time t, which ends in state i
η	Gaussian probability distribution function
λ	Parameters of a hidden Markov model
$\overline{\lambda}$	Reestimated model
μ	Mean vector
$\overline{\mu}$	Reestimated mean vector
$\xi_t(i,j)$	Probability of being in state i at time t, and state j at time t+1, given the model and the observation sequence
π	Initial state distribution
$\overline{\pi}$	Reestimated initial state distribution
ϕ_p	Autoregressive reflection coefficient
$\psi_t^k(j)$	Back-tracking array

List of appendices

Appendix A Mathematical Proof of Equations (2-17) and (2-23) 105
Appendix B Photographs 108
Appendix C Numerical Results 112

Introduction

When two different fluids are simultaneously flowing together, this phenomenon is called two-phase flow. The fluids can be two different substances, or can be two phases of the same substance. In this text, the phases are referred to as the 'liquid phase' (water) and the 'gas phase' (air). Two-phase flows very often exist in industrial applications such as filtration, lubrication, spray processes, natural gas networks and nuclear reactor cooling.

Unlike single-phase flow for which there are only two flow regimes: laminar and turbulent flow, there exist several different flow regimes in the two-phase flow: bubbly flow, slug flow, churn flow and annular flow. In the study of two-phase flow, a flow regime indicates how the phases are distributed and mixed due to the physical nature of the system. These flow regimes appear as different configurations, which are referred to as flow patterns and as a result, flow regimes are sometimes addressed as flow patterns. The two-phase flow regimes depend on the type of fluid-fluid combination, the flow rates and direction, the conduit shape, size and inclination. In addition, heat and mass transfer rates, momentum loss, rate of back mixing and pipe vibration all vary greatly with the flow regimes. Therefore, it is quite important and necessary to identify these regimes and discern their correlation with the flow properties. These correlations are often presented as flow regime maps.

Many experimental and theoretical works and researches have been done in this area and as a result, there are several classification methods, and several two-phase flow

regime maps. The early experimental works were mostly based on direct observations. High-speed photography technique, X-ray attenuation picture and suchlike are some of the methods in which the flow regimes are detected directly by observations. Although these methods are inexpensive and in most of the cases are easy to perform, they are to a great extent subjective methods. Hence, in order to increase the objectiveness, indirect methods were developed. Indirect observation methods deal with the fluctuating characteristics of two-phase flow and utilize them for detecting the regime. It has been proven that there is coherence between flow regimes and the fluctuating characteristics of the two-phase flow. Thus, in this case, mathematical and statistical models are used to analyze these fluctuation characteristics and make judgment on the flow regime. Many theoretical methods have also been developed, most of which aimed to find a criterion for transitions between two-phase flow regimes.

In this project, a new method is developed for identifying two-phase upward flow regimes in a vertical channel, from the local void fraction signals gathered by an optical fiber probe system. The basic idea of this method is to detect flow regimes through analyzing signal patterns. As mentioned, there is a correlation between the fluctuating character of two-phase flow and flow regimes. Moreover, the signals are interpretations of such fluctuating characteristics. Therefore, the signal patterns can be considered as representative of the flow patterns. By analyzing and distinguishing these signal patterns, the flow patterns can be detected. In most of the previous methods of this type, statistical properties such as probability density function (PDF) were used for detecting flow patterns. In these methods, the statistical properties of a given fluctuating characteristic of the flow were obtained for each regime and then were used for comparing different regimes. In this research, in order to analyze the signal patterns in an enhanced and objective manner, the signal patterns were detected using hidden Markov models (HMM).

An HMM is a doubly embedded stochastic process, which has a rich mathematical structure. It has been proven to be a very strong pattern identifier with a good accuracy on most critical applications. HMM has been used in speech recognition starting from

the 60's and in recent decades, it has become more popular and it has been applied in other fields.

A dominant feature of HMM is that this model is effectively capable to compare signals. This feature has made HMM very applicable in many fields such as system condition monitoring, fault detection and so forth. In these applications, the procedure is in two steps: first different possible conditions of the system are simulated and recorded; and second, the unknown conditions are identified through comparing them to the simulated conditions using HMM. In this project, in an approximately similar way, two-phase flow conditions with clearly known regime were created in an experimental test setup. Optical probe measurements were performed on the flow and used for identifying regime of unknown two-phase flow conditions by means of HMM.

In chapter 1, a review of some of the well-known two-phase flow regime identification methods for the case of flow through a vertical tube is presented.

In chapter 2, the hidden Markov model is introduced and all the basic concepts and mathematical issues of it, related to this work are presented.

In chapter 3, the experimental procedure is explained. The information about data acquisition system, test section and like can be found in this chapter.

In chapter 4, the procedure of using HMM in identifying two-phase flow regimes is explained in detail. This chapter also covers the data preprocessing procedure.

In chapter 5, the results of applying different approaches are compared and discussed.

Eventually, in the conclusion, some suggestions for follow-ups to this project are presented.

Chapter 1 An Introduction to Two-Phase Flow and Literature Review

1.1 Introduction

As mentioned previously, it is quite important to investigate two-phase flow regimes and categorize them using pattern maps. Many authors and researchers have been working in this field and, as a result, there are several classification methods, and several two-phase flow regime maps. In this chapter, some of the most widely known and dominant methods for the case of internal two-phase flow in a vertical tube are covered. In order to have a better comprehension of different flow regimes and their transitions, a brief explanation is presented.

1.2 Flow Pattern Classification

A flow regime indicates how the phases are distributed due to the physical nature of the system. In case of two-phase upward gas-liquid flow in a vertical conduit, flow regimes can be categorized as follows:

Bubbles: This flow regime occurs at low gas flow rates where the gas phase is approximately uniformly distributed in the form of discrete bubbles in a continuum of liquid phase. Large deformable bubbles rise with a zigzag motion. Occasional Taylor-type bubbles can also be observed.

Finely dispersed bubbles: At higher velocities, the large bubbles break up due to turbulent forces. The bubbles come in smaller and more dispersed spheres in comparison with the bubbly flow. They behave as rigid spheres.

Slug flow: In this case, most of the gas appears in large bullet shaped bubbles, also known as Taylor bubbles, which have a diameter almost equal to the pipe diameter. The liquid slug area between two Taylor bubbles is filled with small bubbles that are very similar to those in bubbly flow.

Churn flow: Churn flow is a highly disordered flow that happens at high gas flow rates because of instabilities in the slugs. Churn flow can be interpreted as an irregular, chaotic and disordered slug flow. It is also characterized by an oscillatory flow, with the liquid phase moving alternately upward and downward in the channel.

Annular flow: At higher gas flow rates, the oscillations of the churn flow disappear, and there will be a continuum of gas phase along the center of the pipe. The liquid phase is continuously flowing upward, and it is distributed between a liquid film, which is flowing up the pipe wall, and a dispersion of the droplets flowing in the gas core of the flow.

1.3 Different Methods in Flow Regime Detection

There are several methods to detect flow regimes experimentally. One of the easiest and the most general method is to detect flow regimes through visual observation. This method has been being broadly employed whether to detect flow regimes or to verify other methods. This method owes its generality to the definition of different regimes, which is also based on visual observations. Due to their correspondence to visual observation, flow regimes detection methods can be dichotomized into direct and indirect methods.

1.3.1 Direct Observation Techniques

Some of the techniques that are directly connected to visual observation include high-speed photography technique, X-ray attenuation picture, electrical contact probe, multi-beam gamma-ray density measurement.

a. High speed photography technique: Because of its simplicity and inexpensiveness, this method has been used as a very common method in most of the experiments. This technique has been used not only as a basic method for detecting flow patterns, but also has been used along other techniques for verification and validation. Cooper *et al.* (1963), Staub and Zuber (1964), Bennett *et al.* (1965) and Hewitt and Roberts (1969) are some of those who used this method as a basic method.

Since most of the tests have been done using partly or completely transparent tubes, and this type of tubes cannot bear high pressures, some limitations are imposed on pressure increase. It is also declared that there are uncertainties in case of high flow velocities and in case of regime transitions. Nevertheless, this method is still a useful method in both detecting flow regimes and verifying other methods.

b. X-ray attenuation picture: As mentioned, transparent tubes must be used for flow patterns visualization. In order to visualize the flow inside metallic tubes, X-ray pictures

can be taken under some controlled conditions. In order to have better pictures, the thickness and the material of the channel wall must be chosen the way that there would be the least X-ray absorption. Bennett *et al.* (1965) and Hewitt and Roberts (1969) used this technique together with high-speed photography technique.

c. Electrical contact probe: In this method a thin rod shape electrical probe, which is insulated from the channel wall and its tip is positioned at the center of the channel cross section, is used. The channel wall and the probe are parts of an energized electric circuit. Whenever a conducting liquid mass bridges the gap between the probe's tip and the channel wall, the circuit is close, otherwise the circuit in open. Regarding the fact that different regimes have different distribution of gas-liquid, the fluctuation in electrical current that is easily detectable, can represent a schematic of the flow regime. Bergles *et al.* (1968) used this technique and verified it using visual observation and flash photography through a transparent section at the channel exit.

d. Multi-beam, Gamma-ray density measurement: When gamma rays pass through two-phase flow, the amount of attenuation will change with the flow regime changes. By recording the attenuation of several gamma ray beams, which are particularly arranged in a way that beams cross the flow channel along different chords, some useful information about flow regimes can be obtained.

Piper (1974) studied such gamma densitometer and Lassahn (1977) developed the data analysis procedure to estimate the density profile from measurements of a three-beam densitometer on the LOFT (loss of fluid test) reactor pipes. Further description of this approach was given by Kondic and Lassahn (1978). Finally, Prassinos and Liao (1979) used this technique to identify flow regimes.

1.3.2 Indirect Techniques

The direct observation methods always seem to be promising choices. However, due to their subjectiveness and the difficulties in some applications, it has been of interest to find a method, which uses the fluctuating characters of two-phase flow to detect the regimes. These fluctuating characters can be observed in local pressure, instantaneous mixture ratios of vapor and liquid or suchlike. Further, mathematical models have been shown to bring about clear indications of the different flow regimes when they are used to analyze such fluctuations. Thus, by measuring one or more fluctuating features of the flow and by modeling such features, flow regimes can be detected either objectively or subjectively. Some of these techniques are presented as follow:

a. Pressure fluctuation analysis: Using the normalized power spectral density (PSD) of the data gathered from channel wall pressure fluctuation, Hubbard and Dukler (1966) showed that for different regimes there exist different PSDs. Nevertheless, this method had some weak points; the plots of PSD versus frequency for different regimes depend not only on flow regime but also on the homogenous velocity of mixture. Vince and Lahey (1980) clearly illustrated the existence of such problem. Anyhow, Albrecht *et al.* (1982) showed that this method could be recognized as a strong method for flow regime changes.

Tutu (1982) used two pressure transducers while Matsui (1984) employed four transducers for measuring pressure at different locations along flow direction. Statistical properties such as probability density function (PDF) were used by them to predict the flow regimes.

Later, King *et al.* (1988) used an optimum modeling method, which is to fit the two-phase flow pressure signals by autoregressive moving average (ARMA) models using an optimization technique.

Recently, Elperin and Klochko (2002) proposed a novel wavelet transform-based approach and validated using time series of differential pressure fluctuations. The wavelet transform provides time-scale signal decomposition, which is intermediate

between the time and frequency domain representations and has two remarkable properties. One is that there exists a very fast algorithm for computing the coefficients of the discrete wavelet transform, which is faster than the fast Fourier transform (FFT). Another is that the estimation of the wavelet coefficients does not require a large sample size. Thus, it can be used for online identification of flow regimes in two-phase systems, and may be implemented with any measurement device for which the output is related to the gas void fraction of the flow.

b. X-ray attenuation fluctuation analysis: Jones and Zuber (1975) were first to investigate that the probability distribution function (PDF) of void fraction can be used for detecting flow regimes. They used X-ray attenuation through a rectangular channel for obtaining void fraction data. High-speed motion pictures were taken for verifying results.

Vince and Lahey (1980) and Vince and Lahey (1981) employed the same technique using the data obtained by a special X-ray system with six beams and later with a dual beam. They also claimed that using the variance of the PDF distribution is an objective method for flow regime identification, as opposed to using PDF itself, which they stated to be a subjective method.

c. Neutron noise analysis: Some of the key characteristics of the two-phase flow can be determined by measuring neutron density in boiling water reactors. The measured neutron densities demonstrate a fluctuating intensity with respect to fluctuating nature of the two-phase flow, which reflects local and global variation in the flow structure. There are two types of measurements for this case; near field measurements that signify measuring at some points close to channel inside a reactor core, and far field measurements, which correspond to measuring at points around the core. Simultaneous recording of neutron noise via these two types of measuring can provide enough information of the two-phase flow manners.

This method was first suggested by Crowe *et al.* (1977) and developed by Albrecht *et al.* (1980), Kosaly (1980) and Kozma *et al.* (1992) who utilized the statistical interpretation of neutron noise signals.

Also King *et al.* (1989) proposed a technique based on the modeling of neutron signals by autoregressive moving average (ARMA) models using an optimization technique to identify flow pattern by a single index called dynamic signature.

d. Drag disk noise analysis: Albrecht *et al.* (1982) reported that measuring the impact force of two-phase flow on a drag disk located inside the tube could be used for detecting flow regimes. The drag disk in their experiment was supported by a bar, which was attached to the wall and it transmitted the impact force to a measuring system.

e. Electrical impedance methods: A packed mass of two-phase flow mixture has different electrical impedance in different flow regimes. Impedance is given by the resistance in case of conductive flows, or by the reactance in other case. Matuszkiewicz *et al.* (1987), Kelessidis and Dukler (1989), Das and Pattanayak (1993) and Costigan and Whalley (1997) utilized conductance sensing method, whereas, Geraets and Borst (1988), Soldati *et al.* (1996) and Elkow and Rezkallah (1997) used capacitance sensing technique. Statistical analyses such as probability distribution functions PDF, power spectrum distribution functions PSDF or diffusional analyses were applied by most of the mentioned authors.

Xie *et al.* (1989) used data gathered from 8-electrode capacitance system to build a database of fingerprints of flow regimes. Then by comparing the fingerprints, which were normalized capacitance vectors, they detected flow regimes. Also Jeanmeure *et al.* (2002) employed a similar approach called electrical capacitance tomography (ECT). Later, Dong and Jiang (2003) employed electrical resistance tomography (ERT) which was somehow similar to ECT.

Haiqing *et al.* (1992) and Le Corre *et al.* (1999) presented a fuzzy methodology based on local time averaged two-phase parameters obtained from a conductivity multi-sensor

probe. In few words, a fuzzy algorithm is a collection of fuzzy If/Then rules, which is formulated to perform a given task. Further, they argued that fuzzy systems not only determine which flow regime is prevalent, they give the contribution of each flow regime to the two-phase flow system as well.

f. Other techniques: Wang *et al.* (1988, 1990) proposed that analyzing the spectra of void fraction signals obtained by a single light sensor by means of the high frequency contribution fraction (HFCF) technique, the flow patterns can be identified. HFCF is described as the ratio of PSDF of high frequency components to the PSDF of the all the frequency components.

Lu and Zhang (1994) suggested a steady state mathematical model for two-phase flow pattern identification using the interfacial area concentration as the identification parameter. They argued that due to theoretical analysis, the maximum of the interfacial area concentration curve is the transition point between bubble and slug-churn flow patterns and the intersection point of this curve with the typical annular interfacial area concentration curve represents the transition between slug-churn and annular flow patterns. Such intersection points can then be used to construct flow pattern transition lines on proper maps.

Dinh and Choi (1999) and Ulbrich *et al.* (2002) applied an image-processing method to detect flow regimes. In this method, at first continuous images are captured of the two-phase flow in a transparent conduit. In this step, taking more contrast images is a crucial point. Then the images are digitalized using computer codes. Digital image processing techniques will be used to detect flow regimes by analyzing digitalized images.

Trafalis *et al.* (2005) presented a novel method for flow pattern identification based on a multi-class support vector machine (MSVM) model. MSVM model is an extension to support vector machine (SVM) model and is a technique to discover the complex and hidden relationships between variables of the inputs and outputs. The idea of the SVM is to determine support vectors of experimental data, which can be divided into two groups

of the independent variables and the dependent variables, and use them to derive the weights that define the separating surface between the different patterns of the experimental data. These weights represent the level of influence of the independent variables on each dependent variable. For two-phase flow in a pipe, the weights represent the level of influence of pipe diameter, liquid superficial velocity, and gas superficial velocity in the flow regime.

1.4 Flow Regime Transition Mechanisms in Vertical Flow

One of the most crucial and complicated concepts in two-phase flow study is the mechanisms of transition. In order to determine the conditions at which the transition between flow patterns happens, physical mechanisms by which such transition occurs must be investigated. In this section, some of the physical criteria that have been proposed are presented.

1.4.1 Bubble to Slug Transition

Taitel *et al.* (1980) dichotomized the bubbly flow regime into two distinct regimes: finely dispersed bubbles and bubbles. Then they discussed that the density of the bubbles will increase with the gas rate. Consequently, the bubbles will become closer and coalescence rate will increase. On the other hand, as the liquid rate increases, the turbulent fluctuations associated with the flow can cause break up of larger bubbles formed through agglomeration. Hence, the dominance of two above factors (agglomeration and turbulence) must be determined.

In case of low liquid rates, Taitel *et al.* (1980) argued that by an increase in gas flow rate, the bubble density increases and a point is reached where the dispersed bubbles become very closely packed. Therefore, there will be more agglomeration to larger bubbles and it results in the transition to slug flow. Prior to this study, Griffith and Wallis (1961), Griffith and Synder (1964) and Radovicich and Moissis (1962) had

suggested that the transition happens for void fractions around 0.25 to 0.30. As a consequence, Taitel *et al.* (1980) picked 0.25 and gave a condition for transition from bubbly flow to slug flow. Another study was done later by Weisman and Kang (1981) who gave their own criterion, which was based on data correlation for transition from bubbly to slug flow.

In case of high liquid rates, Taitel *et al.* (1980) stated that turbulent forces break and disperse the gas phase into small bubbles. For void fractions higher than 0.25, if the bubbles produced by the turbulent breakup process are large enough, then slug flow will be formed by the process of coalescence. Using the theory that was given by Hinze (1955) and confirmed by Sevik and Park (1973), Taitel *et al.* (1980) obtained a condition for transition from finely dispersed bubble to churn-slug.

Moreover, Mishima and Ishii (1984) suggested a value of 0.3 for void fraction using geometrical consideration and presented a relationship for bubbly to slug transition.

1.4.2 Slug to Churn Transition

There exist different definitions for churn flow and as a consequence, transition from slug to churn is more intricate to study. That is to say, prior to find a transition criterion, physical conception of this transition must be understood. Griffith (1964) and later Golan and Stenning (1970) were the first authors who gave a transition criterion, which was based on their experiments on air-water flow.

Taitel *et al.* (1980) stated that as the gas flow increases, the slug flow pattern develops from a bubbly pattern and it makes bubbles to get closer and coalesce. Then, if the process of coalescence continues, Taylor bubbles which occupy most of the cross sectional area of the pipe, are formed and separated by a liquid slug. Then, the liquid slug cannot support a stable liquid bridge between two consecutive Taylor bubbles. Hence, the falling film around the bubbles breaks through the liquid slug and creates an agitated mixture. This can be considered as churn pattern where an oscillatory motion of the liquid is observed. They also added that the churn flow pattern is an entry region

phenomenon in the process of slug flow formation. Accordingly, whenever slug flow is observed, churn flow must have been formed in the entry. The entry length where churn flow can be observed depends on the flow rates and pipe size. Eventually, Taitel *et al.* (1980) gave a criterion for transition as a function of entry length and tube size.

Mishima and Ishii (1984) defined the limiting mean value of void fraction and gave an expression based on streaming conditions around a Taylor bubble. Then they claimed that for void fractions greater than the limiting mean value there would be a transition from slug to churn.

Brauner and Barena (1986) suggested that the transition to churn flow occurs when the void fraction within the liquid slug reaches the maximum volumetric bubble packing that is 0.52 as they argued. For such region, the organized structure of the slug flow is destroyed repeatedly by regions of high gas concentration in the liquid slug.

McQuillan and Walley (1985) and Govan *et al.* (1991) modeled the transition between slug flow and churn flow under the assumption that flooding of the falling liquid film limits the stability of slug flow. They attributed this transition to the flooding of the liquid film surrounding the Taylor bubble in slug flow and extracted the theoretical relations. Flooding is a phenomenon in which the liquid film in countercurrent flow of gas and liquid breaks down due to the formation of large interfacial waves. Jayanti and Hewitt (1992) compared this method with three other methods and concluded that only the flooding mechanism is capable of predicting the gas velocity required for the transition and so is the most likely cause of the transition.

Mao and Dukler (1993) claimed that no transition from slug to churn exists and the churn flow is simply a continuous extension of the condition of slug flow. They used visual, instrumental and experimental evidences to suggest that there is little justification for considering churn flow to be a distinct flow pattern. However, not much later, Hewitt and Jayanti (1993) prepared a response to that claim and called it confusion.

1.4.3 Transition to Annular Flow

Golan and Stenning (1970) represented a criterion based on their experimental data for this transition.

Taitel *et al.* (1980) gave a criterion for transition to annular flow based on the idea that annular flow cannot exist unless the gas velocity in the gas core is sufficient to lift the entrained droplets.

Weisman and Kang (1981) used a curve-fit correlation method to predict this transition.

Ishii and Mishima (1980) obtained two different criteria, one for small tube sizes and one for large channels and compared their map with those of Mandhane *et al.* (1974) and Duckler and Taitel (1977). They also gave a definition for small tube.

1.5 Conclusion

In this chapter, most of the methods for flow regime detection were introduced. A two-phase system due to its properties can be addressed to be under two conditions. A condition is when the system undergoes a distinct and specified regime, to wit, bubble, churn, slug and annular. In this case, many experimental works have been done to detect the flow regime, which have been somehow successful. Another condition exists when the system undergoes a transition between regimes. In this case, detecting the flow regime is crucially difficult and most of the works were based on theoretical analyses. Moreover, due to complex nature of two-phase flow, theoretical analyses have not been able to describe the system impeccably. Therefore, a technique is still required which, whether experimentally or theoretically, detects and describes the flow regime in conditions near regime transition.

Chapter 2 Hidden Markov Model, Theory and Applications

2.1 Introduction

Signals can be considered as representations of observable outputs of a real-world process, which carry a great deal of information about their sources. Using raw signals for learning about a process is extremely limited in practice. Hence, signal models have been defined and created to derive the characteristics of a process from its signal. Signal models often work very well in practice and can efficiently be used in identification systems, recognition systems, prediction systems and suchlike. Signal models can be categorized into two broad classes of deterministic models and statistical models. Deterministic models are those which contain no stochastic components, and the models are assumed to deal with only one possible result for each alternative course or action. In the case that the randomness of a process is taken into account, the model is a statistical model. In this category, the statistical properties of the signal are characterized. Gaussian process, Poisson process, Markov process and Hidden Markov Model, as an extension to Markov processes, are some examples of this type.

In the late 60's, the basic theory of Hidden Markov Model (HMM) was developed by Baum and his colleagues. Later, Baker (1975) and Jelinek *et al.* (1982) developed and implemented HMMs for speech recognition. Rabiner (1989) published a detailed tutorial on HMM, which he used in speech recognition. Since then, HMM has been used not only in speech recognition but also in many other fields.

Even though the idea behind HMM and its application dates back to the 60's and 70s, its first uses in mechanical engineering was in the early 90's. Heck and McClellan (1991), Ertunc and Loparo (2001), Ertunc *et al.* (2001) and Ertunc and Oysu (2004) employed HMM in the field of tool wear monitoring. They gathered thrust, torque, spindle and servo signals from acceptable and worn tools and then used them to train HMMs. In addition, Owsley *et al.* (1997), Atlas *et al.* (2000), and Wang *et al.* (2002) modeled HMM from vibration data for tool wear monitoring.

Hannaford and Lee (1991) developed a model based on HMM for the prediction and analysis of sensor information recorded from a robotic system during performance of tasks by telemanipulation. The HMM was used to describe the task structure and the operator or intelligent controller's goal structure from the sensor signals such as forces and torques. Hovland and McCarragher (1999) presented a process monitor for robotic assembly based on HMM process using dynamic force and torque signals arising from the interaction between the workpiece and the environment.

Using axial leakage flux and line current data from electromechanical motors, Hatzipantelis and Penman (1993) utilized HMM to diagnose faults in the motors. Later, Ying *et al.* (2000) presented an HMM-based algorithm to solve fault diagnosis problems with partial and imperfect tests. Bunks *et al.* (2000) used vibration measurements to build HMMs and diagnose faults in helicopter gearbox. Ocak and Loparo (2001), Zhang *et al.* (2005), Ocak and Loparo (2005) and Purushotham *et al.* (2005) proposed a fault detection scheme for rolling bearings based on hidden Markov modeling of vibration signals. Lee et al (2002) used continuous HMMs built on acceleration signals to diagnose faults of a lathe. Later, Lee *et al.* (2004) simulated different types of fault in a rotor; they gathered vibration signals from each fault and used continuous HMMs to

model to diagnose the faults. Ge *et al.* (2004) presented an HMM based fault diagnosis for stamping process using strain signals. Li et al (2005) implemented HMM in fault diagnosis for speed-up and speed-down process for rotating machine, using vibration signals.

Smyth (1993) used HMM for online health monitoring of an antenna pointing system from the antenna motor current signal under both normal and fault conditions.

The HMM was applied to power plant accident identification by Kwon and Kim (1999). They created an HMM for each accident from a set of training data obtained from major variables of a power plant such as temperature, pressure, flow, pump on/off status, or valve open/close status.

2.2 Markov Models

HMM is an extension to Markov process, thus in order to have a good knowledge of HMMs, it is quite reasonable to consider the Markov process first. A Markov process is a random process whose future probabilities are determined by its most recent values, depending on the order of the process. The order of a Markov process determines the number of previous values that are taken into account for obtaining the future probabilities. It can be considered as a system, which at any time is in a distinct state chosen from a set of N states, $S_1, S_2, \ldots, S_N$ and any state is subject to change during a discrete time difference. This change can be made from a state to another state or from a state to itself. To be precise, as discrete time passes, the system can face a change in its state or can remain in the preceding state. In order to have a full probabilistic description of the system, the model needs to specify the probability of the system to be in any given current state, given all the previous states. However, according to the definition of first order Markov process, the probabilistic description will be reduced to:

$$P\left[q_{t+1} = S_j \mid q_t = S_i, q_{t-1} = S_k, \ldots\right] = P\left[q_{t+1} = S_j \mid q_t = S_i\right] \qquad (2\text{-}1)$$

where t is the time instants associated with state changes and q_t is the actual state at time t. Moreover, the set of state transition probabilities a, is defined as:

$$a_{ij} = P[q_{t+1} = S_j \mid q_t = S_i], \quad 1 \le i, j \le N, \quad a_{ij} \ge 0 \tag{2-2}$$

$$\sum_{j=1}^{N} a_{ij} = 1 \tag{2-3}$$

In this model, the states correspond to physical outputs of the process, which are observable. In comparison with a hidden Markov process, the above process can be called an observable Markov process.

2.3 Extension to Hidden Markov Models

Markov models in which each state corresponds to an observable (physical) event were introduced. As a matter of fact, Markov models are too restrictive to be applied to many problems of interest. Even though, the concept of Markov models can be extended to include the case where the observations are probabilistic functions of the states. In this case, the resultant model is a doubly embedded stochastic process with an underlying stochastic process that is not observable (it is hidden), but can only be observed through another set of stochastic processes that produce the sequence of observations.

As an example, as shown in Figure 2.1 it can be imagined that in a test setup there are N identical beep producer devices, which produce M different beeps. Every second, a beep is played on a doubly stochastic basis: not only the beep producer devices are randomly chosen from N choices, but also beep frequencies are randomly chosen from M choices. Supposedly, only auditory signals are provided to the analyzer via a microphone and there is no information about the number of devices or about the device that plays the beep at a specific time. Therefore, in this case, the number of devices and

the device that produces the beep at a given time are hidden from the analyzer. This system can be modeled with an HMM in which each state corresponds to a beep producer device and the probability distribution of different beeps is defined for each state. Since the number of devices is unknown and there are different possibilities, there is a serious problem of finding the model that best represents the process. Theoretically, the model that has more states is capable of considering more possibilities and is a better model. However, there are always limitations for increasing the number of model parameters. These limitations are greatly influenced by practical considerations. Therefore, the concept of best model depends on the area of application.

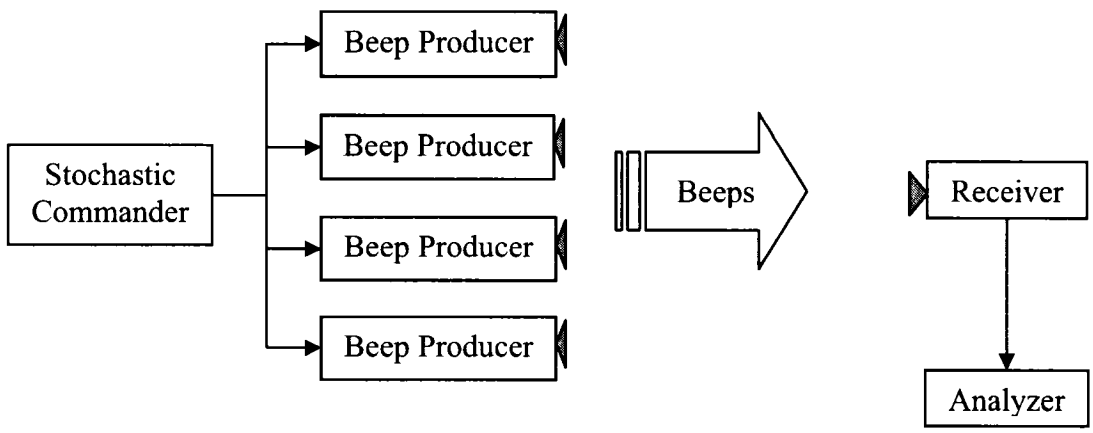

Figure 2-1 An example of a doubly stochastic process.

2.4 Elements of An HMM

A discrete HMM in which the observations are discrete symbols, is characterized by the following parameters:

1) A set of hidden states, which can be denoted as $S = \{S_1, S_2, \ldots, S_N\}$ where N is the number of states in the model. There may be a physical interpretation for states in some application. However, in most of the applications there is no clear physical meaning for states.

2) The states transition probability distribution, $A = \{a_{ij}\}$, which is the same as what it was for Markov models.

3) A set of observation symbols which can be denoted as $V = \{v_1, v_2, \ldots, v_M\}$, where M is the number of observation symbols per any state. This is the observable part of an HMM.

4) The observation symbol probability distribution (emission matrix):

$$B = \{b_j(m)\},$$

where for $1 \le j \le N$, $1 \le m \le M$ and q_t as actual state at time t:

$$b_j(m) = P[v_m \text{ at } t \mid q_t = S_j], \qquad b_j(m) \ge 0 \tag{2-4}$$

$$\sum_{m=1}^{M} b_j(m) = 1 \tag{2-5}$$

5) And finally, the initial state distribution:

$$\pi_i = P[q_1 = S_i], \quad 1 \le i \le N, \qquad \pi_i \ge 0 \tag{2-6}$$

$$\sum_{i=1}^{N} \pi_i = 1 \tag{2-7}$$

These parameters can be presented in the short form: $\lambda = (A, B, \pi)$.

Given an observation sequence $O = o_1 o_2 \ldots o_T$ where each observation o_t is one of the symbols from V, and T is the number of observations in the sequence, the appropriate values of N, M, A, B and π can be calculated. Moreover, the probability of observing a given observation sequence with a previously calculated HMM can be determined. That is to say, if the parameters of an HMM have already been estimated using an observation sequence, then the probability of observing any other observation

sequence by that model can be calculated. This is a feature of HMM that makes it strongly applicable in practice. The procedure of such calculation will be discussed in detail in the following sections.

2.5 Continuous Hidden Markov Model (CHMM)

In the previous section, elements of a discrete HMM were introduced. A discrete HMM is one in which the observations were represented by discrete symbols chosen from a finite alphabet, and therefore a discrete probability density could be used within each state. Actually, in most applications, observations are continuous symbols (or vectors). So the HMM in which the parameters are defined based on discrete observation will not be capable to model continuous observations. Therefore, elements of the HMM must be modified in a way that enables the model to cover continuous observations. Fortunately, there is only one parameter that deals directly with observation and thus must be modified: the probability distribution of the observation symbol, $B = \{b_j(m)\}$. The discrete definition of this element must be replaced with a continuous one.

According to probability concepts, the most general representation of probability distribution function of continuous observations is in the form of a mixture model. A mixture model can be represented as a sum of probability density functions (PDFs) so that each PDF is weighted by a mixture coefficient. Hence, the probability distribution of the observations can be represented as:

$$b_j(\bar{o}) = \sum_{m=1}^{M} c_{jm}\eta[\bar{o}, \mu_{jm}, U_{jm}], \quad 1 \le j \le N \tag{2-8}$$

where c_{jm} is the mixture coefficient for the mth mixture in the state j, μ_{jm} and U_{jm} are respectively the mean vector and covariance matrix for the mth mixture component in state j and η can be any log-concave or elliptically symmetric density. In case of

Gaussian probability distribution function, η is defined as:

$$\eta(\bar{o},\mu,U)=\frac{1}{\sqrt{(2\pi)^n|U|}}\exp\left(-\frac{1}{2}(\bar{o}-\mu)'U^{-1}(\bar{o}-\mu)\right) \qquad (2\text{-}9)$$

where μ is the mean vector, U is the covariance matrix and n is the size of vector $\bar{o}$.

2.6 Procedure for using HMM in Practice

So far the preliminary concepts of HMM were considered and its elements were introduced. Previously, it was stated that the elements of an HMM can be calculated given an observation sequence and the probability of an observation can be calculated using an existing HMM. This feature makes HMM a very strong tool for comparing two or more signals, which is a key to solve several problems in practice.

For example, its use in speech recognition can be considered. It can be supposed that there is a speech recognition device, which receives an auditory signal from a speaker. The speaker is saying a number between 1 to 10 and the recognizer must specify which number is being said. In order to do so, first a library of HMMs must be created in which each HMM corresponds to a number between 1 and 10. Precisely, each HMM has been trained using auditory signals of the pronunciations of the numbers 1 to 10. Then, once the speaker says a number, the auditory signal of the said number will be considered as an observation for all HMMs in the library. Then, the probability of observing such signal is calculated using each of the ten HMMs. The number for which the corresponding HMM has the highest probability is detected to be the said number. So HMMs can be used in many applications. First possible conditions of a system must be simulated and then a library of HMMs of simulated conditions must be created. Then, any unknown condition can be recognized by comparing its observation sequence with the HMMs in the library. This library can be a library of different faults of a

mechanical system, a library of the spoken words in a speech recognition device, or any other events depending on the area of application.

As described, the process of using HMM is achieved in two main steps. The first step is training, that is making an HMM from a signal. The second step is identification, that is calculating of the probability of observing a signal, given an HMM. These steps will be discussed in detail in the next sections.

2.7 Identification

Studying the identification step will lead to some basic definition and concepts that will be used in the other step, so this step will be discussed first. In the identification step it is required that the probability of observing an observation sequence of an unknown signal, $O = o_1 o_2 \ldots o_T$ for a given model $\lambda = (A, B, \pi)$ be determined, i.e., $P(O \mid \lambda)$. The explicit way of doing this is to calculate $P(O \mid \lambda)$ as a function of the model elements $\lambda = (A, B, \pi)$, using probability definitions. The first element that must be considered is the state sequence that matches with the observation. One such sequence can be denoted as $Q = q_1 q_2 \ldots q_T$, in which q_1 is the initial state. Since, at any time, the number of possible states is N, then there are N^T possibilities for the state sequence. The probability of observing O given the sequence of states Q is written as:

$$P(O \mid Q, \lambda) = \prod_{t=1}^{T} P(o_t \mid q_t, \lambda) \qquad (2\text{-}10)$$

The above formulation can be represented as:

$$P(O \mid Q, \lambda) = b_{q_1}(o_1).b_{q_2}(o_2)\ldots b_{q_T}(o_T) \qquad (2\text{-}11)$$

Moreover, the probability of the state sequence Q given $\lambda = (A, B, \pi)$ is:

$$P(Q \mid \lambda) = \pi_{q_1} a_{q_1 q_2} a_{q_2 q_3} \ldots a_{q_{T-1} q_T} \tag{2-12}$$

The joint probability of Q and O, which is the probability that Q and O occur simultaneously, is the product of two previous terms:

$$P(O,Q \mid \lambda) = P(O \mid Q,\lambda) P(Q \mid \lambda) \tag{2-13}$$

The above formulation is very close to the desired formulation of $P(O \mid \lambda)$. The only difference is the extra term Q in the left side of the conditional probability bar. With respect to probability theorems, in order to omit such term, the term $P(O,Q \mid \lambda)$ must be summed over all the possible occurrence of that term. So using the above formulation, $P(O \mid \lambda)$ can be written as:

$$P(O \mid \lambda) = \sum_{over\, Q} P(O \mid Q,\lambda) P(Q \mid \lambda) = \sum_{q_1, q_2 \ldots, q_1} \pi_{q_1} b_{q_1}(o_1) a_{q_1 q_2} b_{q_2}(o_2) \ldots a_{q_{T-1} q_T} b_{q_T}(o_T) \tag{2-14}$$

Equation (2-14) is a complete formulation for calculating the probability of observing an observation sequence O, given model parameters $\lambda = (A, B, \pi)$.

The interpretation of the computation in the above equation is as follows. Initially (at time t = 1) the instantaneous state is q_1 with probability π_{q_1} and it generates the symbol o_1 (in this state) with the probability $b_{q_1}(o_1)$. As time changes from t to t+1 (t = 2) there will be a transition to state q_2, from state q_1 with probability $a_{q_1 q_2}$, and generate symbol o_2 with probability $b_{q_2}(o_2)$. This process continues in this manner until the last transition (at time T) from state q_{T-1} to state q_T with probability $a_{q_{T-1} q_T}$ and generating symbol o_T with probability $b_{q_T}(o_T)$. Using the above equation requires a huge number

of calculations, which is quite inefficient. Precisely, $(2T-1)N^T$ multiplications, and N^T-1 additions will be needed. Even for small models (with a few numbers of states and mixtures), a large number of calculations must be done which cannot be performed by any ordinary computer. Clearly, a more efficient procedure is required to solve this problem. There exists a procedure for solving the mentioned problem, which is called forward-variables procedure.

2.8 Forward Variables

The probability of partial observation sequence until time t, $O = o_1\, o_2 \ldots o_t$, and state S_i at time t given the model λ, is called forward variable $\alpha_t(i)$ for time t and state i and is represented as:

$$\alpha_t(i) = P(o_1 o_2 \ldots o_t, q_t = S_i \mid \lambda) \tag{2-15}$$

Regarding HMM parameters there are two different solutions for $\alpha_t(i)$:

1- Initialization or solution at initial time:

$$\alpha_1(i) = \pi_i b_i(o_1), \qquad 1 \le i \le N. \tag{2-16}$$

At time t=1 the probability of the first observation and state i, given λ, will clearly be the product of initial probability of state i, precisely π_i, and the observation probability distribution of o_1 within such state $b_i(o_1)$.

2-Induction:

$$\alpha_t(j) = \left[\sum_{i=1}^{N} \alpha_{t-1}(i) a_{ij}\right] b_j(o_t), \quad 2 \le t \le T \quad and \qquad 1 \le j \le N \tag{2-17}$$

At any time t other than the initial time, the probability of observation o_t in state j is the observation probability distribution of o_t within such state, $b_j(o_t)$, multiplied by joint probability of observing o_{t-1} in any states and transition from that state to state j which is the summation of the products of all forward variables of previous states and state transition probabilities. The mathematical proof of Equation (2-17) is given in Appendix A. As an example, it can be supposed that there is a model with 3 states and 4 mixtures and it is desired to determine the probability of the second observation (t=2). Since at time t=1 the system could have been in one of the three states, in order to be in state 1 at time t=2, there are three ways for which the state 1 can be reached. In probabilistic terms, it can be written as:

$$P(q_2 = S_1 \mid \lambda) = \pi_1 a_{11} + \pi_2 a_{21} + \pi_3 a_{31} \tag{2-18}$$

If the probability of observations is taken into account then the above formulation will be modified to:

$$\begin{aligned} P(o_1 o_2, q_2 = S_1 \mid \lambda) &= \left(\pi_1 a_{11} b_1(o_1) + \pi_2 a_{21} b_2(o_1) + \pi_3 a_{31} b_3(o_1)\right) b_1(o_2) \\ &= \left[\sum_{i=1}^{N} \pi_i a_{i1} b_i(o_1)\right] b_1(o_2) = \alpha_t(j) = \left[\sum_{i=1}^{N} \alpha_1(i) a_{i1}\right] b_1(o_2) \end{aligned} \tag{2-19}$$

It can be concluded that sum of all forward variables at termination time (t=T) will be the probability of an observation sequence O, given model λ:

$$P(O \mid \lambda) = \sum_{i=1}^{N} \alpha_T(i) \tag{2-20}$$

Using this method for calculating $P(O \mid \lambda)$, as many as N (N+1) (T-1) +N multiplications and N (N-1) (T-1) additions must be performed. If N=3, and T=150, using forward variables method requires about 2700 calculation, while for direct method requires about 10^{74} operations. Therefore, obviously it is a much more enhanced way of calculating $P(O \mid \lambda)$.

2.9 Training

As mentioned earlier, the first and the most difficult step of applying HMM in practice is to model the known signals in HMMs or, precisely, to adjust model parameters $\lambda = (A, B, \pi)$ that will maximize the probability of observing signal $P(O \mid \lambda)$. This step is called training and the observation sequence used to adjust the model parameters is called a training sequence. The training step is crucial for most applications of HMMs, since in this step model parameters are optimally adapted to observe training data.

Unfortunately, there is no optimal analytic way to solve for the model parameters $\lambda = (A, B, \pi)$, which maximizes the probability of the observation sequence $P(O \mid \lambda)$. However, there exist some iterative methods that can be used to choose $\lambda = (A, B, \pi)$ such that $P(O \mid \lambda)$ is locally maximized. Baum-Welch method is one of these iterative methods, which will be introduced. In order to have a good understanding of Baum-Welch method, backward variables must first be introduced.

2.10 Backward Variables

Previously, the probability of the partial observation sequence until time t, $O = o_1 o_2 \ldots o_t$ and state S_i at time t, given the model λ was called forward variable. In a similar manner, the probability of the partial observation sequence from time t+1 to the end, given state S_i at time t and the model λ is called backward variable $\beta_t(i)$ for time t

and state i and is represented as:

$$\beta_t(i) = P(o_{t+1}o_{t+2}\ldots o_T \mid q_t = S_i, \lambda) \qquad (2\text{-}21)$$

Similarly to the case of forward variables, there are two different solutions for $\beta_t(i)$:

1- Initialization or solution at the first iteration:

$$\beta_T(i) = 1, \qquad 1 \le i \le N. \qquad (2\text{-}22)$$

At time t=T, $\beta_t(i)$ is arbitrary assigned to be 1.

2-Induction:

$$\beta_t(i) = \sum_{j=1}^{N} a_{ij}\beta_{t+1}(j)b_j(o_{t+1}), \qquad t = T-1, T-2, \ldots, 1 \quad \textit{and} \quad 1 \le j \le N \qquad (2\text{-}23)$$

At any time t other than the final time T, the probability of transition from state i to any other state j and observing o_{t+1} in state j is the sum of the products of the observation probability distribution of o_{t+1} within destination state $b_j(o_{t+1})$ and state transition probability over all possible destination states. In order to extend the time to the rest of observations after t+1 and since it must be considered for all states, term $\beta_{t+1}(i)$ must be added within the summation. The mathematical proof of the above equation is given in Appendix A.

2.11 Baum-Welch Algorithm

As mentioned before, the Baum-Welch method is an iterative method for choosing $\lambda = (A, B, \pi)$ such that $P(O \mid \lambda)$ is maximized. To do so first, a new term $\xi_t(i, j)$ must be defined, which is the probability of being in state S_i at time t, and state S_j at time t+1, given the model and the observation sequence:

$$\xi_t(i, j) = P(q_t = S_i, q_{t+1} = S_j \mid O, \lambda). \qquad (2\text{-}24)$$

In order to write $\xi_t(i, j)$ as a function of model parameters, it is better to divide the observation into three parts:

Observations between initial time and present time t,

Observation at time t+1,

Observations from time t+2 to the last one.

The joint probability of observing the first part of the observations and being in state i can be written as:

$$P(o_1 o_2 \ldots o_t, q_t = S_i \mid \lambda)$$

which is nothing else than the forward variable at time t and state S_i: $\alpha_t(i)$.

At time t+1, there is a state transition from S_i to S_j and observation o_{t+1} is observed, the probability of this event is $a_{ij} b_j(o_{t+1})$. Further, for the last part of the observations, precisely from t+2 to T, the probability of observing partial observation sequence $o_{t+2} o_{t+3} \ldots o_T$ given state S_j at time t+1 and model parameter is:

$$P(o_{t+2}o_{t+3}\ldots o_T \mid q_{t+1} = S_j, \lambda)$$

which is the backward variable at time t+1 and state S_j, i.e., $\beta_{t+1}(j)$.

The joint probability of these three events can be formulated as:

$$\alpha_t(i)a_{ij}b_j(o_{t+1})\beta_{t+1}(j) = P(q_t = S_i, q_{t+1} = S_j, O \mid \lambda) \tag{2-25}$$

This formulation is very similar to desired one; but the only difference is the term O in the left side of conditional probability line. According to probability theorems, this problem can be fixed by dividing the above term by $P(O \mid \lambda)$ which can be formulated as double summation of term $P(q_t = S_i, q_{t+1} = S_j, O \mid \lambda)$ over all states. Eventually the result is:

$$\xi_t(i,j) = \frac{\alpha_t(i)a_{ij}b_j(o_{t+1})\beta_{t+1}(j)}{\sum_{i=1}^{N}\sum_{j=1}^{N}\alpha_t(i)a_{ij}b_j(o_{t+1})\beta_{t+1}(j)} \tag{2-26}$$

Another useful term that can be defined is the probability of being in state S_i at time t, given the observation sequence O, and the model λ, which can be written as:

$$\gamma_t(i) = P(q_t = S_i \mid O, \lambda) \tag{2-27}$$

Comparing the above equation with equation (2-24) the difference is term $q_{t+1} = S_j$ at the left side of the conditional probability line. This term can be omitted, using probability rules, by summing the equation over all possible states for S_j:

$$P(q_t = S_i \mid O, \lambda) = \sum_{j=1}^{N} P(q_t = S_i, q_{t+1} = S_j \mid O, \lambda) \tag{2-28}$$

and consequently

$$\gamma_t(i) = \sum_{j=1}^{N} \xi_t(i,j) \tag{2-29}$$

furthermore

$$\gamma_t(i) = \sum_{j=1}^{N} \frac{\alpha_t(i) a_{ij} b_j(o_{t+1}) \beta_{t+1}(j)}{\sum_{i=1}^{N}\sum_{j=1}^{N} \alpha_t(i) a_{ij} b_j(o_{t+1}) \beta_{t+1}(j)} = \frac{\alpha_t(i) \sum_{j=1}^{N} a_{ij} b_j(o_{t+1}) \beta_{t+1}(j)}{\sum_{i=1}^{N} \alpha_t(i) \sum_{j=1}^{N} a_{ij} b_j(o_{t+1}) \beta_{t+1}(j)} = \frac{\alpha_t(i)\beta_t(i)}{\sum_{i=1}^{N} \alpha_t(i)\beta_t(i)}$$

(2-30)

In case of a continuous observation sequence, as an extension to $\gamma_t(i)$, $\gamma_t(i,k)$ can be defined as the probability of being in state S_i and observing the kth mixture at time t, given observation sequence $\bar{O}$ and model λ:

$$\gamma_t(i,m) = \gamma_t(i) \left[\frac{c_{jm} \eta(O_t, \mu_{jm}, U_{jm})}{\sum_{l=1}^{M} c_{jl} \eta(O_t, \mu_{jl}, U_{jl})} \right] \tag{2-31}$$

Since each of the above terms is the probability of the event at a specific time t, if they are summed over time the results would be the expected number of occurrences of that event and can be denoted as follow:

$$\sum_{t=1}^{T} \gamma_t(i) = \text{expected number of transitions from } S_i \tag{2-32}$$

$$\sum_{t=1}^{T} \gamma_t(i,m) = \text{expected number of transitions from } S_i \text{ and observing } m\text{th mixture.} \tag{2-33}$$

$$\sum_{t=1}^{T-1} \xi_t(i,j) = \text{expected number of transitions from } S_i \text{ to } S_j \tag{2-34}$$

Using the above formulas and with respect to the concept of counting event occurrences, the model parameters can be estimated. Given the current model $\lambda = (A, B, \pi)$, the reestimated model that is denoted as $\overline{\lambda} = (\overline{A}, \overline{B}, \overline{\pi})$ can be formulated as follows:

$$\overline{\pi}_i = \text{expected number of times in state } S_i \text{ at time } (t{=}1) = \gamma_1(i) \tag{2-35}$$

$$\overline{a}_{ij} = \frac{\text{expected number of transitions from state } S_i \text{ to state } S_j}{\text{expected number of transitions from state } S_i} = \frac{\sum_{t=1}^{T-1} \xi_t(i,j)}{\sum_{t=1}^{T-1} \gamma_t(i)} \tag{2-36}$$

$$\overline{b}_j(m) = \frac{\text{expected number of times in state } j \text{ and observing } m\text{th mixture}}{\text{expected number of times in state } j} \tag{2-37}$$

which for discrete observation:

$$\bar{b}_j(m) = \frac{\sum_{t=1}^{T} \gamma_t(j)}{\sum_{t=1}^{T} \gamma_t(j)} \quad \text{s.t} O_t \text{ is } m\text{th symbol} \tag{2-38}$$

and in case of continuous observation:

$$b_j(\vec{o}_t) = \sum_{m=1}^{M} c_{jm} \eta[\vec{o}_t, \mu_{jm}, U_{jm}] \tag{2-39}$$

where

$$\bar{c}_{jm} = \frac{\sum_{t=1}^{T} \gamma_t(j,m)}{\sum_{t=1}^{T} \sum_{m=1}^{M} \gamma_t(j,m)} \tag{2-40}$$

$$\bar{\mu}_{jm} = \frac{\sum_{t=1}^{T} \gamma_t(j,m).\vec{o}_t}{\sum_{t=1}^{T} \gamma_t(j,m)} \tag{2-41}$$

$$\bar{U}_{jm} = \frac{\sum_{t=1}^{T} \gamma_t(j,m).(\vec{o}_t - \vec{\mu}_{jm})(\vec{o}_t - \vec{\mu}_{jm})'}{\sum_{t=1}^{T} \gamma_t(j,m)} \tag{2-42}$$

Baum Welch and his colleagues have proved that for any iteration, the probability of the observation in the new iterated model is greater than that of the previous iteration. Using the above equation and given an observation sequence, model parameters can be determined. However, there are some practical considerations that will be studied in the next sections.

2.12 Multiple Observation Sequence

So far, it was considered that there is only one sequence of observation. Nevertheless, sometimes it is necessary to deal with more than one observation sequence. In this case, some changes must be made in the iteration methods. In the case of a single observation sequence, the model parameters were all interpreted in terms of the expected numbers of an event for a given observation sequence. In a similar manner, this concept can be extended to deal with the case of more than one observation by summing the expected numbers over all of the observation sequences. Since forward-backward variables and their derivatives are functions of time, all of them get an index of k. So the modified model parameters for K observation sequences will be as below:

$$\overline{\pi}_i = \frac{\sum_{k=1}^{K} \gamma_1^k(i)}{K} \tag{2-43}$$

$$\overline{a}_{ij} = \frac{\sum_{k=1}^{K}\sum_{t=1}^{T-1} \xi_t^k(i,j)}{\sum_{k=1}^{K}\sum_{t=1}^{T-1} \gamma_t^k(i)} \tag{2-44}$$

for discrete observation:

$$\bar{b}_j(m) = \frac{\sum_{k=1}^{K}\sum_{t=1}^{T}\gamma_t^k(j)}{\sum_{k=1}^{K}\sum_{t=1}^{T}\gamma_t^k(j)} \quad s.t\ O_t is\ mth\ symbol \tag{2-45}$$

and for continuous observation:

$$b_j(\vec{o}) = \sum_{m=1}^{M} c_{jm}\eta[\vec{o}, \mu_{jm}, U_{jm}] \tag{2-46}$$

where

$$\bar{c}_{jm} = \frac{\sum_{k=1}^{K}\sum_{t=1}^{T}\gamma_t^k(j,m)}{\sum_{k=1}^{K}\sum_{t=1}^{T}\sum_{m=1}^{M}\gamma_t^k(j,m)} \tag{2-47}$$

$$\bar{\mu}_{jm} = \frac{\sum_{k=1}^{K}\sum_{t=1}^{T}\gamma_t^k(j,m).\vec{o}_t^k}{\sum_{k=1}^{K}\sum_{t=1}^{T}\gamma_t^k(j,m)} \tag{2-48}$$

$$\bar{U}_{jm} = \frac{\sum_{k=1}^{K}\sum_{t=1}^{T}\gamma_t^k(j,m).(\vec{o}_t^k - \vec{\mu}_{jm})(\vec{o}_t^k - \vec{\mu}_{jm})'}{\sum_{k=1}^{K}\sum_{t=1}^{T}\gamma_t^k(j,m)} \tag{2-49}$$

2.13 Initial Estimation

Regarding reestimation procedure, it is clear that the first iteration of calculating model parameters requires an initial estimation. One way is to estimate either randomly or uniformly the initial parameters with respect to the constraints of each parameter. As

mentioned earlier, solutions to model parameters often result in local answers. So initial estimations plays an important role in obtaining better answers. There exist some methods that can be used for a possibly good estimation. One of these methods is k-means segmentation with clustering. This method is carried out in three steps that are clustering, best state sequence tracking and segmental k-mean clustering. All of these three steps will be presented for the general case of multiple continuous observation sequence.

2.13.1 Clustering

In this step for each set of observation sequence, the observations must first be clustered into $N \times M$ clusters where N is the number of states and M is the number of mixtures. In order to do so, N observations that have the most distant value among others are selected as centers for groups. For measuring the distance value, Euclidean distortion measure can be used. Then all the observation, due to their distance, to N centers observation, are grouped into N groups which are denoted as s_n. Thus, there will be N groups in which the observations are close together in terms of Euclidean measure. Then, each group is divided into M groups using the same criterion, resulting in $N \times M$ clusters. If a cluster is denoted as x_{nm}, in case of continuous observation sequence the initial values for mean, covariance and mixture gain are obtained as follow:

$$\bar{\mu}_{nm} = \text{sample mean vector of the observations clustered in } x_{nm} \qquad (2\text{-}50)$$

$$U_{nm} = \text{sample covariance matrix of the observations clustered in } x_{nm} \qquad (2\text{-}51)$$

$$c_{nm} = \frac{\text{number of observation vectors in } x_{nm}}{\text{number of observations in } s_n} \qquad (2\text{-}52)$$

Using the values above, the initial values of B are obtained according to equation 2-46. In case of a discrete observation sequence, the initial value of B is obtained using the same formula used for obtaining the mixture gain (Equation 2-52). The initial values of A and π in this step can be assigned arbitrarily. It must be noticed that these initial values are preliminary values, not major initial estimations that are used in training step. These preliminary values will be used as initial estimation for the next step, i.e., the best state sequence.

2.13.2 Best State Sequence

The best state sequence can have different definitions. The definition used in this work is as follows: for an observation sequence $O^k = \{o_1^k, o_2^k, \ldots, o_T^k\}$, the best state sequence is the one for which $P(Q, O^k \mid \lambda)$ is maximized. This definition takes into account both the effects of the transition probabilities and the observation probabilities within a state. There is a technique called Viterbi algorithm, which is used to find such best sequence. In order to use this technique, first the maximum probability of the observation sequence along a single path until time t, which ends in state S_i, is formulated as:

$$\delta_t^k(i) = \max_{q_1, q_2, \ldots, q_{t-1}} P(q_1 q_2 \ldots q_t = i, O^k \mid \lambda) \qquad (2\text{-}53)$$

Obviously there are different paths with different probabilities to get to state i at time t, the variable $\delta_t^k(i)$ is the path with the highest probability. Since it is needed to have a record of the state sequence at any time and for any state, an array $\psi_t^k(j)$ is used. The iterative procedures for obtaining $\delta_t^k(i)$ and $\psi_t^k(j)$ are presented as follow:

1- Initialization:

$$\delta_1^k(i) = \pi_i b_i(O_t^k), \qquad 1 \le i \le N \tag{2-54}$$

$$\psi_1^k(i) = 0. \tag{2-55}$$

2- Recursion:

$$\delta_t^k(j) = \max_{1 \le i \le N}[\delta_{t-1}^k(i)a_{ij}]b_j(O_t^k), \qquad 2 \le t \le T, \qquad 1 \le j \le N, \qquad 1 \le k \le K \tag{2-56}$$

$$\psi_t^k(j) = \arg\max_{1 \le i \le N}[\delta_{t-1}^k(i)a_{ij}], \quad 2 \le t \le T, \qquad 1 \le j \le N \tag{2-57}$$

where argmax stands for the argument of the maximum, that is to say, the value of the argument for which the value of the given expression attains its maximum value.

3- Termination:

$$P^{k^*} = \max_{1 \le i \le N}[\delta_T^k(i)] \tag{2-58}$$

$$q_T^{k^*} = \arg\max_{1 \le i \le N}[\delta_T^k(i)] \tag{2-59}$$

4- Path backtracking:

$$q_t^{k^*} = \psi_{t+1}^k(q_{t+1}^{k^*}) \qquad t = T-1, T-2, \ldots, 1 \qquad k = 1,2,\ldots,K \tag{2-60}$$

Eventually q^k is the best state sequence for the kth set of observations.

2.13.3 Segmental k-mean Clustering

This is the final step of calculating the initial estimation. Using segmental k-means clustering, the model parameters can be estimated as:

$$\overline{\pi}_n = \frac{\sum_{k=1}^{K} \Delta(q_1^{k^*} - s_n)}{K} \qquad n = 1,2,\ldots,N \tag{2-61}$$

$$\overline{a}_{ij} = \frac{\sum_{k=1}^{K}\sum_{t=2}^{T} \Delta((q_{t-1}^{k}{}^{*} - s_i) + (q_t^{k^*} - s_j))}{\sum_{k=1}^{K}\sum_{t=2}^{T} \Delta(q_{t-1}^{k}{}^{*} - s_i)} \qquad i = 1,2,\ldots,N \; j = 1,2,\ldots,N \tag{2-62}$$

$$\overline{\overline{\mu}}_{nm} = \frac{\sum_{k=1}^{K}\sum_{t=1}^{T} \Delta((q_t^{k^*} - s_n) + (r_t^k - x_{nm})) \times \overline{o}_t^k}{\sum_{k=1}^{K}\sum_{t=1}^{T} \Delta(q_t^{k^*} - s_n)} \tag{2-63}$$

$$\overline{U}_{nm} = \frac{\sum_{k=1}^{K}\sum_{t=1}^{T} \Delta((q_t^{k^*} - s_n) + (r_t^k - x_{nm})) \times (\overline{o}_t^k - \overline{\overline{\mu}}_{nm}) \times (\overline{o}_t^k - \overline{\overline{\mu}}_{nm})'}{\sum_{k=1}^{K}\sum_{t=1}^{T} \Delta(q_t^{k^*} - s_n)} \tag{2-64}$$

$$\overline{c}_{nm} = \frac{\sum_{k=1}^{K}\sum_{t=1}^{T} \Delta((q_t^{k^*} - s_n) + (r_t^k - x_{nm}))}{\sum_{k=1}^{K}\sum_{t=1}^{T} \Delta(q_t^{k^*} - s_n)} \tag{2-65}$$

$$\Delta(y) = \begin{cases} 1 & for\ y = 0, \\ 0 & otherwise \end{cases} \tag{2-66}$$

Where $q_t^{k^*}$ is the best state at time t, s_n represents nth state, x_{nm} represents the mth mixture in nth state, and r_t refers to the cluster in which observation at time t belongs. To illustrate the above procedure, it can be assumed that the observation at t=5 is clustered into a cluster for which n=2 and m=3, in this situation the result of $r_t - x_{nm}$ is zero only when t=5, n=2 and m=3 in above formula. For the case $q_t^* - s_n$, this term is zero, only when the state number presented by q at time t is the same as index n. Using this method, any parameter will be adjusted in a manner that matches with the best state sequence tracking and clustering division.

This step and the previous one will be repeatedly iterated until the distance measurement between two subsequent models becomes less than a predetermined error. A least squared error method can be used for measuring such distance. Then the last model obtained from iteration will be the initial estimation for training.

2.14 Scaled Forward-Backward Variables

Calculating forward-backward variables requires multiplication of a large number of probabilities, which are always a number between 0 and 1. As the number of the observations increases, these two terms get too small and dealing with such numbers is out of precision of the computers. One way for solving this problem is to use scaled variables. Scaled variables can be obtained by multiplying variables by a scaled coefficient, which will be cancelled out automatically. For both forward and backward variable, a scaling coefficient c_t, which is independent of i and depends only on t is used and defined as:

$$c_t = \frac{1}{\sum_{i=1}^{N} \alpha_t(i)} \qquad (2\text{-}67)$$

To have a better understanding, computation of $\alpha_t(i)$ can be considered. At each time $\alpha_t(i)$ is computed using the induction formula, it is also multiplied by the scaling coefficient. So the equation for $\alpha_t(i)$ is:

$$\alpha_t(i) = \left[\sum_{j=1}^{N} \hat{\alpha}_{t-1}(j) a_{ji}\right] b_i(O_t), \tag{2-68}$$

then the scaled term $\hat{\alpha}_t(i)$ is obtained by multiplying $\alpha_t(i)$ by c_t:

$$\hat{\alpha}_t(i) = \frac{\sum_{j=1}^{N} \hat{\alpha}_{t-1}(j) a_{ji} b_i(O_t)}{\sum_{i=1}^{N}\sum_{j=1}^{N} \hat{\alpha}_{t-1}(j) a_{ji} b_i(O_t)} \tag{2-69}$$

due to induction $\hat{\alpha}_t(i)$ can be written as

$$\hat{\alpha}_{t-1}(j) = \left(\prod_{\tau=1}^{t-1} c_\tau\right) \alpha_{t-1}(j) \tag{2-70}$$

so the scaled forward variable is

$$\hat{\alpha}_t(i) = \frac{\sum_{j=1}^{N} \left(\prod_{\tau=1}^{t-1} c_\tau\right) \alpha_{t-1}(j) a_{ji} b_i(O_t)}{\sum_{i=1}^{N}\sum_{j=1}^{N} \left(\prod_{\tau=1}^{t-1} c_\tau\right) \alpha_{t-1}(j) a_{ji} b_i(O_t)} = \frac{\alpha_t(i)}{\sum_{i=1}^{N} \alpha_t(i)} \tag{2-71}$$

The above equation shows that the defined c_t properly works in induction. Using the same approach it can be shown that the defined c_t is the right one for backward

variables as well. Regarding reestimation equations for a, π and b, it is obvious that this term will not affect the final result of those terms and is easily cancelled out. This is because of the fact that in reestimation equations for model parameters, the forward backward variables appear in both the denominator and the numerator. Nevertheless, this is not true for calculating $P(O \mid \lambda)$ which formerly was shown to be:

$$P(O \mid \lambda) = \sum_{i=1}^{N} \alpha_T(i). \tag{2-72}$$

Fortunately, this problem can be solved easily. At time T the scaling variable is:

$$c_T = \frac{1}{\sum_{i=1}^{N} \alpha_T(i)} \tag{2-73}$$

or

$$c_T = \frac{1}{P(O \mid \lambda)} \tag{2-74}$$

due to induction c_T can be written as:

$$c_T = \prod_{t=1}^{T} c_t \tag{2-75}$$

and eventually $P(O \mid \lambda)$ can be written as:

$$P(O \mid \lambda) = \frac{1}{\prod_{t=1}^{T} c_t} \tag{2-76}$$

which can be rewritten in logarithm scale as:

$$\log P(O \mid \lambda) = -\sum_{t=1}^{T} \log c_t \tag{2-77}$$

2.15 Conclusion

In this chapter, theory, concepts and practical issues of hidden Markov model were discussed in detail. It was shown that there is a strong mathematical structure behind this model, although in some parts the analytical methods were replaced by numerical ones. Depending on the area of application of the HMM, there would be some more practical problems that must be considered. The concepts discussed in this chapter were the most general and common ones, which would occur in most of the applications. Even though there are some limitations in using HMM, this model is very strong and effective model in practice.

Chapter 3 Experimental and Data Acquisition Procedure

In order to study some aspects of two-phase flow and obtain the data, different conditions of two-phase flow were simulated in a test section. In this chapter, the test section and experimental procedure for obtaining data from two-phase flow is presented.

3.1 Test Section

3.1.1 Tube and Mixer

For the case of vertical upward flow, liquid-gas two-phase flow was simulated with air-water two-phase flow. In the test section as shown in Figure 3.1, air and water were fed into a mixer and the two-phase mixture entered from the bottom end of a transparent tube. The transparent tube was made of polycarbonate and had 2 meters of length, 0.019

meters of inside diameter and 0.003 meters of tube's wall thickness. The pipe was mounted vertically using two clamps at the two ends of the tube. The mixer consisted of two pipe connectors that were installed in a way that let air enter with an angle of 45 degrees, and water with an angle of 90 degrees. Inside the mixer, a screen net helped water and air to be mixed in a well-distributed form. The mixer was equipped with a manometer for measuring the pressure of the mixture at the entrance of the transparent tube.

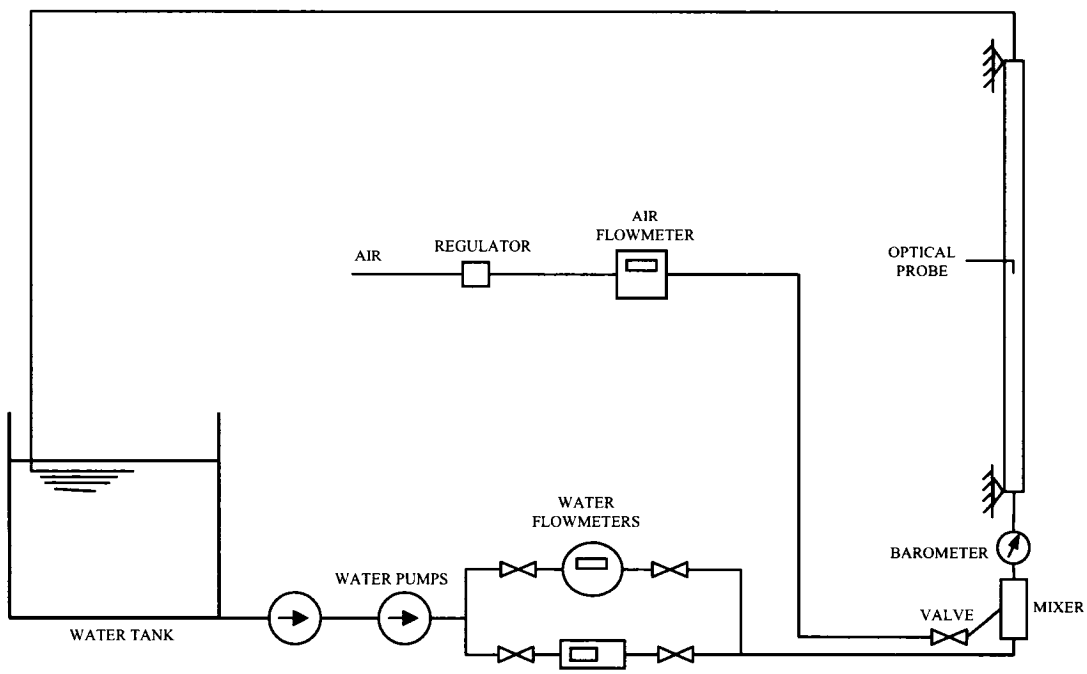

Figure 3-1 Experimental setup.

3.1.2 Air Supply

The air was supplied to mixer from the main air support line in the laboratory. The rate of airflow was controlled with a regulator and a valve and it was measured by an electronic mass flowmeter. The flowmeter had an accuracy of 1% of full scale (FS). The specifications of this flowmeter are presented in Table 3.1.

3.1.3 Water Supply

The water was supplied from a constant head tank to the mixer using two pumps that were arranged in series. One of the pumps was used for low flow rates and the other one for higher flow rates. Two different flow meters were used for measuring high and low water flow rates. For lower flow rates, a magnetic flowmeter with the accuracy of 0.5% of actual flow and for higher flow rates, a turbine flowmeter with the accuracy of 1% of FS were used. The specifications of these two flowmeters are given in Table 3.1. Disregarding vaporizing from tank and possible leakages, the water cycle was a closed loop. The flow rate was controlled using a valve.

Table 3-1 Measuring instruments.

No.	Type	Fluid	Label	Model	Operation Range	Accuracy and Resolution
1	Turbine Flowmeter	Water	Blue-White	FHXX10M2	7.6-75.7 LPM	1% of FS
2	Magnetic Flowmeter	Water	Rosemount	9711TSA30FU5N0	0.65-25.00 LPM	0.5% of actual flow
3	Mass Flowmeter	Air	Omega	FMA-A2322	0.85-75.00 SLPM	1% of FS

3.2 Adjustment Procedure

In this experiment, two-phase flow conditions for seven different velocities of the mixture, from 0.5 m/s to 5 m/s, and nine different void fractions, from 10% to 90%, were simulated in the test section. In this thesis, these two-phase conditions are referred to by condition numbers given in Table 3.2. The conditions indicated by hyphen (-) are those for which the test was not performed, because they exceeded the operating range of the flowmeters.

Table 3-2 Test numbers, and two-phase flow conditions simulated in test section.

		Void Fraction (%)								
		10	**20**	**30**	**40**	**50**	**60**	**70**	**80**	**90**
Mixture Velocity (m/s)	**0.5**	1	2	3	4	5	6	7	8	9
	1	10	11	12	13	14	15	16	17	18
	1.5	19	20	21	22	23	24	25	26	27
	2	28	29	30	31	32	33	34	35	36
	3	37	38	39	40	41	42	43	44	45
	4	46	47	48	49	50	51	52	53	54
	5	-	55	56	57	58	59	60	-	-

Since in this case, the liquid and gas flow rates were the only parameters that could be controlled and adjusted, first the relations between flow rates and two-phase flow velocity and void fraction are discussed.

3.2.1 Notations and Definitions

Some preliminary definitions in the study of two-phase flow are presented as follow:

Void Fraction α **:** In a stationary mixture, the void fraction is the ratio of the volume occupied by gas to the total volume:

$$\alpha = \frac{V_g}{V_g + V_l} \tag{3-1}$$

where V_l and V_g are respectively the liquid and gas volume.

Volumetric Quality β **:** The volumetric quality is the ratio of the gas volume flow rate to the sum of gas and liquid flow rates:

$$\beta = \frac{Q_g}{Q_g + Q_l} \tag{3-2}$$

where, Q_g is the gas flow rate and Q_l is the liquid flow rate.

Phase Velocities: The area-averaged velocities for the liquid(U_l) and gas(U_g) phases are written as:

$$U_l = \frac{Q_l}{A(1-\alpha)} \tag{3-3}$$

$$U_g = \frac{Q_g}{A\alpha} \tag{3-4}$$

where A is the sectional area of the channel.

Superficial Velocities: The superficial velocity is defined as the ratio of the fluid volume flow rate to the channel area, and for the liquid(U_{ls}) and gas(U_{gs}) phases are formulated as:

$$U_{ls} = \frac{Q_l}{A} \tag{3-5}$$

$$U_{gs} = \frac{Q_g}{A} \tag{3-6}$$

Slip Ratio S: The slip ratio is defined as the ratio of the average gas velocity to the average liquid velocity:

$$S = \frac{U_g}{U_l} \tag{3-7}$$

where U_g is the average gas velocity and U_l is the average liquid velocity.

The relation between void fraction and volumetric ratio in terms of slip ratio is written as:

$$\frac{1-\beta}{\beta} = \left(\frac{1-\alpha}{\alpha}\right)\frac{1}{S} \tag{3-8}$$

3.2.2 Homogeneous Model

There are some mathematical models for modeling two-phase flow, none of which describes the two-phase flow perfectly. One of these models is the homogeneous model that is, to some extent, the simplest one. In this model, the phases are considered to be homogeneously mixed and traveling at the same velocity through the channel. Hence, the slip ratio S is equal to 1 and the velocities of the gas phase and the liquid phase are replaced with the homogeneous velocity:

$$U_l = U_g = U_{\text{hom}} \tag{3-9}$$

Moreover, with respect to the relationship between void fraction α and volumetric ratio β, it is clear that these two parameters are equal. Further, the total flow rate and the flow rates of gas and liquid phases can be written as follow:

$$Q_{total} = U_{\text{hom}} A \tag{3-10}$$

$$Q_g = \beta Q_{total} = \beta U_{\text{hom}} A \tag{3-11}$$

$$Q_l = (1-\beta) Q_{total} = (1-\beta) U_{\text{hom}} A \tag{3-12}$$

Thus, given the void fraction (volumetric quality) and the homogeneous velocity, the gas and liquid flow rates can be obtained and adjusted in the test section using the above equations.

3.2.3 Gas Flow Rate Correction

Because gases are compressible fluids, their volume and consequently their flow rate changes with pressure. In the experiment of two-phase flow, the pressure of the gas changes as the gas enters the mixer because of the existence of the liquid and its pressure. Therefore, the gas flow rate measured at the flowmeter is not the flow rate inside the tube and this will bring about some inaccuracies. In order to solve this problem, the following equation is derived from the ideal gas law, and is applied to air as an ideal gas at constant temperature:

$$Q_{g(corrected)} = Q_{g(measured)} \frac{P_{std} + P_{(mixer)}}{P_{std}}, \qquad (3\text{-}13)$$

where $Q_{g(corrected)}$ is the corrected gas flow rate, $Q_{g(measured)}$ is the gas flow rate measured by the flowmeter, P_{std} is standard pressure (i.e., 101 kPa) and P_{mixer} is the pressure measured at the entrance of the tube.

The correction procedure is as follows: first, the air flow rate is adjusted to $Q_{g(theory)} = \beta U_{\text{hom}} A$, where β and U_{hom} are selected arbitrarily for different flow parameters. Then the pressure at the tube entrance $Q_{g(measured)}$ is measured. Then the air flow rate is adjusted to $Q_{g(corrected)}$ which is calculated using equation 3-13. After that, the pressure at the tube entrance is again measured and the air flow rate is adjusted to the new $Q_{g(corrected)}$ obtained from equation 3-13, but using the new pressure P_{mixer}. This cycle continues until P_{mixer} converges to an approximately constant pressure.

3.3 Measurement System

In this experiment, void fraction data were gathered using an optical fiber probe system linked to a numeric data acquisition system. Besides, for each test, two-phase flow patterns were captured using a digital camera for being used as a comparative tool. The procedure and instrument were used in this experiment are presented in this section.

3.3.1 Optical Probe System

The basic principle of using optical fiber in two-phase flow is that the reflection states of the system changes as liquid-gas interfaces pass by the tip of the probe. This principle is based on the Snell-Descartes reflection law.

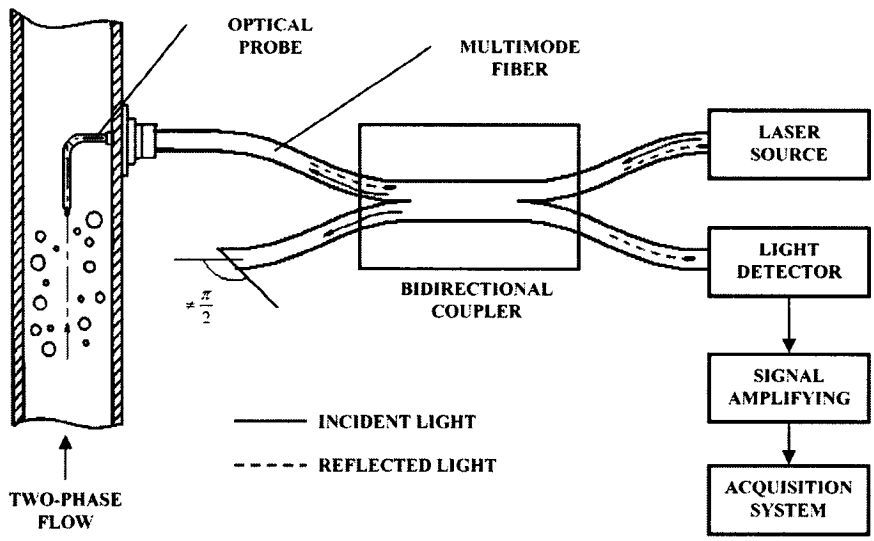

Figure 3-2 Optical probe system.

A block diagram of the optical probe system is shown in Figure 3.2. An electroluminescence diode is used as a laser producer. The exit fiber from the diode joins to one of the branches of a biconical fused bidirectional coupler. In this way, a fraction of the input light is sent to the probe tip. The angle of the cut branch is unequal to 90

degrees, so the light reflected at this branch is negligible.

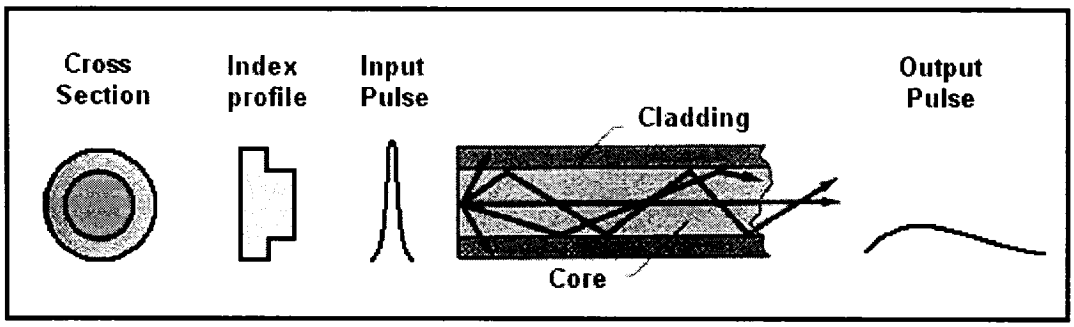

Figure 3-3 Step index multimode fiber.

The probe consists of a single step index multimode fiber (Fig. 3.3) placed in a stainless steel tube. The stainless steel tube holds the fiber firmly for piercing the bubbles without moving around. The optical fiber probe is installed in the middle of the tube length at a distance of 1 meter from the mixer where the flow is assumed to be completely developed. The probe's tip is positioned at the center of tube cross section, along the flow direction. The fiber probe reflects the light with different reflection coefficients due to the phase of the flow. Then a fraction of the reflected light is coupled back to a detector diode placed in the other branch of the coupler. The detector diode produces electrical signals. The electrical signals are amplified using an amplifier card and transmitted to both an oscilloscope and the acquisition system. The signals produced by this system come in two distinguishable, but irresolute values. That is to say, the local phase of the flow can be determined from instantaneous value of the signals. However, a constant value cannot be assigned to each phase because of the existence of noise. This will be discussed further in chapter 4. Another point that must be noted here is that the mean value of the signal is not steady during the time of experiment and it is subject to unexpected changes. These changes happen especially when the optical fibers, anywhere in the system, are shaken. Therefore, in order to have possibly smooth and steady signals in which the major fluctuations are due to phase change, signals are monitored during acquisition time using an oscilloscope. Moreover, to facilitate the subsequent signal

processing steps, it was tried to maintain the mean of the signal on the zero line by changing the gain of the output signal from optical system set. In this way, the positive values show the gas phase and negative values indicate liquid phase.

3.3.2 Data Acquisition System

The amplified signals produced by optical probe system were transmitted to a personal computer through a National Instruments terminal. LabVIEW software was used to process the signals and to store them into text files, which can be used by most of the programming software. For each condition simulated in the test section, one minute of the signals at a sampling frequency of 99 kHz was stored for future data processing.

Using an E4500 Nikon digital camera, ten photos were taken of each test for determining flow regimes and verifying the results. All the photos were taken at the speed of 1/2000s and from a distance of about 35 cm from tube. For better resolutions, camera's flash together with an external light was used.

3.3.3 Void Fraction Verification

As mentioned, given the void fraction (volumetric quality) and the homogeneous velocity, the gas and liquid flow rates are adjusted using theoretical equations. In order to verify the accuracy of such adjustment, nine different conditions of two-phase flow were simulated and for each condition, void fraction was measured and compared to the theoretical values. For measuring void fraction, first the local void fraction was measured at four points on the tube radial line using the optical fiber probe. Then the values obtained for local void fractions at four points were averaged. In each test, 20 seconds of data were gathered at a frequency of 99 kHz. The test results are given in Table 3.3.

Table 3-3 Results of void fraction verification test.

Point	Distance from the tube center(mm)	Void fraction (%)								
		U_{hom}=0.5 m/s			U_{hom}=2 m/s			U_{hom}=5 m/s		
Theoretical Volumetric quality		10	50	90	10	50	90	20	40	70
1	0	19	51	64	9	60	87	25	71	89
2	3	18	52	62	9	61	88	24	68	87
3	6	13	51	73	8	60	87	20	51	75
4	8	2	30	67	15	31	59	17	23	37
Average (measured)		12	46	67	10	52	79	21	51	70
Error		2	4	23	0	2	11	1	11	0

Except for one case in which the error between the theoretical and measured values is 23, all other cases show an error of less than 11% void fraction. The overall results are within the expected experimental precision, and therefore, they are acceptable.

Chapter 4 Modeling Two-Phase Flow Regimes using Continuous Hidden Markov Models

So far, in the previous chapters, different methods for identifying two-phase flow were introduced. Besides, the theory and some practical issues of the hidden Markov model were explained. It was stated that HMM has been used in many applications and it has been shown to be a very strong pattern identifier. In this chapter, a new approach for identifying two-phase flow regimes based on continuous hidden Markov model (CHMM) is presented.

As mentioned in chapter two, implementing HMM in most of the applications is carried out through two main steps. The first step is to train HMM based on observation

data and the other one is to calculate the probability of observing data given one or more pre-trained HMMs. Furthermore, prior to modeling the data with HMM, it is necessary in most applications to preprocess data or signals. Therefore, it is more appropriate to explain preprocessing before the other steps.

4.1 Data Preprocessing

The preprocessing of the data gathered by an optical fiber probe was performed in four stages: de-noising signals, down sampling, feature extraction and feature vector derivation. These steps are presented in this section.

4.1.1 De-noising Signals

Theoretically, the signals provided by the optical fiber probe in the study of two-phase flow are binary. One quantity represents the liquid phase and the other one represents the gas phase. Nevertheless, as for any other signal gathered from a real source, there are noise along with the pure signal. The noise are mostly produced in multimode optical fibers because of their sensitivity to thermal fluctuation and mechanical vibration. Hence, the first step of preprocessing data is to reduce or possibly remove the noises from the data. In most applications, noise reduction is very intricate. Fortunately, this is not the case for this experiment.

As mentioned in previous the chapter, the stored probe signals have roughly two arbitrary values with opposite mathematical signs. The quantities with a positive sign denote the gas phase and quantities with a negative sign denote the liquid phase. Hence, zero line is used as a threshold for specifying the phase. Then, using a simple computer program and applying the mentioned criterion, noisy data is converted to data that consists of only two values, -1 and +1; that represent the gas and liquid phases, respectively. Figure 4.1 shows a real signal and the resulting de-noised signal.

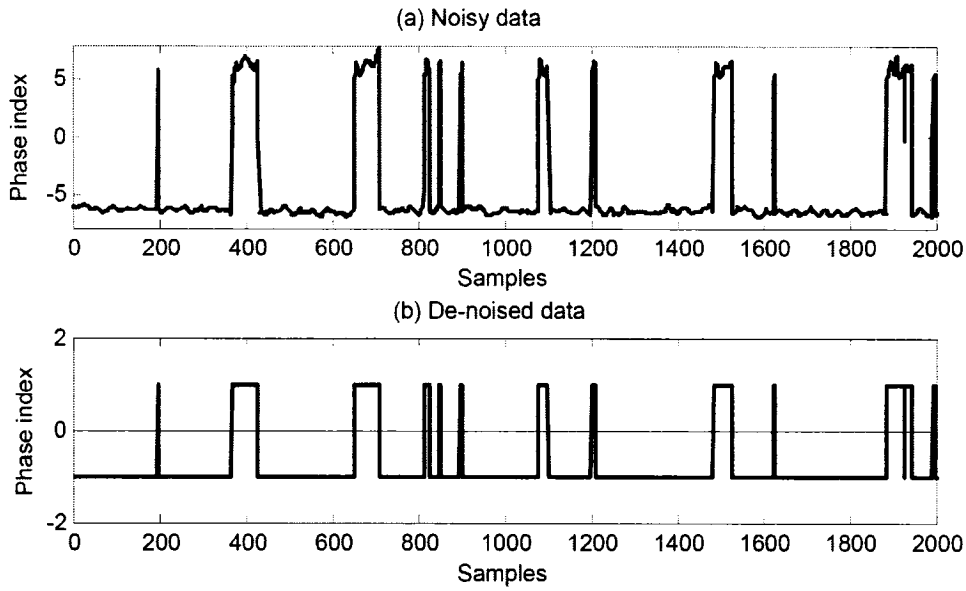

Figure 4-1 An example of de-noising data: (a) measured signal and (b) de-noised signal.

4.1.2 Down Sampling

In this experiment, two-phase conditions with a variety of homogeneous velocities were simulated and all of the data were recorded at the same frequency. The problem with this approach is that the conditions with different velocities but similar pattern will not be recognized as being similar. For example if a slug with the length of 4 cm passes across the probe at the velocity of 5 m/s, the signal recorded will be the same as that of a slug with the length of 0.4 cm passing at the velocity of 0.5 m/s. With this example, it is quite clear that the data must be down sampled due to the homogenous velocity at which they were recorded. The down-sampling ratios for all the velocities are given in Table 4.1. The 'desired frequencies' were obtained based on the idea that in each condition for a given length of flow, the same number of samples must be recorded. In other words, the length of the passing flow between two successive samples must be the same for all conditions. Through dividing the recording frequency (i.e. 99 kHz) by desired frequencies the down sampling rates are obtained. Moreover, since the down sampling

ratio must be a positive integer, the theoretical down sampling rates are rounded to real down sampling rates.

Table 4-1 Down sampling ratios for different mixture velocities.

Velocity (m/s)	Desired frequency (Hz)	Down-sampling rate (theory)	Down-sampling rate (real)	Obtained frequency (Hz)	Length of flow between two samples (mm)
0.5	2000	49.5	50	1980	0.2525
1	4000	24.75	25	3960	0.2525
1.5	6000	16.5	17	5823.53	0.2575
2	8000	12.375	12	8250	0.2424
3	12000	8.25	8	12375	0.2424
4	16000	6.18	6	16500	0.2424
5	20000	4.95	5	19800	0.2525

4.1.3 Feature Extraction

Using raw signals as observations in the procedure of implementing HMM is not efficient. Hence, in order to have the best judgment, the signal features, which represent specific characteristics of the signals, must be extracted. As an example, Lee *et al.* (2004) simulated different faults of the rotor in a test section and then measured the vibration amplitude at some specific points. Then they showed that for different faults there are different frequency spectra. Moreover, they argued that for different faults, the system would be excited at only some specific frequency and it is redundant to study the entire frequency range. Thus, they used filter bank method to draw auto power spectra at just some specific frequencies. Precisely, they extracted the features that efficiently carried information about the source regarding their field of research.

In this experiment, after de-noising and down sampling, the data turn out to be a collection of -1 and 1. Then, the next step of preprocessing is to extract features from the mentioned collection, which are somewhat complicated to deal with. Several approaches were tried and examined. In this section, some of the dominant approaches are discussed.

Deriving the auto-power spectrum from the data was one of the examined approaches. However, as shown in Figure 4.2, it is in some way clear that using frequency related methods is not an appropriate choice. For example if two tests are carried out at the same velocity but with different void fractions and the flow regime in both tests is slugs and supposedly there is no change in the regimes, then longer bullet shaped (Taylor bubbles) bubbles show up in the test with the greater void fraction. Therefore, during the same period the number of longer bubbles passing across the probe in less than the number of shorter bubbles. Moreover, however similar the flow regime is in both of the tests, the frequency of passing bubbles is different. Therefore, this approach is not a promising choice.

The results of examining this approach and other approaches of feature extraction are presented in the next chapter.

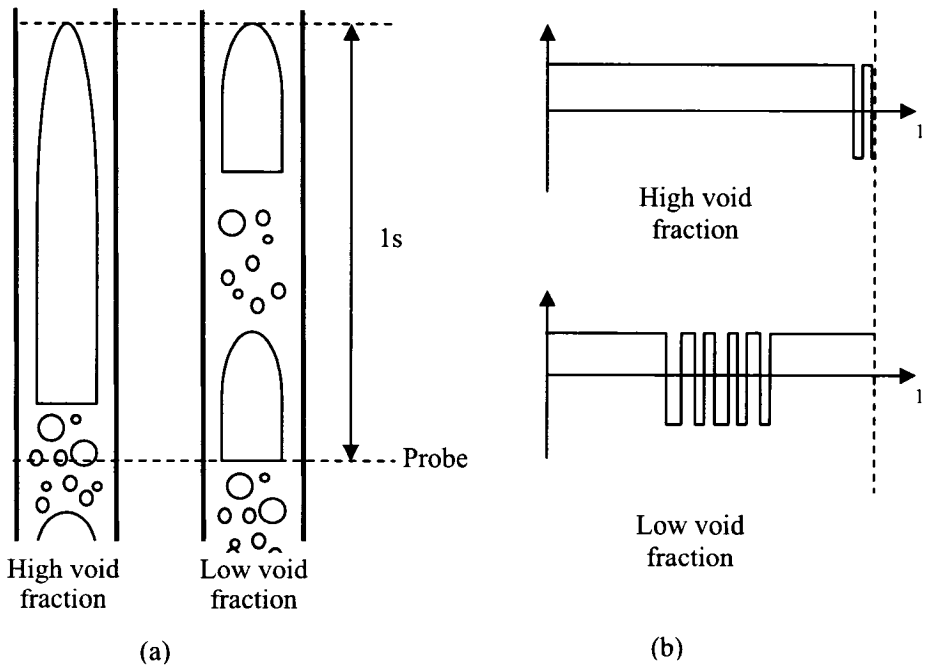

Figure 4-2 Comparison of two tests with same velocity and different void fraction: (a) schematic of the two-phase flows, (b) resulting de-noised, down-sampled data.

Another approach is to use autoregressive reflection coefficients. Autoregressive models are created with the idea that the present value of a time series x_t, can be explained as a function of p past values, $x_{t-1}, x_{t-2}, ..., x_{t-p}$ where p determines the order of the autoregressive model. An autoregressive model of order p can be written as:

$$x_t = \phi_1 x_{t-1} + \phi_2 x_{t-2} + ... + \phi_p x_{t-p} + w_t$$

where $\phi_1, \phi_2, ..., \phi_p$ are constants called autoregressive coefficients and w_t is white noise. As long as the present and past values of a signal are determined, for a given white noise w_t the reflection coefficients can be obtained and used as features. There are several methods for calculating autoregressive coefficients. In this project, the Burg method was used to fit an AR model to the data, by minimizing the least square errors while constraining the AR parameters to satisfy the Levinson-Durbin recursion.

The last approach that is presented in this section is a new inventive approach based on the passage length of the liquid and gas phases. As long as a mass of liquid flow passes across the probe, the signal value is +1. When the phase switches from liquid to gas, there will be a change in the signal value from +1 to -1. The approach can be explained as follows: The length of a distinct mass of liquid phase passes across the probe is recorded as a positive number with the index of its switch turn. In a similar manner, the length of a distinct mass of gas passes across the probe is recorded as a negative number. Then these numbers can be depicted respectively, versus their switch turn. An easy way for recording such lengths is to count the number of samples. Hence, the number of samples that have a value of +1 is counted until it switches to -1. Then the same approach is applied for -1 (Figure 4.3). Thus, the extracted features are given as phase lengths versus switch turns. In the case that the features are too dispersed, the logarithm of the absolute values can be used instead.

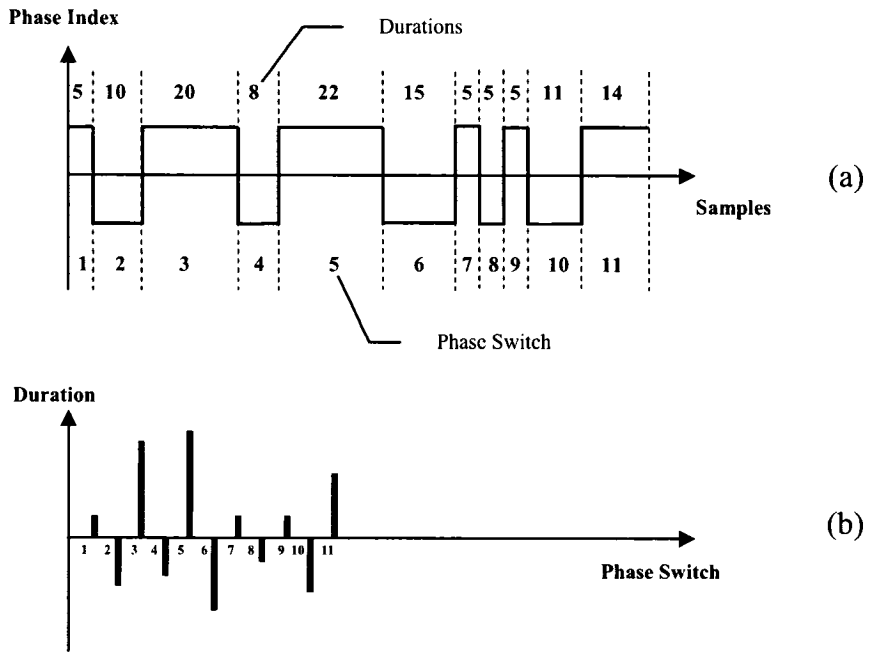

Figure 4-3 Feature extraction based on the passage length of each phase: (a) de-noised, down-sampled data, and (b) resulting feature.

4.1.4 Feature Vector Derivation

In this step, data were divided into segments and vectors, which constitute observation vectors for the hidden Markov modeling. Depending on the feature extraction approach, this step can be done after or prior to feature extraction. First, a finite length of data was selected. This selection should be made in such way that the selected data be long enough to cover various behaviors of the signal source. Then, the selected data were divided into a number of segments, which were separated with a segment offset. In a similar way, each segment was divided into vectors with 50% overlap as shown in Figure 4.4. In the implementation of the CHMM, the segments have the role of observation sequences and vectors have the role of observations. In the case

that the divisions to segments and vectors are made on raw data, the feature extraction is performed on vectors.

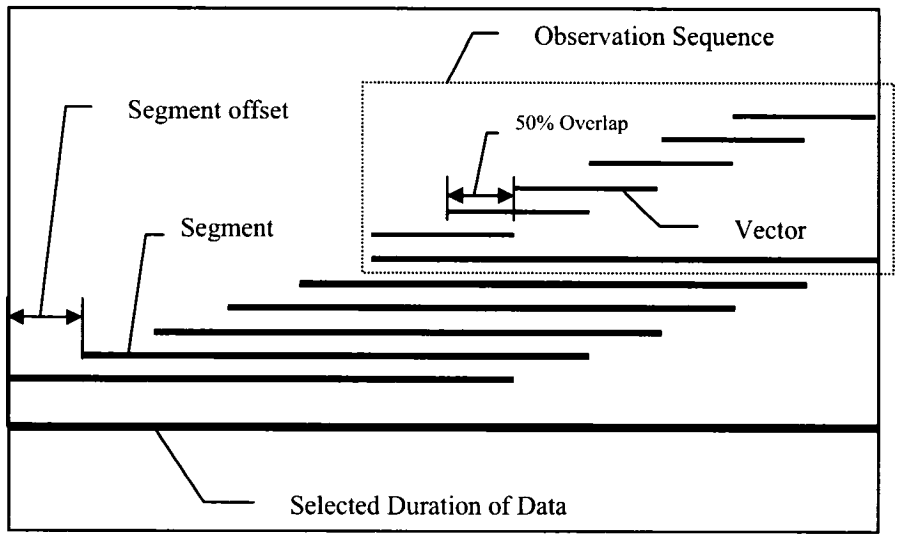

Figure 4-4 Feature vector derivation.

4.2 Procedure of Implementing the CHMM

Once the signals are filtered and the feature vectors are extracted, hidden Markov Modeling can be implemented. The idea behind using CHMM in two-phase flow identification is to use the data corresponding to two-phase flow conditions with a clearly known flow regime (i.e., conditions far away from transition regions) for training, and to detect the conditions with unclear flow regime (i.e., conditions close to transition regions). The general procedure of doing so is shown in Figure 4.5. In order to train the CHMM, some features corresponding to conditions with known regimes are selected among all the features. Photos of different conditions were employed to select such conditions. Further, in order to reduce subjectiveness, an existing two-phase flow pattern map, precisely the one planned for a vertically upward flow based on the Taitel *et al.* (1980) criteria is used. In addition, to make sure that the criteria of other authors

are satisfied, effort was made to select conditions that have a reasonable distance from boundaries provided by Taitel *et al.* (1980). Then, the features extracted from the data of the selected conditions are modeled with CHMM through training step. Finally, the log-likelihood (i.e. the logarithm scaled probability) of all other conditions is calculated using pre-trained CHMMs.

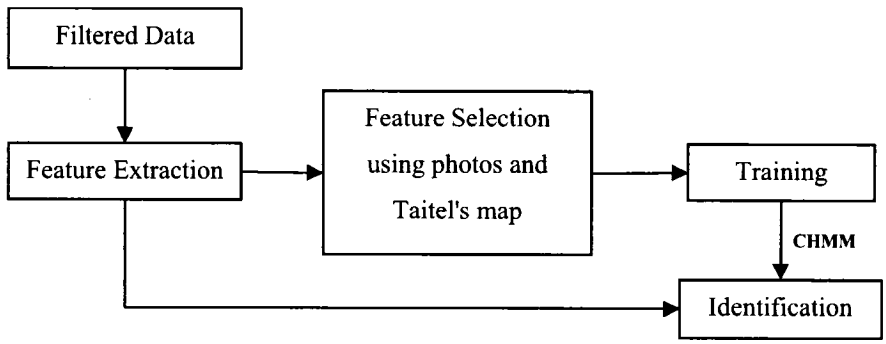

Figure 4-5 Procedure of implementing CHMM in identifying two-phase flow regimes.

4.2.1 Training

The Training procedure is shown in Figure 4.6. First, the number of states and mixtures are selected. Then with respect to the number of states and mixtures, the feature vectors are grouped into clusters. The number of states, mixtures and clusters used are given in chapter 5. After that, the initial state distribution π and the states transition probability distribution $A = \{a_{ij}\}$ are equivalently assigned. The next step is initial estimation using segmental k-means loop. During this step, in any iteration, the best state sequence is tracked using Viterbi algorithm and then the CHMM parameters $\lambda = (A, \pi, \mu, U, C)$ are calculated with respect to best state sequence using k-means clustering algorithm. This loop is iterated until the convergence criterion is met. In this project, the mean square error of all model parameters $\lambda = (A, \pi, \mu, U, C)$ were summed, and the difference between two consequent iterations was used as a convergence

criterion. After that, the obtained initial estimates are used for re-estimating model parameter by means of Baum-Welch algorithm. This step is the main step of the training. The re-estimation continues until the difference between the log-likelihood of two iterations became less than an error (in this project an error equal to 1 was chosen). Finally, the re-estimated parameters are stored for being used in the identification step.

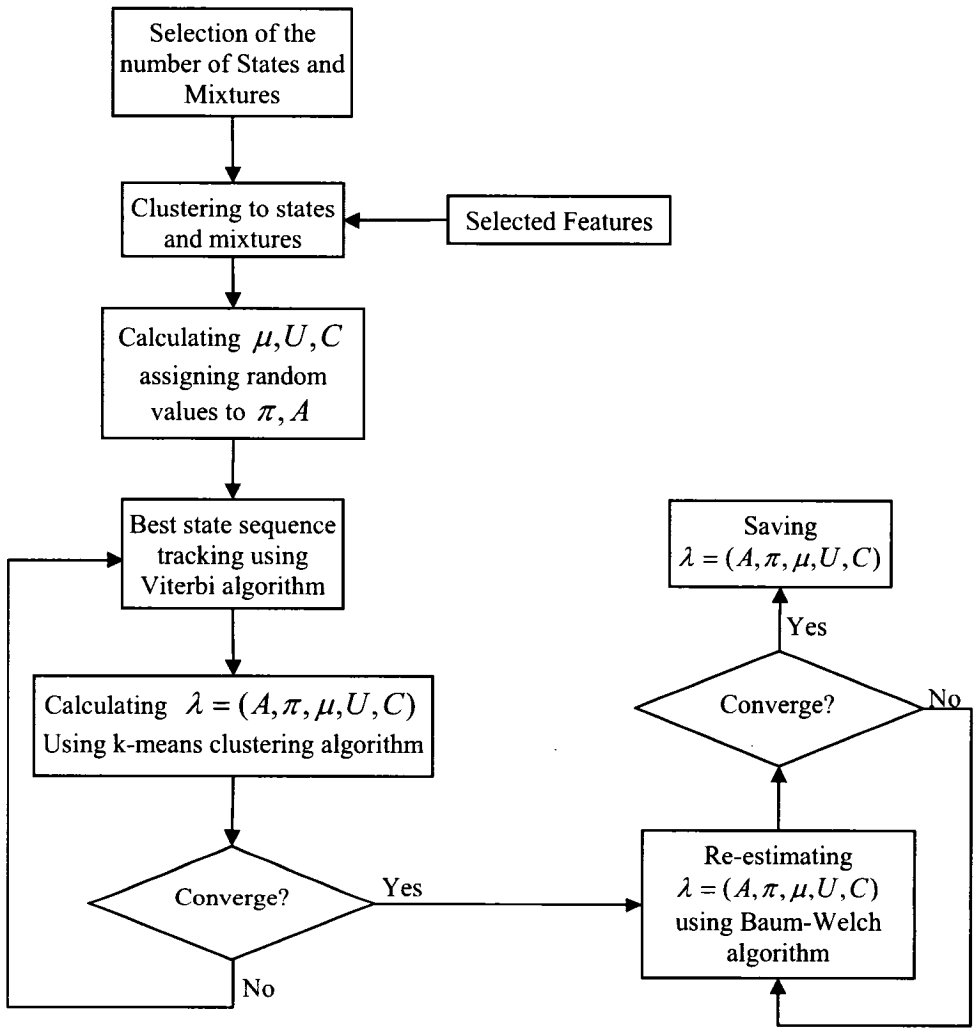

Figure 4-6 Training procedure.

4.2.2 Identification

In this step, the probability of observing feature vectors from each condition of the two-phase flow is calculated in terms of log-likelihood and based upon pre-trained CHMMs. As shown in Figure 4.7 the log-likelihood of each condition is obtained with respect to all CHMMs and this is used as a measure of making decision about the regime of that condition. The results of such evaluation will be presented in the next Chapter.

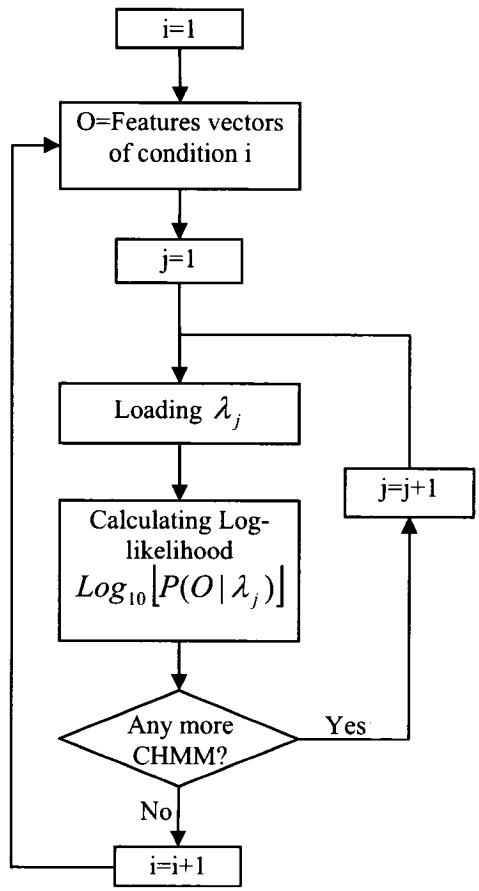

Figure 4-7 Identification procedure.

Chapter 5 Results and Analysis

In this chapter, the results of employing different methods of feature extraction in regime identification based on CHHM are presented and compared. As discussed in previous chapters, in order to implement hidden Markov modeling in two-phase flow pattern identification, some of two-phase flow conditions with clearly known regime must be selected for training. Therefore, before comparing between different methods, the selection procedure is explained.

5.1 Condition Selection

Sixty conditions of two-phase flow were produced in the test section, including seven different homogenous velocities, from 0.5 m/s to 5 m/s, and nine different void fractions, from 10% to 90% (Table 3.2). These conditions were depicted on a flow pattern map (Figure 5.1). This map was suggested by Taitel *et al.* (1980) for tubes with small diameter (i.e. $D \leq 5cm$, where D is tube diameter). It shows four flow pattern regions with respect to gas and liquid superficial velocities (U_{gs} and U_{ls}). As they argued, for smaller tube diameters (including 19 mm), the rising bubbles approach the back of the occasional Taylor bubble coalescing with it, increasing its size, and as a result the regime corresponding to bubbles flow does not exist. Hence the existing flow patterns are finely dispersed bubbles, churn, slug and annular flows. At low flow velocities (low gas- and low liquid- superficial velocity), the flow regime is slug. Finely dispersed bubble regime exists at higher liquid velocities. At higher gas velocities, the flow regime is churn. At very high gas velocities, the regime is said to be annular. To calculate their map, Taitel *et al.* used physical models to develop theoretically based transition equations. They showed that each transition depends on the flow rate pair (U_{gs} and U_{ls}), fluid properties and pipe size. However the nature of the dependence is different for each transition due to different physical transition mechanisms. These mechanisms were presented in section 1.4. Since the annular regime is easily detectable and difficult to reach with the available equipments, this regime was not studied in this project. Therefore, the two-phase flow conditions that were used as reference conditions for training were chosen among three different regimes.

Figure 5.2 shows a map of the test conditions in which the points corresponding to the reference conditions were circled. For each regime three reference conditions were selected. The reason of selecting three points for each regime is that there can be some differences between two-phase flow conditions due to their velocity and void fraction even though they are categorized in a same regime. For example in slug regime, Taylor bubbles appear with different size as the velocity or void fraction change. Therefore, in

order to cover such variations within a regime, three points were selected for each regime.

As mentioned earlier, in each test during experiments, photos of flow patterns were taken and were used in addition to Taitel's map to make such selection. The photos of all the tests are given in Appendix B.

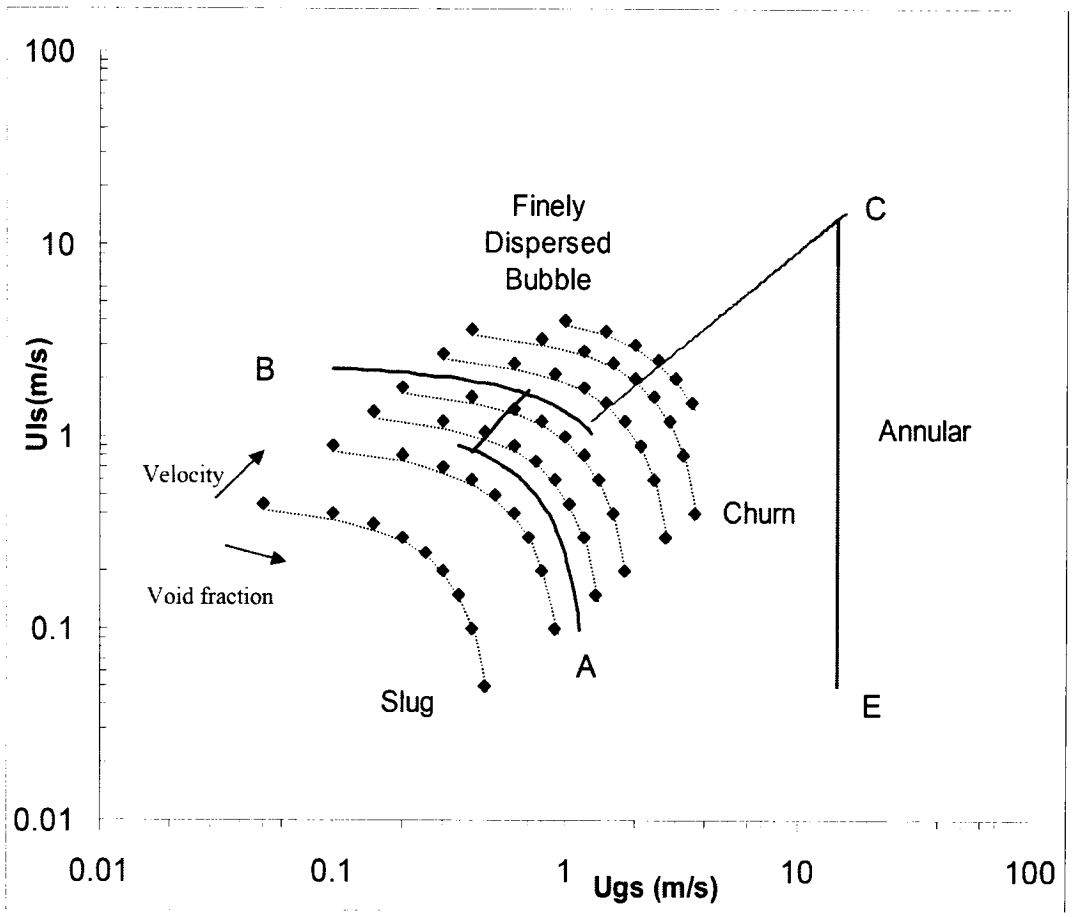

Figure 5-1 Test point on the map of Taitel et al. (1980).

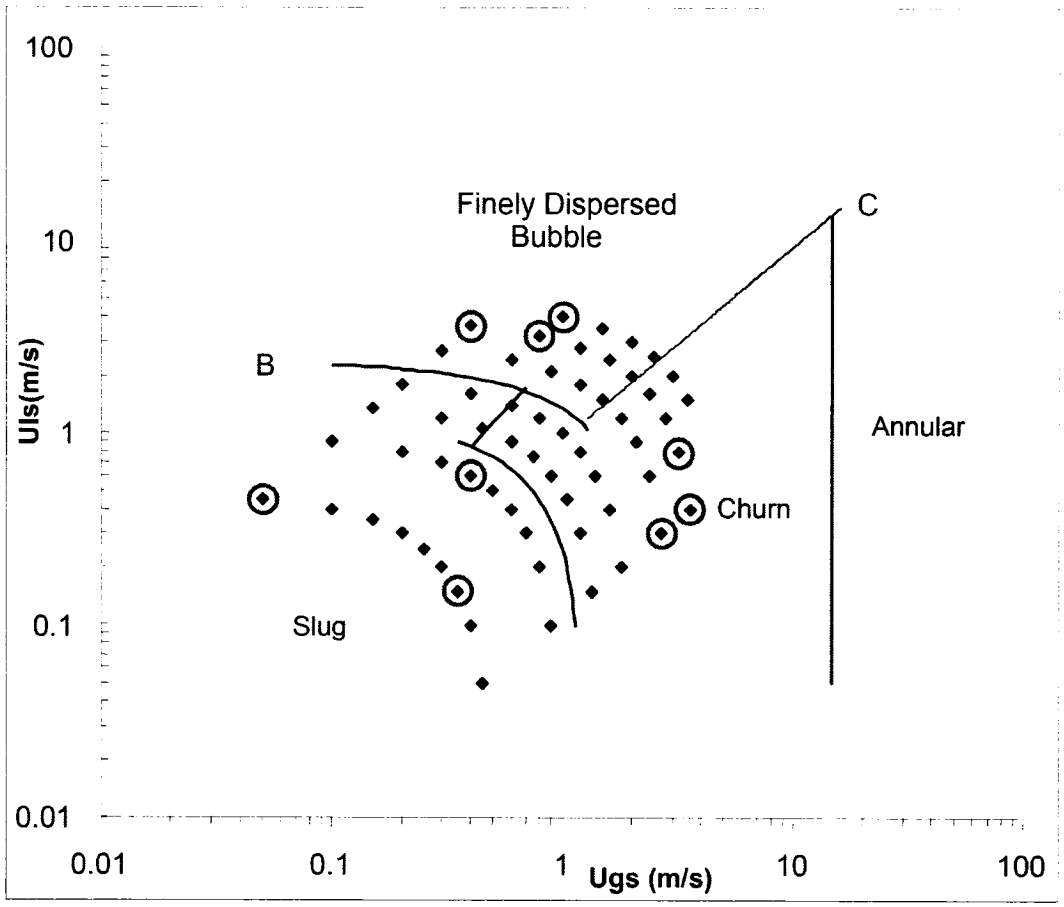

Figure 5-2 Reference conditions on Taitel's map.

5.2 Comparison between Different Methods of Feature Extraction

De-noising and down-sampling of the raw data are performed in same way, regardless of the feature extraction method. These two operations are done prior to feature extraction.

5.2.1 Power Spectral Density Method

As discussed in the previous chapter, the frequency related feature extraction does not seem to be a promising choice. In this section, this presumption is investigated

through analytical and experimental results. First, it is very helpful to contemplate the power spectrum of different conditions in order to find or highlight a frequency range or possibly some certain frequency peaks. Figure 5.3 shows the power spectrum of three different conditions. These conditions correspond to the two-phase flow at 0.5 m/s and void fractions of 10%, 20% and 30%. As shown, at a constant velocity as the void fraction increases, the lower frequencies are mostly excited. This experience was predicted and discussed in the previous chapter. Moreover, photos and direct observations demonstrate that these three conditions have the same regime: slug. Therefore, for three conditions of a regime, there are three very different spectrums and it is not possible to single out one or more peak frequencies.

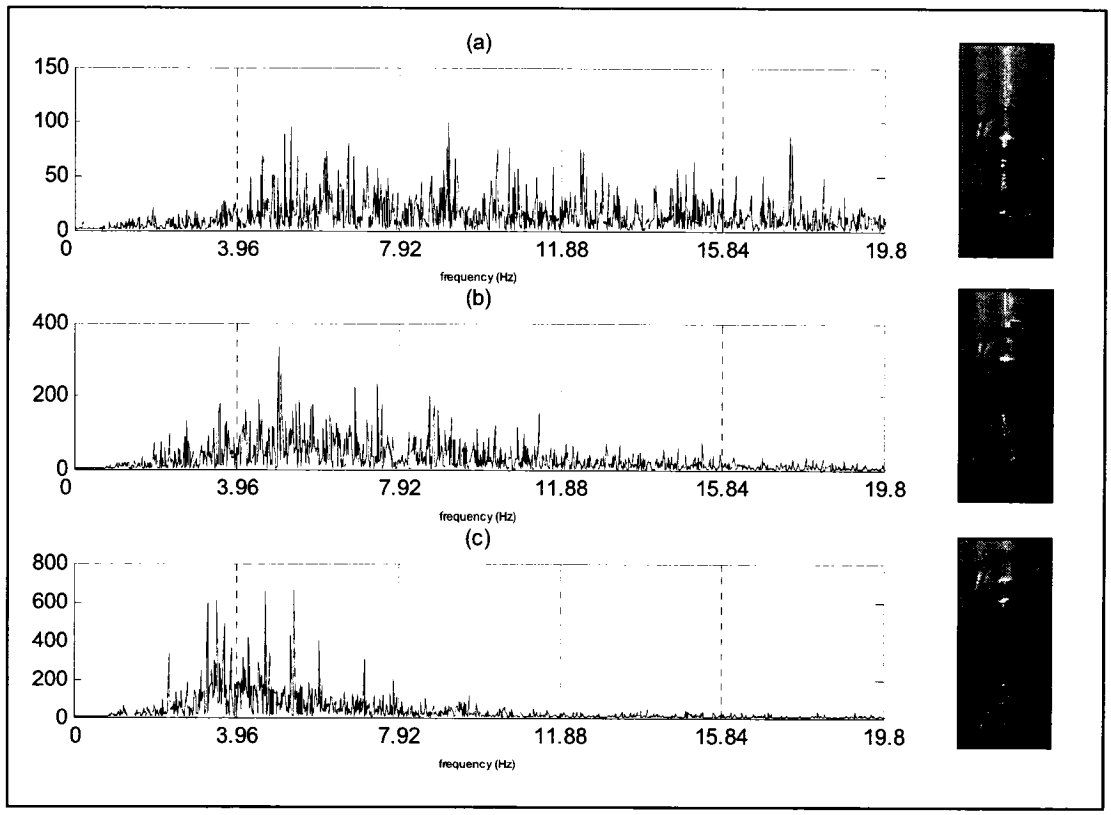

Figure 5-3 Power spectra and photos of three different conditions with same regime: (a) α =10%, Uhom=0.5m/s (b) α =20%, Uhom=0.5m/s (c) α =30%, Uhom=0.5m/s.

Anyway, the data were divided into vectors and the power spectrum of each vector was derived using FFT (Fast Fourier Transform) function. Then a frequency range that covers most of the excited frequencies over all conditions was selected and used as features in CHMM procedure (Table 5.1). It must be noted that, two-phase flow under some conditions, especially at higher void fractions, comes in very long mass of gas (i.e., Taylor bubbles or churns), and consequently the corresponding value of signal does not change for a considerable duration. Further, since extracting features from a constant value signal is neither possible nor meaningful, the vector derivation parameters must be chosen so that such problem is avoided.

Table 5-1 Parameters of vector derivation and CHMM.

Feature Extraction Method	Power Spectrum
Data length	100000 points
Segment length	60000 points
Segment Offset	4000 points
Vector length	10000 points
Number of Segments	11
Number of Vectors	11
Number of states in CHMM (N)	3
Number of Mixtures in CHMM (M)	1
Frequency range	~50 Hz

Unfortunately, because of either underflow or divergence problems during the training step of some conditions, the HMM procedure could not be carried out completely and as a result, there is no result available for this assessment. The underflow problem occurs mostly when the value of the variables exceed the precision

range of the computer. In HMM procedure, this problem happens mostly when the data are not statistically dispersed and consequently the determinant of covariance matrix becomes very small. The divergence problem is the one for which, after each iteration the error does not converge to a specific number and the iteration would never end.

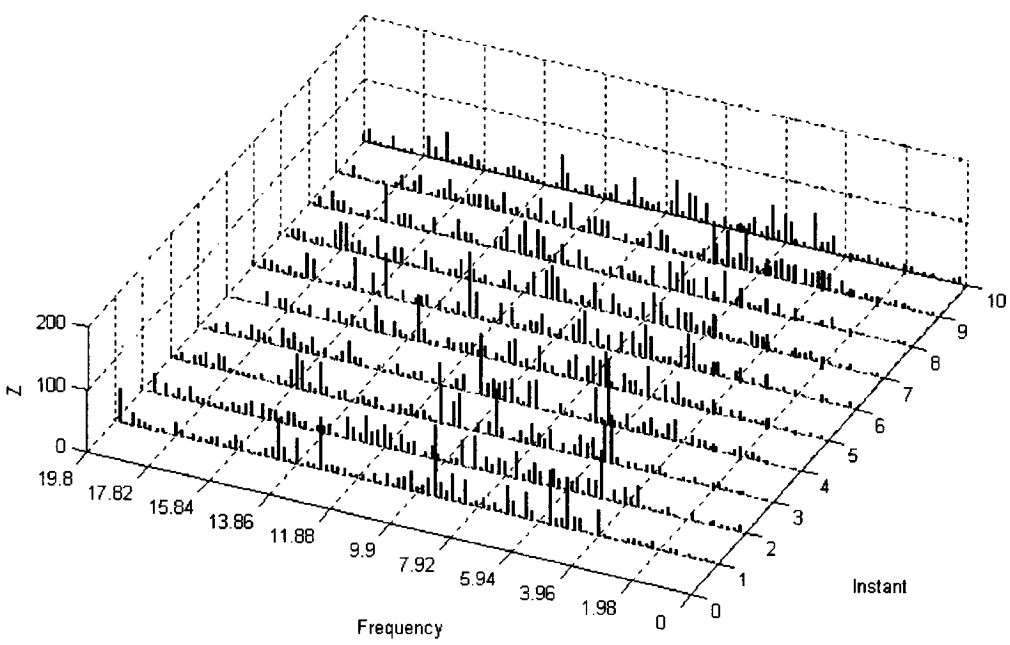

Figure 5-4 Spectrogram of two-phase flow at 0.5 m/s and 10%.

The arbitrary changes in the frequency spectra of feature vectors can be suggested as a reason for having such problems in training CHMM. For illustration, the spectrogram of the condition corresponds to 0.5 m/s and 10% was studied (Figure 5.4). As shown, peak frequencies vary continuously as time passes. That is to say, at any given instant, some frequencies are excited but this excitation does not last long. It can be stated that the frequency spectrum changes arbitrarily as time goes by. Therefore, in this case no clear pattern associated with power spectrum was found two-phase flow data.

5.2.2 Autoregressive Method

Another feature extraction method that was used is autoregressive (AR) method. As for the power spectrum method, the vector derivation is done prior to the feature extraction. The vector derivation parameters are given in Table 5.2.

Table 5-2 Parameters of vector derivation and CHMM

Feature Extraction Method	AR Models with the order of 10
Data length	100000 points
Segment length	60000 points
Segment Offset	2000 points
Vector length	10000 points
Number of Segments	21
Number of Vectors	11
Number of states in CHMM (N)	3
Number of Mixtures in CHMM (M)	1

The reflection coefficients of the autoregressive model with the order of 10 were obtained using the Burg method provided by Matlab software and were used as features. The numerical results of identification in terms of log-likelihood are shown in Table 5.3 (Also Table C.1).

Table 5-3 Log-likelihood results of using AR.

Condition Numbers as in Table 3.2.	Reference Condition Numbers								
	1	7	13	46	55	47	45	53	54
		Slug			Finely Dispersed Bubble			Churn	
1	**4015.1**	2064.9	1633.6	-4382	-21232	-3130.5	-1365.4	-3891.4	819.95
2	2707.1	2797.6	**2957.3**	-7476.9	-25077	-5022.4	-2054.9	-4781.9	447.49
3	1275.1	3087	**3228.9**	-7031.6	-24264	-4788.2	-2112.2	-4714.6	392.85
4	370.3	**3215.9**	3007	-4013.8	-21690	-4465.4	-761.04	-4066.5	839.44
5	768.17	**3295.1**	2954.3	-3541.9	-21343	-3262.2	-119.51	-2992.4	945.45
6	-159.85	**3114**	2916	-4051	-24777	-5063.1	-125.83	-3121.5	1401.5
7	383.12	**3702.4**	2419.1	-2262.9	-23196	-4058.3	116.22	-2810.8	1404.9
8	-277.48	**2810.9**	2172.9	-1581	-23421	-4541.6	583.19	-2164.8	1723
9	719.83	2464.1	**2490.6**	-5507.9	-27603	-6539.8	-229.9	-2763.3	1178.5
10	1186.9	2478	**2965**	-9116.4	-23686	-5673.2	-3035.6	-6557.8	40.591
11	-95.852	1919.4	**2505.9**	-10779	-25185	-6732.9	-3404.2	-7396.4	-394.92
12	-578.23	2291.5	**3091.1**	-9596.3	-23656	-5693.5	-2459.7	-5812.3	35.206
13	189.42	2933.4	**3785.7**	-4834.5	-21336	-3821.3	-549.05	-3099.6	1144.7
14	-2702.9	**2429.9**	2374	-2912	-24774	-6244	720.54	-1188	1323
15	-1913	1939	912.62	185.94	-22861	-4219.3	1837.1	-10.893	**1987.9**
16	-2316.7	1140.3	168.71	-64.253	-26822	-7318.3	1885.2	109.31	**2432.1**
17	-2591	2386.9	1139.8	-603.39	-30066	-7458.9	1943.9	-84.375	**2445.2**
18	-4042.5	1437.5	229.64	-1231.2	-30829	-9067.6	1825.7	234.44	**2152.7**
19	602.64	2211.7	**2975.6**	-10187	-25538	-6223.6	-2538.6	-6278.8	-5.6833
20	1210.2	2558.6	**3240.4**	-9693.5	-23834	-4725	-2738.4	-5756.2	22.801
21	-298.58	**2561.9**	2084.3	-968.01	-20378	-3510.1	992.46	-1609.8	1450.1
22	-664.46	1926.4	1159.9	-945.57	-24014	-5097.8	1457	-484.48	**2136.2**
23	-3947.3	690.44	-641.36	145.44	-26355	-6310.7	2052.8	820.73	**2524**
24	-4932.9	-105.32	-2316.7	902.96	-29415	-7854.2	2541.8	1447.1	**2752.8**
25	-8278.7	-1707.5	-3552.3	-215.2	-34202	-12996	2412.5	1762	**2569**
26	-10343	-3377.3	-6570.3	-1598.9	-41016	-18415	2693.7	2134.8	**2749**
27	-3802.8	696.05	-1753.5	-729.97	-34817	-10901	2463	1137.9	**2731.5**
28	997.78	2967.1	**3211.9**	-4624.7	-20741	-3759.8	-1144.5	-4194	755.28
29	2054.2	**2917.9**	2807	-4116.6	-20029	-2635.9	-786.04	-3351.1	996.94
30	-299.26	1127.1	606.93	1585.2	-18374	-2060.2	1632.9	-10.124	**2131.5**
31	-7624.7	-4831.4	-3877.4	1676.5	-24697	-6592.4	2114.9	1833.2	**2554.4**
32	-11294	-7517.9	-6135.7	1582.5	-26876	-7592.3	1867.9	**2128.1**	2053.2
33	-13318	-8093.7	-8555.8	235.68	-33884	-13997	2401.6	2796.4	**2799**
34	-14636	-6514.9	-8310.3	-640.84	-37921	-16858	2348.9	2393.4	**2516.4**
35	-12672	-5298.6	-7287.9	-1820.6	-42082	-20905	2482.6	2275.2	**2640.4**
36	-10954	-2502.5	-5627.6	-3491	-50517	-24819	2749.6	1978.3	**2930.5**
37	620.76	**2545.3**	1725.7	624.19	-18831	-1866.9	1302.8	-1144.2	1846.8
38	-5908.5	-9632.5	-3780.8	692.1	-10103	**1415.9**	-315.62	-543	1106
39	-21754	-23140	-10538	**1941.3**	-7895.2	954.59	-1079.1	256.14	780.31
40	-49139	-42887	-21640	**487.55**	-11013	-2140	-2763.1	427.42	471.99
41	-65643	-57775	-27914	-1238.6	-16122	-8474.4	-4471.4	-219.1	**-53.999**
42	-54958	-43594	-26146	-2634.6	-34712	-17916	-1948.8	**1564.7**	1018.5
43	-29006	-21556	-17350	-2056.5	-39033	-20005	879.74	**2658**	2100.9
44	-22298	-11195	-15721	-4939.9	-58447	-31430	2421	**2836.7**	2589
45	-17319	-5062.8	-11224	-8498.4	-66954	-36710	**3265.6**	1665.6	1809.4
46	-11462	-7942.2	-6501.1	**3880.9**	-15915	-3876	1402.5	1347.2	1769.8
47	-42969	-55219	-25187	-1189.5	-302.29	**4058.5**	-6253.1	-3451.1	-1692
48	-70997	-71068	-49183	-5951.5	1441.4	**2661.3**	-13444	-7354.2	-4156.6
49	-71068	-71068	-61917	-6087.5	-4100.6	**-2393.3**	-15837	-7321.2	-4427.1
50	-71068	-71068	-59757	-7908.3	-24101	-15540	-13160	-3246.3	**-3091.8**
51	-70695	-68913	-45509	-7140.4	-38308	-25660	-7031.3	**-11.984**	-917.43
52	-47984	-35856	-23637	-3754.2	-45217	-25458	-976.47	**2483**	1412.2
53	-26110	-14765	-19794	-6448.7	-65387	-37714	2214.6	**3472.4**	2324.2
54	-23481	-8467.6	-14196	-11478	-61319	-43909	1761.7	716.65	**3154**
55	-71068	-71068	-67683	-9844.2	**4062.3**	1068.4	-20242	-12262	-7135.2
56	-71068	-71068	-71068	-15189	**1203.8**	-853.92	-29402	-18037	-10098
57	-71068	-71068	-71068	-12229	**-4630.4**	-5715.4	-27124	-12855	-8531.7
58	-71068	-71068	-70372	-12099	-24399	-16871	-19329	-6158.7	**-5493.8**
59	-71068	-70451	-56527	-11562	-48037	-32572	-9745	**-1096.2**	-1982.9
60	-54345	-41752	-33767	-8909.7	-66006	-39391	-1102.6	**1983.5**	943.31

Two-phase flow maps were extracted from the numerical results using two different approaches. One approach was to find the maximum likelihood of each condition in comparison with the nine reference conditions and then recognize the regime of that reference condition as the flow regime. For example, the maximum likelihood of the condition number 10 in comparison with the nine reference conditions is equal to 2965 as indicated in bold format in Table 5.3, and it corresponds to reference condition number 13. Since the regime of the condition number 13 is slugs, the condition number 10 is classified as slugs. Another approach is to sum the likelihood values of the same regime and then find the maximum among them and recognize it as the governing regime. For example, for identifying the regime of condition number 10, the three values correspond to each regime are summed. This results in 6629.9 for slugs (i.e. the sum of the likelihoods of reference condition numbers 1, 7 and 13),-38475.6 for finely dispersed bubbles and -9552.81 for churns. Therefore, since the maximum value is equal to 6629.9 and corresponds to slug regime, the flow regime under condition number 10 is slugs.

The map obtained using these two approaches in comparison with Taitel's map are shown in Figure 5.5. It must be noted that, most transition boundaries suggested in the literature, have regular and undistorted shape when mapped with respect to U_{gs} and U_{ls}. This holds for both cases of theoretical and empirical based methods. Hence, the resulting boundaries are expected to have a reasonably regular and smooth shape.

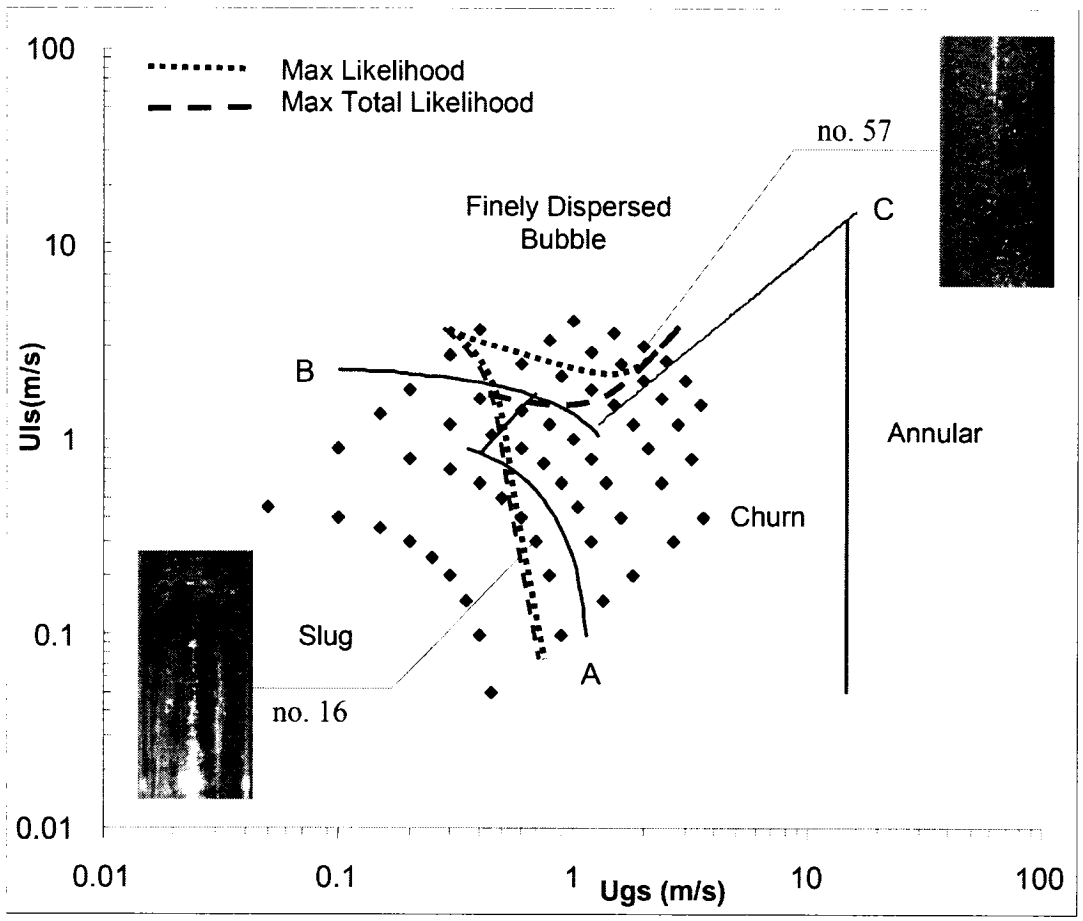

Figure 5-5 Resulting map of using AR feature extraction method.

The resulting boundaries shown in Figure 5.5 have a regular shape; however, in comparison with Taitel's map and photos, there are some disagreements. For example, condition number 16 is classified as churn regime, whereas the photo shows that the regime is slug. In the same manner condition number 57 is misidentified as finely dispersed bubbles, while the actual regime is churn. Therefore, the results of the AR method are not satisfactory.

5.2.3 Passage Time Based Feature Extraction

5.2.3.1 Method Verification

Unlike the previous methods, in this method feature vector derivation was done after feature extraction. In this case, the two different approaches for treating numerical results were used, as described in section 5.2.2. Further, for any approach, CHMMs with different number of states were tried. The resulting map is shown in Figure 5.6 and the modeling parameters are given in Table 5.4. The numerical results in term of log-likelihood for this trial as well as all other trials are given in Appendix C.

The vector derivation parameters must be chosen so that the characteristics of the signals are competently covered. Unfortunately, there is no clear theoretical concept associated with this selection and as a result, this step was done on a trial basis. In most of the cases, pondering on the signals can be helpful. In some cases, as mentioned before, the selection must be done in order that underflow problem is avoided. Moreover, long vectors make the execution time consuming, whereas, short vectors bring about poor results. The numbers represented in Table 5.4 and so forth were selected after trying different numbers and they seem to be the best choices.

As shown, the resulting boundaries obtained by implementing the passage time based feature extraction method are smooth in both cases of using maximum likelihood and maximum total likelihood approaches. Further, there are dissimilarities between the obtained boundaries and Taitel's map, especially the boundary between finely dispersed bubble and churn regions for which the difference is remarkable. On the other hand, the obtained boundaries are in good agreement with the photos, though they have dissimilarities with Taitel's map. A good example for this case is condition number 22. According to Taitel's map, this condition belongs to the churn region, while the photo shows slugs. A reason for having such considerable mismatch between photos and Taitel's map is that Taitel's map was derived based mostly on theoretical concepts and it is obvious that there are always mismatches between theory and experiment. Another

Table 5-4 Parameters of vector derivation and CHMM.

Feature Extraction Method	Passage time Based Method
Data length	1000 points
Segment length	200 points
Segment Offset	100 points
Vector length	20 points
Number of Segments	9
Number of Vectors	19
Number of states in CHMM (N)	3
Number of Mixtures in CHMM (M)	1

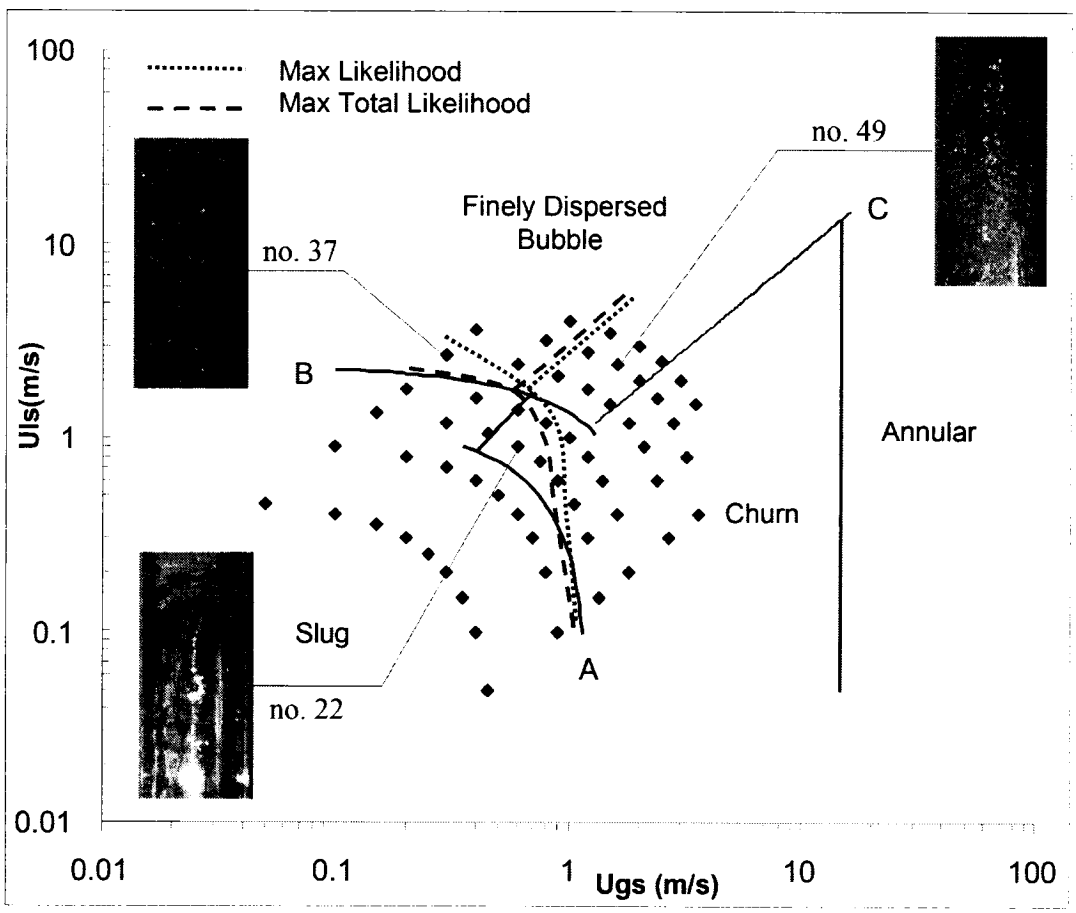

Figure 5-6 Resulting map of using passage time feature extraction method (N=3).

reason that can be suggested is that if the mixer does not mix the two phases evenly the unexpected changes in flow regime can happen.

Anyway, the results of this method among other methods are most acceptable, especially in case of applying total likelihood approach, as they were compared to photos and Taitel's map. Therefore, this method was chosen for feature extraction.

5.2.3.2 The Effect of Changing CHMM Parameters

The only adjustable parameters of a CHMM are N, the number of states and M, the number of mixture. A point that must be made here is that, M and N cannot be increased unrestrictedly, due to underflow problems. That is to say, by increasing any of these two parameters, the elements of the covariance matrix decrease. As a result, the determinant of the covariance matrix appearing in the denominator of Equation (2-9), becomes very small and causes underflow problems. Another point is that the states of an HMM are not related to any physical interpretation. Therefore, in this work it would be incorrect to deduce that the number of states (N) in the HMM was given the same value as the number of possible flow regimes. The number of mixtures in all the executions was kept equal to unity (i.e., M=1 as given in Tables 5.5 and 5.6.). In fact, using models with more than one mixture (i.e., M>1) is mostly applicable in applications where the signals are too statistically dispersed, so that the model with a single mixture is not capable to represent the signals proficiently. Since the signals in this application were not so statistically dispersed, there was no necessity to increase the number of mixtures. Even though, in order to check the probable changes in the results, the number of mixtures was increased and in all the cases, the CHMM training procedure faced the underflow problem during execution. Hence, the only parameter to change was N, number of states. The results of such changes are shown in Figures 5.7 and 5.8.

Table 5-5 Parameters of vector derivation and CHMM.

Feature Extraction Method	Passage time Based Method
Data length	1000 points
Segment length	200 points
Segment Offset	100 points
Vector length	20 points
Number of Segments	9
Number of Vectors	19
Number of states in CHMM (N)	5
Number of Mixtures in CHMM (M)	1

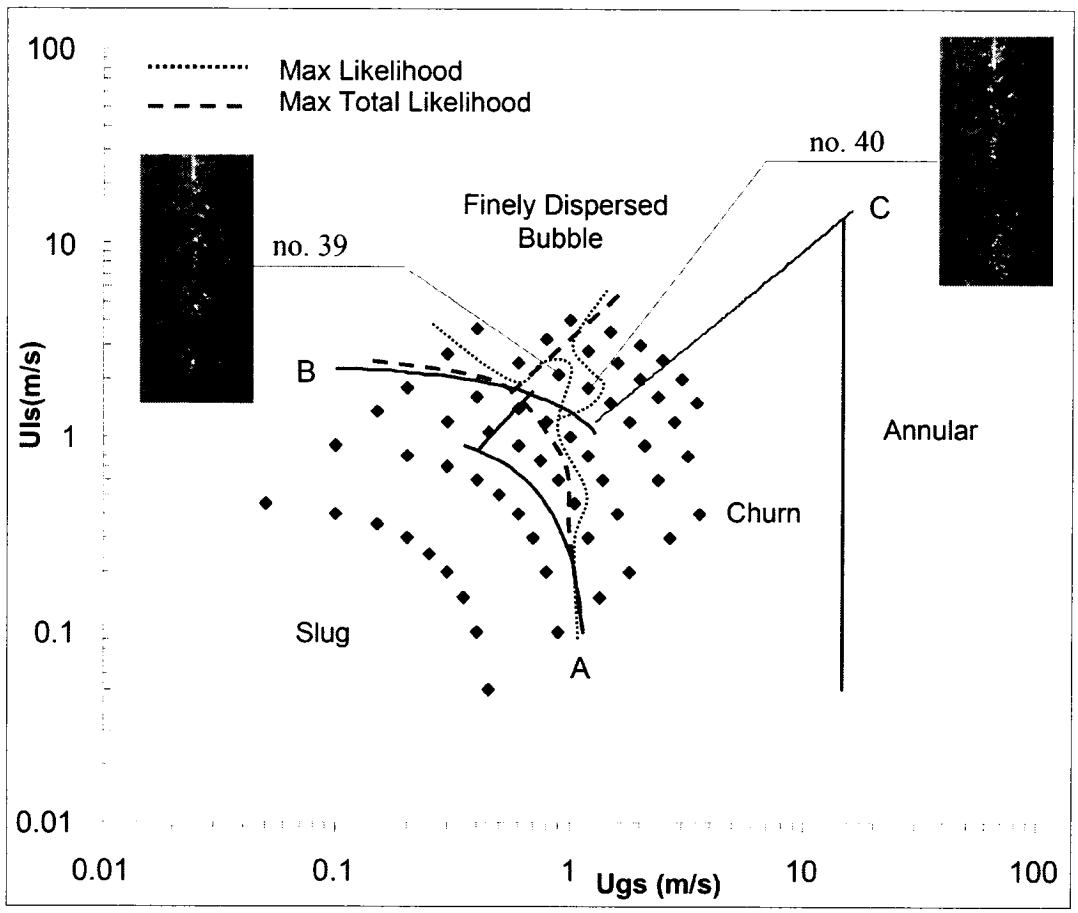

Figure 5-7 Resulting map of using passage time feature extraction method (N=5).

Table 5-6 Parameters of vector derivation and CHMM.

Feature Extraction Method	Passage time Based Method
Data length	1000 points
Segment length	200 points
Segment Offset	100 points
Vector length	20 points
Number of Segments	9
Number of Vectors	19
Number of states in CHMM (N)	7
Number of Mixtures in CHMM (M)	1

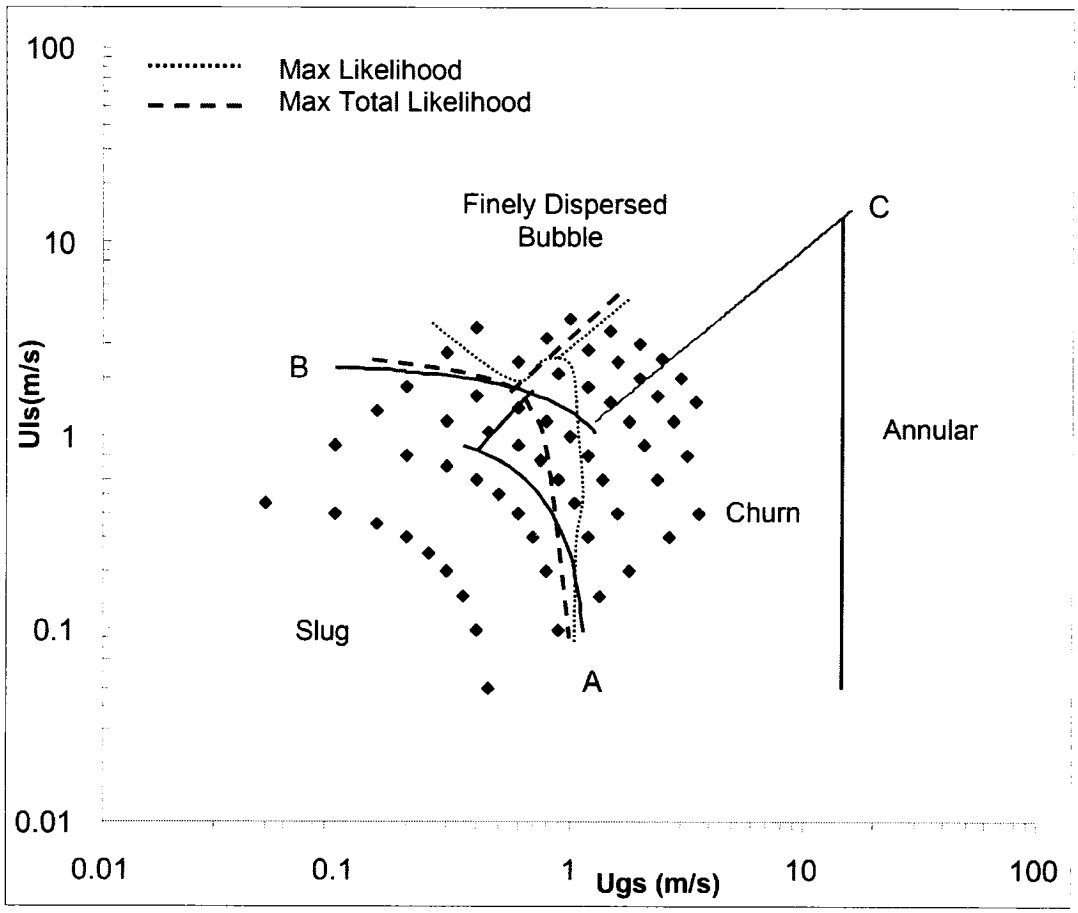

Figure 5-8 Resulting map of using passage time feature extraction method (N=7).

The boundaries depicted based on the results of maximum likelihood approach in the cases that N=5 and N=7 as shown in the Figures, and the case N=2, do not have a regular shape and there are some arbitrariness in comparison with the case N=3. Moreover, no certain coherence can be observed between changing number of states and difference in the shape of the boundaries. On the other hand, the boundaries resulting from the maximum total likelihood approach, not only are smooth, but also there is no significant change as the number of states changes. Therefore, it can be concluded that the maximum total likelihood approach is more reliable and has better performance.

5.2.3.3 The Effect of Selecting Different Reference Conditions

So far, the results were all obtained using a specific selection of conditions as reference conditions. By analyzing those results, the passage time based method and the maximum total likelihood approach were selected among others to be the best method. In this section, the results of using a different set of reference conditions are presented and discussed. It must be noted that this change was made just for the slug and the churn regions. For the finely dispersed bubbles region, because of the limited number of conditions in this region, the previous reference conditions were maintained (Figure 5.9).

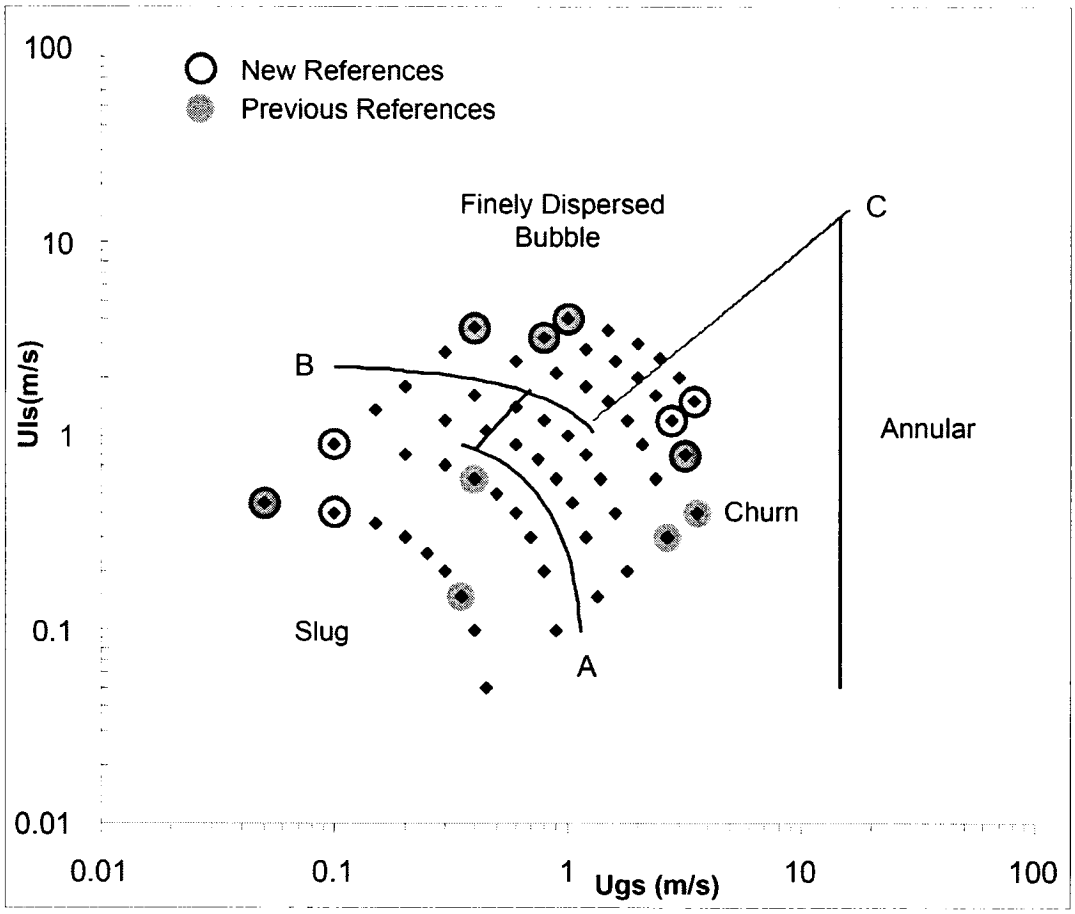

Figure 5-9 New reference conditions on Taitel's map.

The resulting map is shown in Figure 5.10 and the CHMM parameters are given in Table 5.7.

Table 5-7 Parameters of vector derivation and CHMM.

Feature Extraction Method	Passage time Based Method
Data length	1000 points
Segment length	200 points
Segment Offset	100 points
Vector length	20 points
Number of Segments	9
Number of Vectors	19
Number of states in CHMM (N)	3
Number of Mixtures in CHMM (M)	1

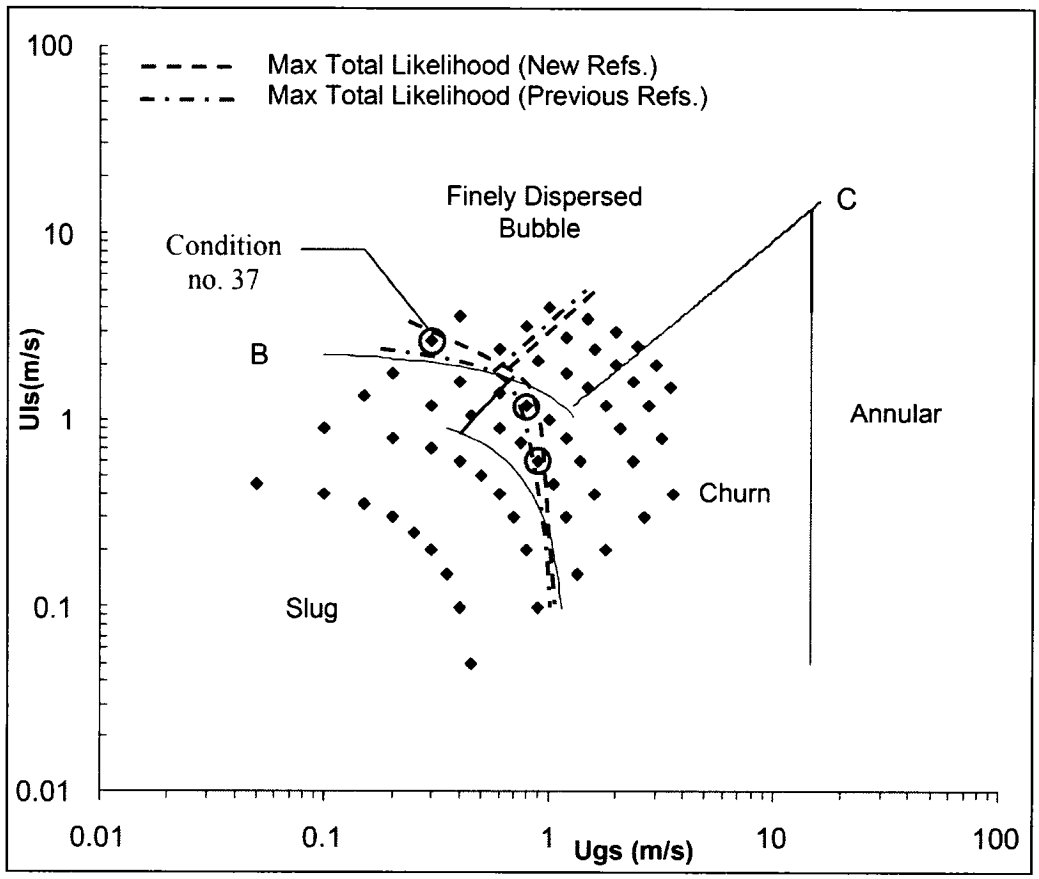

Figure 5-10 Resulting map of using passage time feature extraction method with different reference conditions (N=3).

As shown, there are slight variations in the obtained boundaries due to selecting different reference conditions in comparison with other methods. The circled points are the points for which the identification is different in comparison with map shown in Figure 5.6. The only point that can be considered as not being correctly categorized is the one close to the boundary between finely dispersed bubble regime and slug regime (i.e., condition number 37). The boundary between churn regime and slug regime in comparison with other method did not face important change (in either case, the two other circled points are very close to the transition border).

5.3 Confidence Evaluation

In this section, it is of interest to study the confidence of the results. As previously mentioned, in order to extract a flow map from the numerical log-likelihood results, the maximum likelihood value was selected among others and said to be the actual regime. For this case, the 'confidence difference' can be defined as: the difference between the maximum value and the second largest value among the log-likelihood values obtained by comparing a given flow condition with the reference conditions (i.e. values in a given row of likelihood table). According to this definition, a large confidence difference will show that the condition bears exclusively the characteristics of the given regime. Therefore, the confidence level for the regime detection will be high. On the contrary, a small difference will show that the characteristics of the flow are almost equally comparable to two different regimes. Even though a flow regime was determined, the confidence in this result will be poor.

Figure 5.11 shows a map on which the condition points are classified with respect to their confidence difference. This map was produced based on the results from the passage time based method, and using total likelihood values and an HMM with three states (N=3). Defining the 'full range' as the interval between the maximum and minimum confidence differences, the confidence difference values can be divided into three ranges: low confidence range (0-500) which covers about 10% of the full range,

medium confidence range (500-1400) which covers about 20% of the full range and high confidence range (1400-5200) which covers 70% of the full range. These ranges are selected in a way that the resulting flow pattern map reflects the regions where the confidence is low. The numerical likelihood values and confidence difference values are given in Appendix C (Table C.5).

As shown in Figure 5.11, the conditions with high confidence are mostly those located away from the transition boundaries obtained using HMMs. Close to transition boundaries, the confidence is low. In fact, near transition boundaries, two phase flow bears the characteristics of both regimes between which transition occurs, and the confidence difference is expected to be low. Therefore, the boundaries obtained using the HMM method are reasonably accurate.

One peculiarity on this map is that most conditions in the finely dispersed region have a low confidence difference. This can be explained from the optical probe measuring system. If a group of very small and closely packed bubbles crosses the probe, it is probable that the probe will misinterpret it as a mass of air. In fact, when two bubbles are very close, the liquid film between them is very thin so that the passage time of such film is less than the summation of the signal's rising and falling time. Therefore, the change in phase corresponding to the passage of the liquid film is not recorded completely. For example, if the summation of the rising and falling time is 0.4 ms (as in Figure 5.12), a liquid film between two bubbles flowing at 4 m/s, must be at least 1.6 mm of thickness, for the phase changes to be fully recorded. The passage of closely packed bubbles can happen in the finely dispersed bubbles regime. As a result, such misinterpretation causes the corresponding signal to look as if it was gathered from a flow condition with churn or slug regime. Thus, conditions in the finely dispersed bubbles region are detected as such, but they show relatively high log-likelihoods with the churn or slug reference conditions, causing low confidence levels.

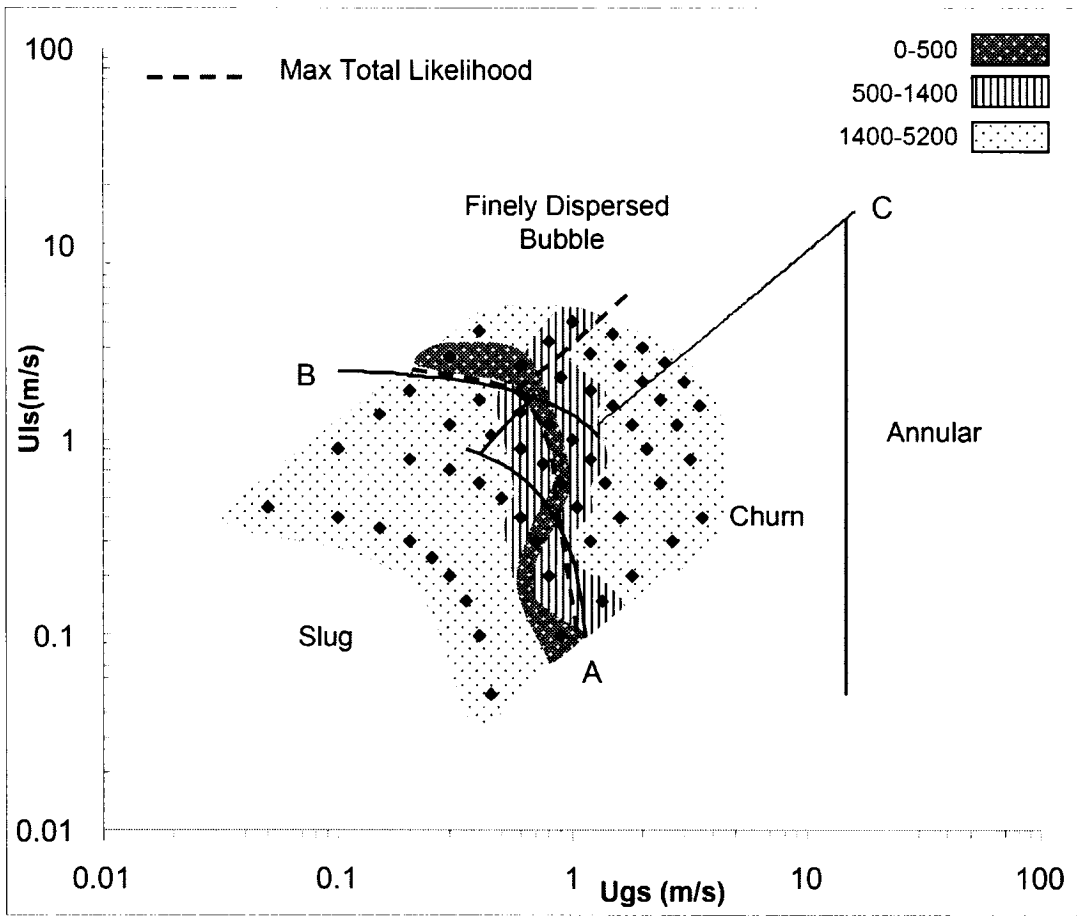

Figure 5-11 Confidence regions for period based method with a 3 states HMM on Taitel's map.

Figure 5.12 shows a short interval of the raw time signal (recorded at 99 kHz) of condition number 46. According to Taitel's map this condition is in the finely dispersed region and is at a reasonably good distance from transition boundaries. From the signal shape, it can be observed that at different times, there are some abrupt changes in the signal. These abrupt changes reflect a change in the phase of the flow, but the step is insufficient for the signal to cross the zero line. Consequently, during de-noising, due to selecting the zero line as a threshold, such changes in the phase will be missed. One may think of using other thresholds than zero to resolve this problem. Due to existence of noise, unpredictable variations in the signal shape and inconsistency in the amplitude of the signal, applying such resolution, seems to be very difficult. Hence, low confidence

in the mentioned region can be considered as being caused by weaknesses in the measurement method. Taking such weaknesses into account, it can be concluded that there is an acceptable correlation between the likelihood values and physical significance of the measured signals.

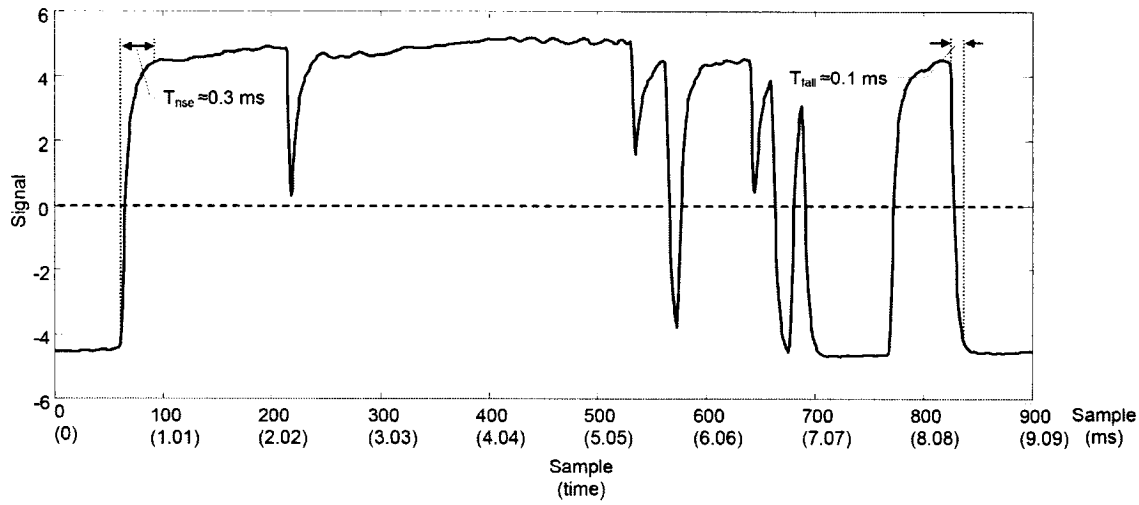

Figure 5-12 An interval of the raw time signal (recorded at 99 kHz) of condition number 46.

5.4 Conclusion

In this chapter, several feature extraction methods were presented and compared and passage time based method was selected among others. In addition, for depicting boundaries using log-likelihood values, two different approaches were tried and it was shown that using maximum total likelihood has a better precision.

Further, the results of changing the reference condition were given and it was discussed that there was some differences.

In all of the cases the map of Taitel *et al.* (1980) together with photos taken during the test were used to justify the results, however these two methods of justification are not perfect. In fact, in studying two-phase flow regimes identification, there is no perfect

method for justification. The map of Taitel was derived based mostly on the theoretical concepts, while there are always mismatches between theory and experiment. Moreover, photography technique in some cases is not that helpful. For example, at higher velocities and for the case of finely dispersed bubble, the photos cannot show what is happening at the center of tube.

Another point that must be noted here is that even though the tests were carried out with the highest possible degrees of accuracy, there are still some inaccuracies. For example if the mixer in the test does not mix the two phases in an even way, then it may cause unexpected changes in the flow regime.

With respect to the mentioned points and the maps obtained by CHMM were to good extent acceptable, it can be concluded that hidden Markov model is able to detect two-phase flow patterns.

Conclusion

In this research, the practicability of hidden Markov modeling in identifying two-phase flow regime was tried out. It was shown that this method, which has been proven to be a very strong pattern identifier in different fields of engineering, has also a good potential in identifying two-phase flow pattern regimes. It was also shown that the performance of this method is significantly affected by choosing different feature extraction methods.

This research can be considered as a leading trial to so many follow-ups that can be practiced in this field. Some of the suggestions for future works on this subject are as follow:

- There exist many methods for extracting signal features. In this project, three feature extraction methods were examined and it was shown that the feature extraction plays an important role in the implementation of the HMM. Therefore, the performance of other methods can be examined as a new project.

- Instead of using optical probe signal, pressure fluctuation signals or any other type of signal for which the nature of the fluctuations depends on the flow regime can be used. In this case, more accurate results are expected for when there is high coherence between the nature of the fluctuation and the flow regime.

- Moreover, it is possible to modify hidden Markov model and enable it to deal with a fusion of different kinds of signals. For example a fusion of optical probe signals and pressure fluctuation signals.

- It is also suggested to use this method of regime identification for the case of two-phase flow crossing tube bundles.

- In this project, HMMs were trained based on the signals gathered from two-phase flow in a tube with 19 mm of diameter, and then the HMMs were used to identify the patterns of the flow in the same tube. As a follow-up, the feasibility of identifying the regimes of the two-phase flow in a given tube using HMMs pre-trained based on data gathered from other tubes with different diameter can be investigated.

- The multiple observation approach was used in the HMM procedure. In this project, signals corresponded to each condition were divided into several segments and each segment was used as an observation sequence. As a result, multiple observations (or equally multiple segments) were gathered from the same condition. Further, for each regime, three points (conditions) were selected as reference points and for any reference point an HMM was built. As an alternative approach, instead of making a single HMM for any reference point, it is suggested to construct multiple observations out of a combination of data corresponding to different reference points of a same regime for training only one HMM. Hence, by applying this approach there would be just one HMM for each regime. As an extension to this method and to the previous suggestion, HMMs can be trained based on data gathered from the two-phase flow inside channels with different tube sizes. Therefore, there would be an HMM for each regime that can be used for identifying regimes of two-phase flow inside channels with different sizes.

Bibliography

Albrecht R. W., Crowe R. D., Dailey D. J., Damborg M. J., Koslay G. (1982) "Measurement of two-phase flow properties using the nuclear reactor instrument." Prog. Nucl. Energy, 9. 37-50.

Albrecht R. W., Tubridy E., Eklund G. (1980) "Two-phase flow characterization by local and global neutronic fluctuation measurements." Trans Am. nucl. Soc, 34. 806-807.

Atlas L., Ostendorf M., Bernard G. D. (2000) "Hidden Markov models for monitoring machining tool-wear." IEEE Intl. Conf. on Acoustics, Speech, and Signal Processing. Proceedings, 6:6. 3887-3890.

Baker J. K. (1975) "The dragon system-An overview." IEEE Trans. Acoustic. Speech signal processing, ASSP-23:1. 24-29.

Baum L. E. (1972) "An inequality and associated maximization technique in statistical estimation for probabilistic functions of Markov processes." Inequalities, 3, 1-8.

Baum L. E., Petrie T., Soules G., Weiss N., (1970) "A maximization technique occurring in the statistical analysis of probabilistic functions of Markov chains." Annals of Mathematical Statistics, 41: 1, 164-171.

Bennett A. W., Hewitt G. F, Kearsey H. A., Keeys R. K. F., Lacey P. M. C. (1965) "Flow visualization studies of boiling at high pressure." Proc. Instn mech. Engrs, 180 (3C). 260-270.

Bergles A. E., Roos J. P., Boume J. G. (1968) "Investigation of boiling flow regimes and critical heat flux." NYO-3304-l3, Dynatech Corp., Cambridge, Mass.

Brauner N., Barena D. (1986) "Slug-to-churn transition in upward gas-liquid flow." Chemical Eng. Sci., 41:1. 159-163.

Bunks C., McCarthy D., Al-Ani T. (2000) "Condition-based maintenance of machines using hidden Markov models." Mechanical Systems & Signal Processing, 14:4. 597-612.

Cooper R. D., Hewitt G. F., Pinchin B. (1963) "Photography of two-phase flow." AERE-R4301.

Costigan G., Whalley P. B. (1997) "Slug flow regime identification from dynamic void fraction measurements in vertical air-water flows." Intl. J. Multiphase Flow, 23. 263-282.

Crowe R. D., Eisenhawer S. W., McAfee F. D., Albrecht R. W. (1977) "A study of two-phase flow characteristics using reactor noise techniques." Prog. Nucl. Energy, 1. 85-97.

Das R. K., Pattanayak S. (1993) "Electrical impedance method for flow regime identification in vertical upward gas-liquid two-phase flow." Meas. Sci. Techno., 4. 1457-1463.

Dempster A. P., Laird N. M., Rubin D. B. (1976) "Maximum likelihood from incomplete data via the EM algorithm." Journal of Royal Statistical Society., 39:1, 1-38.

Dinh T. B., Choi T. S. (1999) "Application of image processing techniques in air/water two-phase flow." Mechanical Research Communications, 26:4. 463-468.

Dong F., Jiang Z. X. (2003) "Application of electrical resistance tomography to identification two-phase flow regime." Intl. Conference on Machine Learning and Cybernetics, 4. 2217-2222.

Dukler A. E., Taitel Y. (1977) "Flow regime transitions for vertical upward gas liquid flow: A preliminary approach through physical modeling." Progress Report No. 1, University of Houston, NUREG-0162.

Elkow K. J., Rezkallah K. S. (1997) "Statistical analysis of void fluctuations in gas-liquid flows under 1-g and m-g conditions using a capacitance sensor." Int, J. Multiphase Flow, 23. 831-844.

Elperin T., Klochko M. (2002) "Flow regime identification in a two-phase flow using wavelet transform." Experiments in Fluids, 32:6. 674-682.

Ertunc H. M., Loparo K. A. (2001) "A decision fusion algorithm for tool wear condition monitoring in drilling." International Journal of Machine Tools & Manufacture, 41:9. 1347-1362.

Ertunc H. M., Loparo K. A., Ocak H. (2001) "Tool wear condition monitoring in drilling operations using hidden Markov models." International Journal of Machine Tools & Manufacture, 41:9. 1363-1384.

Ertunc H. M., Loparo K. A., Ozdemir E., Ocak H. (2001) "Real time monitoring of tool wear using multiple modeling." IEEE International Electric Machines and Drives Conference, 687-691.

Ertunc H. M., Oysu C. (2004) "Drill wear monitoring using cutting force signals." Mechatronics, 14:5. 533-548.

Ge M., Du R., Xu Y. (2004) "Hidden Markov model based fault diagnosis for stamping processes." Mechanical Systems and Signal Processing, 18:2. 391-408.

Geraets J. J. M., Borst J. C. (1988) "A capacitance sensor for two-phase void fraction measurement and flow pattern identification." Int, J. Multiphase Flow, 14:3. 305-320.

Ginoux J. J. (1978) "Two-phase flows and heat transfer with application to nuclear reactor design problems." Hemisphere Publishing Corporation.

Golan L. P., Stenning A. H. (1970) "Two-phase vertical flow in vertical tubes." Proc. Instn. Mech. Engrs, 184:3C. 105-114.

Govan A. H., Hewitt G. F., Richter H. J., Scott A. (1991) "Flooding and churn flow in vertical pipes." Int. J. Multiphase Flow, 17:1. 27-44.

Griffith P. (1964) "Two-phase flow in pipes, in developments in heat transfer." (Editor Rohsenow W. M.) M.I.T. Press, Cambridge, Mass.

Griffith P., Synder G. A. (1964) "The bubbly-Slug transition in a high velocity two-phase flow." MIT Report 5003-29 (TID-20947).

Griffith P., Wallis G. B. (1961) "Two-phase slug flow." Trans. ASME J. Heat Transfer, 83. 307-320.

Haiqing L., Zequi Z., Chiying H. (1992) "Measurement and evaluations of two-phase flow parameters." IEEE Trans. Inst. Measur., 41:2. 298-303.

Hannaford B., Lee P. (1991) "Hidden Markov model analysis of force/torque information in telemanipulation." The Intl. Journal of Robotics Research, 10:5. 528-539.

Hatzipantelis E., Penman J. (1993) "The use of hidden Markov models for condition monitoring electrical machines." Sixth International Conference on Electrical Machines and Drives, 376. 91-96.

Heck L. P., McClellan J. H. (1991) "Mechanical system monitoring using hidden Markov models." Proc. Intl. conf. on Acoustics, Speech and Signal Proc, 3. 1697-1700.

Hewitt G. F., Roberts D. N. (1969) "Studies of two-phase flow patterns by simultaneous X-ray and flash photography." AERE-M 2159.

Hewitt G. F., Jayanti S. (1993) "To churn or not to churn." Int. J. Multiphase Flow, 19:3. 527-529.

Hinze J. O. (1955) "Fundamentals of the hydrodynamic mechanism of splitting in dispersion processes." AIChE J., 1. 289-295.

Hovland G. E., McCarragher B. J. (1999) "Hidden Markov models as a process monitor in robotic assembly." Modeling, Identification and Control, 20:4. 201-223.

Hubbard M. G., Dukler A. E. (1966) "The characterization of flow regimes for horizontal two-phase flow." Proceedings of the 1966 Heat Transfer and Fluid Mechanics Institute (Editors Saad M. A. and Miller J. A.) pp.100-121, Stanford University Press. Palo Alto.

Ishii M., Mishima K. (1980) "Study of two-fluid model and interfacial area." Argonne National Laboratory, ANL-80- 111, NUREG/CR-1873.

Jayanti S., Hewitt G. F. (1992) "Prediction of the slug-to-churn flow transition in vertical two-phase flows." Int. J. Multiphase Flow, 18:6. 847-860.

Jeanmeure L. F. C., Dyakowski T., Zimmerman W. B. J., Clark W. (2002) "Direct flow-pattern identification using electrical capacitance tomography." Experimental Thermal and Fluid Science, 26:6-7. 763-773.

Jelinek F., Bahl L. R., Mercer R. L. (1982) "Continuous speech recognition: Statistical methods." Handbook of Statistics II.

Jones O. C., Zuber N. (1975) "The interrelation between void fraction fluctuations and flow patterns in two-phase flow." Int. J. Multiphase Flow, 2. 273-306.

Kelessidis V. C., Dukler A. E. (1989) "Modeling flow pattern transitions for upward gas-liquid flow in vertical concentric and eccentric annuli." Int, J. Multiphase Flow, 15:2. 173-191.

King C. H., Ouyang M. S., Pei B. S., Lee S. C. (1988) "Identification of two-phase flow regimes by neutron noise analysis." Nuclear Technology, 86:1. 211-226.

King C. H., Ouyang M. S., Pei B. S., Wang Y. W. (1988) "Identification of two-phase flow regimes by an optimum modeling method." Nuclear Technology, 82:2. 211-226.

Kondic N. D., Lassahn G. D. (1978) "Nonintrusive density distribution measurement in dynamic high temperature systems." 24th International Instrumentation Symposium, Albuquerque, N .M.

Kosaly G. (1980) "Noise investigation in boiling water and pressurized water reactors." Prog. Nucl. Energy, 5. 145-199.

Kozma R., van Dam H., Hoogenboom J. E. (1992) "Identification of flow patterns by neutron noise analysis during actual coolant boiling in thin rectangular channels." Nuclear Technology, 100:1. 97-110.

Kwon K. C., Kim J. H. (1999) "Accident identification in nuclear power plants using hidden Markov models." Engineering Applications of Artificial Intelligence, 12:4. 491-501.

Lassahn G. D. (1977) "LOFT three-beam densitometer data interpretation." EG&G Idaho, Inc., TREE-NUREG-1111.

Le Corre J. M., Aldorwish Y., Kim S., Ishii M. (1999) "Two phase flow pattern identification using a fuzzy methodology." Intl. Conf. Info. Intel. Sys., 155-161.

Lee J. M., Kim S. J., Hwang Y. (2002) "Mechanical signal analysis using hidden Markov model." 9th Intl. Congress on Sound and Vibration.

Lee J. M., Kim S. J., Hwang Y., Song C. S. (2004) "Diagnosis of mechanical fault signals using continuous hidden Markov model." Journal of sound and Vibration, 276. 1065-1080.

Levinson S. E., Rabiner L. R., Sondhi M. M., (1983) "An introduction to the application of the theory of probabilistic functions of a Markov process to automatic speech recognition." Bell System Technical Journal, 62: 4, 1035-1074.

Li Z., Wu Z., He Y., Fulei C.(2005) "Hidden Markov model-based fault diagnostics method in speed-up and speed-down process for rotating machinery." Mechanical Systems and Signal Processing, 19:2. 329-39.

Lu Z., Zhang X. (1994) "Identification of flow patterns of two-phase flow by mathematical modeling." Nuclear Engineering and Design, 149. 111-116.

Mandhane J. M., Gregory G. A., Aziz K. (1974) "A flow pattern map for gas -liquid flow in horizontal pipes, Int. J. Multiphase Flow, 1. 537-553.

Mao Z. S., Dukler A. E. (1993) "The myth of churn flow." Int. J. Multiphase Flow, 19:2. 377-383.

Matsui, G. (1984) "Identification of flow regimes in vertical gas-liquid two-phase flow using differential pressure fluctuations." Int. J. Multiple Flow, 10:6. 711-719.

Matusziwicz A., Flamand J. C., Bource J. A. (1987) "The bubble-slug flow pattern transition and instabilities of void fraction waves." Int, J. Multiphase Flow, 13:2. 199-217.

McQuillan K. W., Walley P. B. (1985) "Flow patterns in vertical two-phase flow." Int. J. Multiphase Flow, 11:2. 161-175.

Mishima K., Ishii M. (1984) "Flow regime transition criteria for upward two-phase flow in vertical tubes." Intl. J. Multiphase Flow, 27:5. 723-737.

Morris D., Teyssedou A., Lapierre J., Tapucu A. (1987) "Optical fiber probe to measure local void fraction profiles." Applied optics, 26:21. 4660-4664.

Ocak H., Loparo K. A. (2001) "A new bearing fault detection and diagnosis scheme based on hidden Markov modeling of vibration signals." IEEE Intl. Conference on Acoustics, Speech and Signal Processing, 5. 3141-3144.

Ocak H., Loparo K. A. (2005) "HMM-based fault detection and diagnosis scheme for rolling element bearings." Journal of Vibration and Acoustics, Transactions of the ASME, 127:4. 299-306.

Owsley L. M. D., Atlas L. E. Bernard G. D. (1997) "Self-organizing feature maps and hidden Markov models for machine-tool monitoring." IEEE trans. Signal processing, 45:11. 2787-2798.

Piper T. C. (1974) "Dynamic gamma attenuation density measurements." Aerojet Nuclear Co., ANCR-1160.

Prassinos P. G., Liao C. K. (1979) "An investigation of two-phase flow regimes in LOFT piping during loss-of-coolant experiments." EG&G Idaho, Inc., NUREG/ CR-0606, TREE- 1244.

Purushotham V., Narayanan S., Prasad S. A. N. (2005) "Multi-fault diagnosis of rolling bearing elements using wavelet analysis and hidden Markov model based fault recognition." NDT and E International, 38:8. 654-664.

Rabiner L. R. (1989) "A tutorial on hidden Markov models and selected applications in speech recognition." Proceeding of IEEE, 77:2. 257-286.

Radovcich N. A., Moissis R. (1962) "The transition from two-phase bubble flow to slug flow." Department of Mechanical Engineering, Report 7-7673-22, MIT Cambridge. Mass.

Rouhani S. Z., Sohal M. S. (1983) "Two-phase flow patterns: a review of research results." Progress in Nuclear Energy, 11:3. 219-259.

Sevik M., Park S. H. (1973) "The splitting of drops and bubbles by turbulent fluid flow." Trans. ASME, J. Fluids Eng, 95. 53-60.

Smyth P. (1993) "Hidden Markov models and neural networks for fault detection in dynamic systems." Neural Networks for Processing III Proceedings of the 1993 IEEE-SP Workshop, 582-592.

Soldati A., Paglianti A., Giona M. (1996) "Identification of two phase flow regimes via diffusional analysis of experimental time series." Experiments in Fluids, 21:3. 151-160.

Staub F. W., Zuber N. (1964) "A program of two-phase flow investigation." General Electric Co., Report, EURAEC 1171, GEAP 4631.

Taitel Y., Borena D., Dukler A. E. (1980) "Modeling flow pattern transitions for steady upward gas-liquid flow in vertical tubes." AIChE J., 26. 345-354.

Trafalis T. B., Oladunni O., Papavassiliou D. V. (2005) "Two-phase flow regime identification with a multiclassification support vector machine (SVM) model." Industrial and Engineering Chemistry Research, 44:12. 4414-4426.

Tutu, N. K. (1984) "Pressure fluctuations and flow pattern recognition in vertical two phase gas-liquid flows." Int. J. Multiple Flow, 8. 443-447.

Ulbrich R., Krotkiewicz M., Szmolke N., Anweiler S., Masiukiewicz M., Zajac D. (2002) "Recognition of two-phase flow patterns with the use of dynamic image analysis." Journal of Process Mechanical Engineering, 216:4. 227-234.

Vince M. A., Lahey R. T., Jr, (1980) "Flow regime identification and void fraction measurement techniques in two-phase flow." Rensselaer Polytechnic Institute, NUREG/CR-1692.

Vince M. A., Lahey R. T., Jr, (1982) "On the development of an objective flow regime indicator." Int. J. Multiphase Flow, 8:2. 93-124.

Wang L., Mehrabi M. G., Asibu E. K. (2002) "Hidden Markov model-based tool wear monitoring in turning." Transactions of the ASME. Journal of Manufacturing Science and Engineering, 124:3. 651-658.

Wang Y. W., Pei B. S., King C. H., Lee S.C. (1990) "Identification of two-phase flow patterns in a nuclear reactor by high-frequency contribution fraction." Nuclear Technology, 89:2. 217-226.

Wang Y. W., Pei B. S., King C. H., Pei B.S. (1988) "Identification of two-phase flow patterns by single void fraction sensor." Nuclear Technology, 83:1. 56-64.

Weisman J., Kang S. Y. (1981) "Flow pattern transitions in vertical and upwardly inclined tubes." Intl. J. Multiphase Flow, 7. 271-291.

Xie C. G., Plaskowski A., Beck M. S. (1989) "8-electrode capacitance system for two-component flow identification." II. Flow regime identification. IEE proceeding A, 136:4. 184-190.

Ying J., Kirubarajan T., Pattipati K. R., Patterson-Hine, A.(2000) "Hidden Markov model-based algorithm for fault diagnosis with partial and imperfect tests." IEEE Transactions on Systems, Man and Cybernetics Part C: Applications and Reviews, 30:4. 463-473.

Zhang X., Xu R., Kwan C., Liang S.Y., Xie Q., Haynes L.(2005) "An integrated approach to bearing fault diagnostics and prognostics." Proceedings of the 2005 American Control Conference IEEE, 4:4. 2750-5.

Appendix A

Mathematical Proof of Equations (2-17) and (2-23)

Induction:

$$\alpha_t(j) = \left[\sum_{i=1}^{N} \alpha_{t-1}(i) a_{ij}\right] b_j(o_t), \quad 2 \le t \le T \quad and \qquad 1 \le j \le N \quad (2\text{-}17)$$

In fact, since $\alpha_t(i) = P(o_1 o_2 \ldots o_t, q_t = S_i \mid \lambda)$, for a given λ and $t \ge 2$, the $\alpha_t(j)$ can be written as:

$$\alpha_t(j) = \sum_{i=1}^{N} P(o_1 \ldots o_t, q_{t-1} = S_i, q_t = S_j) \qquad (A\text{-}1\text{-}a)$$

$$= \sum_{i=1}^{N} P(q_{t-1} = S_i, q_t = S_j) P(o_1 \ldots o_t \mid q_{t-1} = S_i, q_t = S_j) \qquad (A\text{-}1\text{-}b)$$

$$= \sum_{i=1}^{N} P(q_t = S_j \mid q_{t-1} = S_i) P(q_{t-1} = S_i) P(o_1 \ldots o_{t-1} \mid q_{t-1} = S_i) P(o_t \mid q_1 = S_j)$$

(A-1-c)

$$= \sum_{i=1}^{N} a_{ij} P(o_1 \ldots o_{t-1}, q_{t-1}) b_j(o_t) \quad \text{(A-1-d)}$$

$$= \sum_{i=1}^{N} a_{ij} \alpha_{t-1}(i) b_j(o_t) \quad \text{(A-1-e)}$$

$$= \left[\sum_{i=1}^{N} a_{ij} \alpha_{t-1}(i) \right] b_j(o_t) \quad \text{(A-1-f)}$$

That is to say

$$\alpha_t(j) = \left[\sum_{i=1}^{N} a_{ij} \alpha_{t-1}(i) \right] b_j(o_t), \quad 2 \le t \le T \quad \text{(A-1-g)}$$

In the similar way, since $\beta_t(i) = P(o_{t+1} \ldots o_T \mid q_t = S_i, \lambda)$ for a given λ and $t < T$, the $\beta_t(i)$ can be written as:

$$\beta_t(i) = \sum_{j=1}^{N} P(o_{t+1} \ldots o_T, q_{t+1} = S_j, q_t = S_i) / P(q_t = S_i) \quad \text{(A-2-a)}$$

$$= \sum_{j=1}^{N} P(o_{t+1} \ldots o_T \mid q_{t+1} = S_j, q_t = S_i) P(q_{t+1} = S_j, q_t = S_i) / P(q_t = S_i)$$

(A-2-b)

$$= \sum_{j=1}^{N} P(o_{t+1} \ldots o_T \mid q_{t+1} = S_j) P(q_{t+1} = S_j \mid q_t = S_i) \quad \text{(A-2-c)}$$

$$= \sum_{j=1}^{N} P(o_{t+1} \mid q_{t+1} = S_j) P(o_{t+2} \ldots o_T \mid q_{t+1} = S_j) P(q_{t+1} = S_j \mid q_t = S_i)$$

(A-2-d)

$$= \sum_{j=1}^{N} b_j(o_{t+1})\beta_{t+1}(j)a_{ij} \qquad \text{(A-2-e)}$$

That is to say

$$\beta_t(i) = \sum_{j=1}^{N} a_{ij}\beta_{t+1}(j)b_j(o_{t+1}), \quad 1 \le t < T \qquad \text{(2-23)}$$

Appendix B

Photographs

For each two-phase flow condition a photo, the most representative one, was selected and is presented here. The photos are numbered according to condition numbers given in Table 3.2. (Recalled here).

Table 3-2 Test numbers and two-phase flow conditions simulated in test section

		Void Fraction (%)								
		10	**20**	**30**	**40**	**50**	**60**	**70**	**80**	**90**
Mixture Velocity (m/s)	**0.5**	1	2	3	4	5	6	7	8	9
	1	10	11	12	13	14	15	16	17	18
	1.5	19	20	21	22	23	24	25	26	27
	2	28	29	30	31	32	33	34	35	36
	3	37	38	39	40	41	42	43	44	45
	4	46	47	48	49	50	51	52	53	54
	5	-	55	56	57	58	59	60	-	-

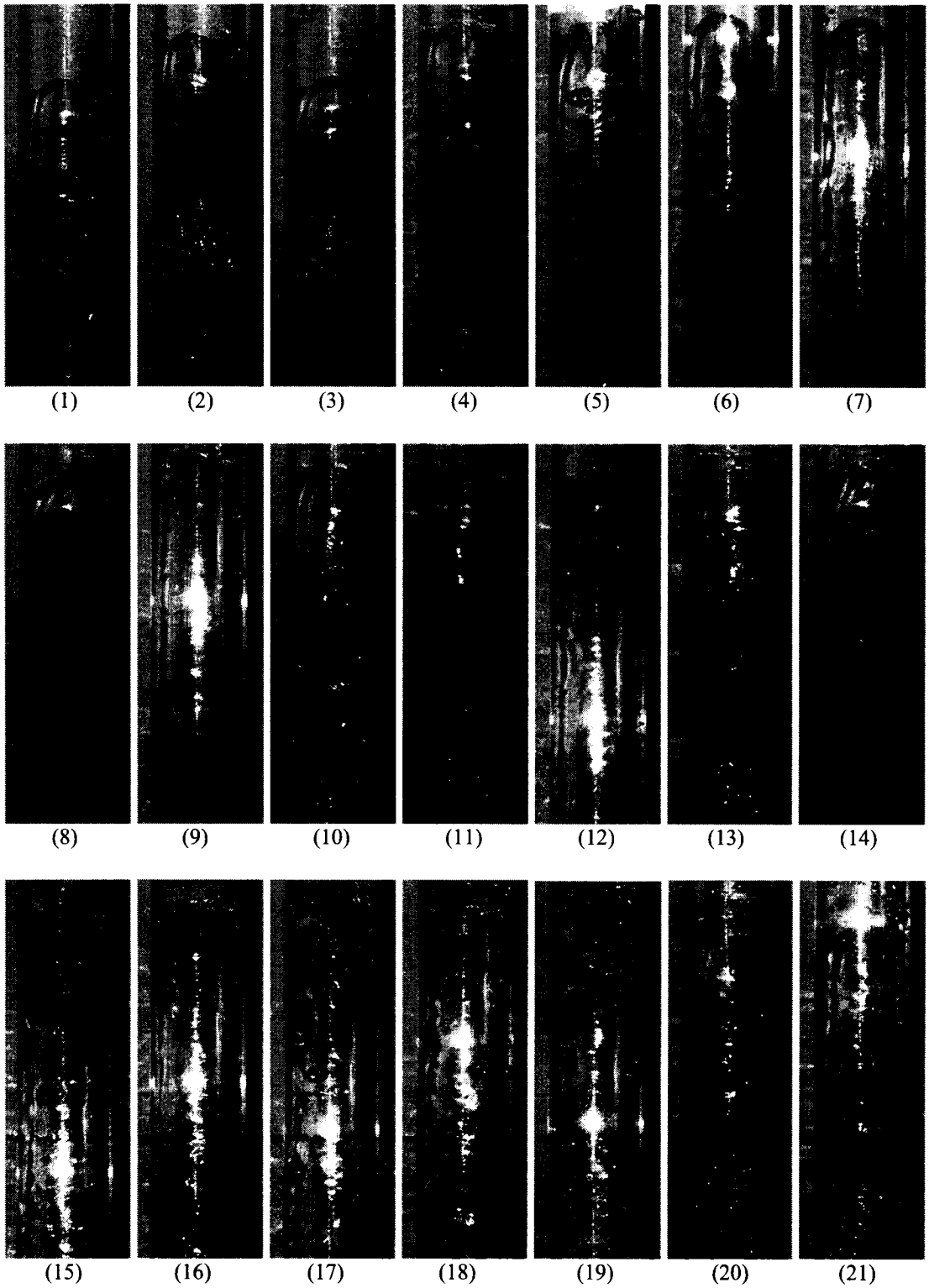

Figure B-1 Photographs of two-phase flow conditions, simulated in test section.

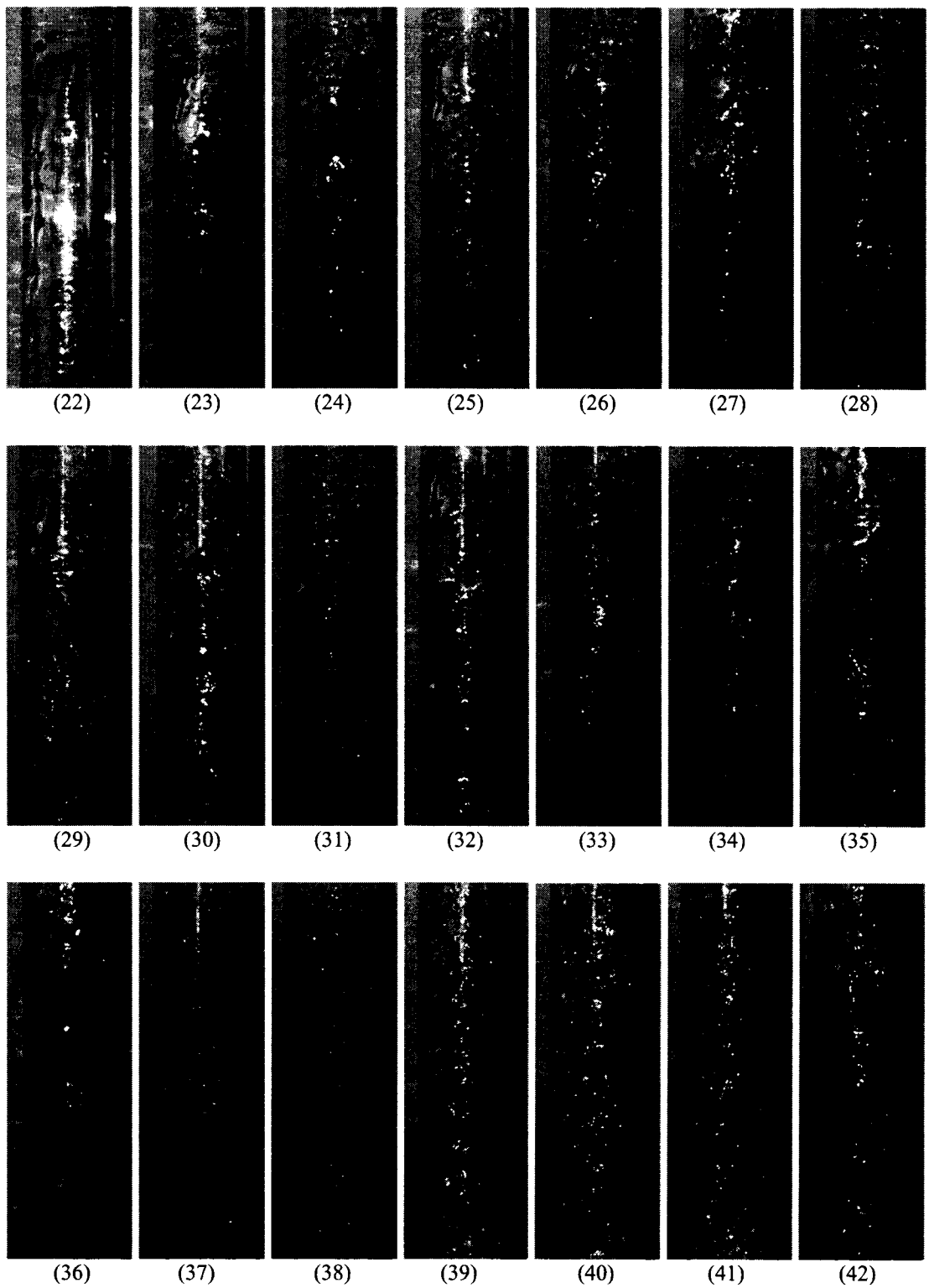

Figure B-1 Photographs of two-phase flow conditions, simulated in test section (continued).

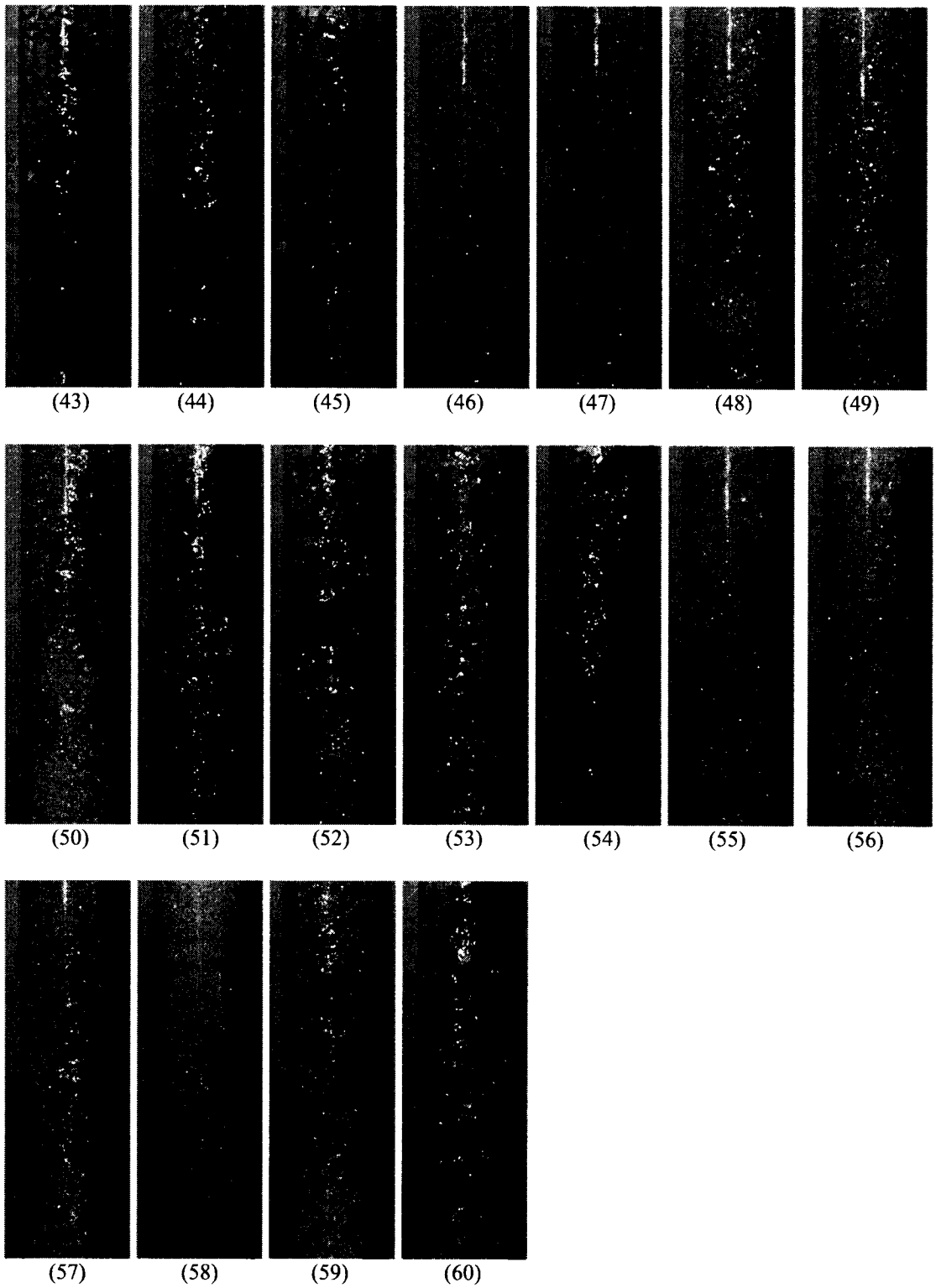

Figure B-1 Photographs of two-phase flow conditions, simulated in test section (continued).

Appendix C

Numerical Results

The numerical results of all trial are presented in terms of log-likelihood. These results are obtained using the Matlab software.

Table C-1 Log-likelihood results from the Autoregressive method.

Condition Numbers as in Table 3.2.	Reference Condition Numbers								
	1	7	13	46	55	47	45	53	54
		Slug			Finely Dispersed Bubble			Churn	
1	**4015.1**	2064.9	1633.6	-4382	-21232	-3130.5	-1365.4	-3891.4	819.95
2	2707.1	2797.6	**2957.3**	-7476.9	-25077	-5022.4	-2054.9	-4781.9	447.49
3	1275.1	3087	**3228.9**	-7031.6	-24264	-4788.2	-2112.2	-4714.6	392.85
4	370.3	**3215.9**	3007	-4013.8	-21690	-4465.4	-761.04	-4066.5	839.44
5	768.17	**3295.1**	2954.3	-3541.9	-21343	-3262.2	-119.51	-2992.4	945.45
6	-159.85	**3114**	2916	-4051	-24777	-5063.1	-125.83	-3121.5	1401.5
7	383.12	**3702.4**	2419.1	-2262.9	-23196	-4058.3	116.22	-2810.8	1404.9
8	-277.48	**2810.9**	2172.9	-1581	-23421	-4541.6	583.19	-2164.8	1723
9	719.83	2464.1	**2490.6**	-5507.9	-27603	-6539.8	-229.9	-2763.3	1178.5
10	1186.9	2478	**2965**	-9116.4	-23686	-5673.2	-3035.6	-6557.8	40.591
11	-95.852	1919.4	**2505.9**	-10779	-25185	-6732.9	-3404.2	-7396.4	-394.92
12	-578.23	2291.5	**3091.1**	-9596.3	-23656	-5693.5	-2459.7	-5812.3	35.206
13	189.42	2933.4	**3785.7**	-4834.5	-21336	-3821.3	-549.05	-3099.6	1144.7
14	-2702.9	**2429.9**	2374	-2912	-24774	-6244	720.54	-1188	1323
15	-1913	1939	912.62	185.94	-22861	-4219.3	1837.1	-10.893	**1987.9**
16	-2316.7	1140.3	168.71	-64.253	-26822	-7318.3	1885.2	109.31	**2432.1**
17	-2591	2386.9	1139.8	-603.39	-30066	-7458.9	1943.9	-84.375	**2445.2**
18	-4042.5	1437.5	229.64	-1231.2	-30829	-9067.6	1825.7	234.44	**2152.7**
19	602.64	2211.7	**2975.6**	-10187	-25538	-6223.6	-2538.6	-6278.8	-5.6833
20	1210.2	2558.6	**3240.4**	-9693.5	-23834	-4725	-2738.4	-5756.2	22.801
21	-298.58	**2561.9**	2084.3	-968.01	-20378	-3510.1	992.46	-1609.8	1450.1
22	-664.46	1926.4	1159.9	-945.57	-24014	-5097.8	1457	-484.48	**2136.2**
23	-3947.3	690.44	-641.36	145.44	-26355	-6310.7	2052.8	820.73	**2524**
24	-4932.9	-105.32	-2316.7	902.96	-29415	-7854.2	2541.8	1447.1	**2752.8**
25	-8278.7	-1707.5	-3552.3	-215.2	-34202	-12996	2412.5	1762	**2569**
26	-10343	-3377.3	-6570.3	-1598.9	-41016	-18415	2693.7	2134.8	**2749**
27	-3802.8	696.05	-1753.5	-729.97	-34817	-10901	2463	1137.9	**2731.5**
28	997.78	2967.1	**3211.9**	-4624.7	-20741	-3759.8	-1144.5	-4194	755.28
29	2054.2	**2917.9**	2807	-4116.6	-20029	-2635.9	-786.04	-3351.1	996.94
30	-299.26	1127.1	606.93	1585.2	-18374	-2060.2	1632.9	-10.124	**2131.5**
31	-7624.7	-4831.4	-3877.4	1676.5	-24697	-6592.4	2114.9	1833.2	**2554.4**
32	-11294	-7517.9	-6135.7	1582.5	-26876	-7592.3	1867.9	**2128.1**	2053.2
33	-13318	-8093.7	-8555.8	235.68	-33884	-13997	2401.6	2796.4	**2799**
34	-14636	-6514.9	-8310.3	-640.84	-37921	-16858	2348.9	2393.4	**2516.4**
35	-12672	-5298.6	-7287.9	-1820.6	-42082	-20905	2482.6	2275.2	**2640.4**
36	-10954	-2502.5	-5627.6	-3491	-50517	-24819	2749.6	1978.3	**2930.5**
37	620.76	**2545.3**	1725.7	624.19	-18831	-1866.9	1302.8	-1144.2	1846.8
38	-5908.5	-9632.5	-3780.8	692.1	-10103	**1415.9**	-315.62	-543	1106
39	-21754	-23140	-10538	**1941.3**	-7895.2	954.59	-1079.1	256.14	780.31
40	-49139	-42887	-21640	**487.55**	-11013	-2140	-2763.1	427.42	471.99
41	-65643	-57775	-27914	-1238.6	-16122	-8474.4	-4471.4	-219.1	**-53.999**
42	-54958	-43594	-26146	-2634.6	-34712	-17916	-1948.8	**1564.7**	1018.5
43	-29006	-21556	-17350	-2056.5	-39033	-20005	879.74	**2658**	2100.9
44	-22298	-11195	-15721	-4939.9	-58447	-31430	2421	**2836.7**	2589
45	-17319	-5062.8	-11224	-8498.4	-66954	-36710	**3265.6**	1665.6	1809.4
46	-11462	-7942.2	-6501.1	**3880.9**	-15915	-3876	1402.5	1347.2	1769.8
47	-42969	-55219	-25187	-1189.5	-302.29	**4058.5**	-6253.1	-3451.1	-1692
48	-70997	-71068	-49183	-5951.5	1441.4	**2661.3**	-13444	-7354.2	-4156.6
49	-71068	-71068	-61917	-6087.5	-4100.6	**-2393.3**	-15837	-7321.2	-4427.1
50	-71068	-71068	-59757	-7908.3	-24101	-15540	-13160	-3246.3	**-3091.8**
51	-70695	-68913	-45509	-7140.4	-38308	-25660	-7031.3	**-11.984**	-917.43
52	-47984	-35856	-23637	-3754.2	-45217	-25458	-976.47	**2483**	1412.2
53	-26110	-14765	-19794	-6448.7	-65387	-37714	2214.6	**3472.4**	2324.2
54	-23481	-8467.6	-14196	-11478	-61319	-43909	1761.7	716.65	**3154**
55	-71068	-71068	-67683	-9844.2	**4062.3**	1068.4	-20242	-12262	-7135.2
56	-71068	-71068	-71068	-15189	**1203.8**	-853.92	-29402	-18037	-10098
57	-71068	-71068	-71068	-12229	**-4630.4**	-5715.4	-27124	-12855	-8531.7
58	-71068	-71068	-70372	-12099	-24399	-16871	-19329	-6158.7	**-5493.8**
59	-71068	-70451	-56527	-11562	-48037	-32572	-9745	**-1096.2**	-1982.9
60	-54345	-41752	-33767	-8909.7	-66006	-39391	-1102.6	**1983.5**	943.31

Table C-02 Log-likelihood results from the passage time based method (N=2).

Condition Numbers as in Table 3.2.	Reference Condition Numbers								
	1	7	13	46	47	55	45	53	54
	Slug			Finely Dispersed Bubble			Churn		
1	**1.4604**	-818.89	-316.16	-1333.3	-899.66	-1692.1	-545.29	-2885.4	-480.42
2	-472.8	-913.79	**-387.42**	-2749.8	-1775.6	-2703.6	-1139.6	-3613.6	-988.91
3	-913.69	-1119.6	**-378.37**	-3777.7	-2587.3	-3547.4	-1604.2	-3898	-1488.9
4	-1711.9	**-435.95**	-1020.3	-7513.2	-3509.7	-4924.7	-2652.8	-2210.3	-2624.3
5	-1105	-1313.9	**-361.01**	-3742.4	-2392.9	-3368.3	-1604.2	-3222.5	-1498.3
6	-1500.7	**-400**	-1093.5	-6503.6	-3000.4	-4196.2	-2242.6	-2211	-2171.3
7	-1244.8	**-239.15**	-977.57	-5614.6	-2566.1	-3631.1	-1949.6	-2054.1	-1982.8
8	-1153.9	**-322.08**	-952.16	-5233.5	-2254.8	-3136.1	-1646.2	-1757.8	-1655.9
9	-1051.5	**-349.19**	-850.28	-4644.4	-2013.1	-2923.7	-1501.8	-1617.6	-1534.1
10	**-239.01**	-837.13	-323.44	-2241.5	-1755.3	-2832.7	-1013.3	-4217.6	-891.25
11	-743.37	-1005.5	**-380.99**	-3844.5	-2601.4	-3766.9	-1618.9	-4460.6	-1419.7
12	-1035.5	-1211.9	**-386.14**	-4241.5	-2861	-4055.7	-1836	-4282.4	-1594.8
13	-1038.3	-1295.6	**-308.2**	-3460.6	-2268.9	-3169.2	-1527.4	-3232.1	-1401.5
14	-1214.1	-1454.8	**-535.47**	-3339	-2128.1	-2981.6	-1375.9	-2661.7	-1270.6
15	-1042.1	-1345.8	**-397.73**	-2387.8	-1448.2	-1934.1	-975.93	-1814	-966.9
16	-1010.9	**-583.13**	-879.33	-3339.4	-1305.6	-1855.2	-849.26	-1078.1	-908.91
17	-1117.4	**-505.33**	-955.01	-3966.6	-1650.7	-2339.4	-1125.3	-1353.5	-1183.9
18	-1108.9	-1270.3	**-540.86**	-2531.4	-1218.3	-1791.3	-892.24	-1217.3	-903.48
19	**-276.89**	-932.17	-381.03	-2146.9	-1730.4	-2646.2	-972.27	-4167.6	-824.88
20	-592.91	-980.46	**-348.88**	-3143.1	-2102.5	-3263.6	-1343.1	-3934.1	-1231.2
21	-1466.2	**-575.78**	-927.05	-5502.6	-2403.7	-3360.5	-1771.6	-1403.2	-1798.2
22	-1368.9	**-461.83**	-1002.8	-5116.3	-2166.9	-3041.1	-1538	-1363.6	-1581
23	-889	-1375.6	**-445.05**	-1949.6	-1090.3	-1673.3	-768.22	-1694.3	-690.8
24	-925.8	-1344.4	**-456.45**	-1649.5	-806.65	-1249.1	-627.19	-1188.4	-649.86
25	-997.17	**-521.25**	-887.58	-3006.6	-1087.2	-1534	-620.03	-833.7	-719.14
26	-923	-705.72	-831.58	-2132.2	-690.59	-916.71	**-231.51**	-686.88	-307.77
27	-1210	-1081.8	-683.95	-2608.3	-1083.6	-1439.1	-748.5	**-611.7**	-806.76
28	**-151.11**	-894.95	-402.2	-1381.9	-1154.3	-1916.7	-609.42	-3280.3	-530.08
29	-1619.8	**-453.69**	-843.43	-6492.8	-2906.3	-3926.9	-2262.6	-1218.9	-2289.1
30	-1222.5	**-435.64**	-841.06	-4496.4	-1796.4	-2461.8	-1433.9	-901.67	-1428.5
31	-875	-1296	-487.39	-1515.7	-767.38	-1137.1	**-476.54**	-1213.2	-501.08
32	-757.22	-1170.8	-380.29	-1060.3	-415.95	-660.24	**-313.47**	-671.42	-396.5
33	-895.34	-1261.2	-459.09	-1205.7	-518.12	-652.8	**-375.77**	-567.07	-411.61
34	-905.19	-612.63	-869.33	-2119	-545.38	-819.22	**-142.71**	-395.38	-158.5
35	-1142.8	-1248.1	-619.73	-1621.5	-549.62	-919.78	-406.71	**-135.15**	-536.32
36	-934.27	-949.19	-781.92	-1693.8	-616.64	-869.87	**-202.62**	-822.8	-206.73
37	**-62.268**	-1221.8	-213.71	-192.06	-396.08	-818.99	-154.5	-1988.8	-105.98
38	-238.05	-1003.8	-245.41	-496.47	-169.86	-492.6	**-123.13**	-1151.8	-147.65
39	-807.04	-315.94	-689.2	-2746.9	-710.97	-1016.1	-385.42	**-136.76**	-465.36
40	-716.26	-1160.2	-441.43	-577.61	-27.573	-139.94	**-9.5654**	-104.81	-79.701
41	-948.46	-660.11	-809.79	-1685.6	-330.59	-434.72	**93.438**	-75.15	41.565
42	-1025.7	-890.78	-821.55	-1263.8	-230.63	-190.38	**238.23**	16.615	233.7
43	-1080.9	-1134.5	-635.47	-1265.2	-329.05	-392.97	-66.118	**151.92**	-158.16
44	-976.6	-936.95	-852.25	-1259.8	-265.52	-340.61	**176.72**	-237.59	151.07
45	-962.95	-1178.2	-817.54	-1062.9	-397.46	-461.41	**55.342**	-575.83	-23.762
46	-187.11	-1505.8	-123.94	**496.94**	196.8	55.317	103.98	-930.16	105.93
47	-240.18	-941.59	-225.08	-1.8757	**403.87**	260.21	163.07	-161.61	72.77
48	-669.41	-540.33	-550.32	-1356.1	-102.55	-206.42	62.843	**85.883**	3.8433
49	-872.69	-838.05	-708.13	-1073.6	-76.372	-45.63	**214.28**	132.2	177.69
50	-1069.5	-998.83	-852.61	-1158.9	-190.11	-134.55	**283.41**	117.67	252.93
51	-1096.4	-1018.1	-881.36	-1017.3	-200.04	-87.023	**303**	44.177	266.37
52	-1037.4	-1071.3	-849.23	-992.87	-167.67	-96.867	**291.35**	-11.331	273.3
53	-1289.3	-1193.9	-803.48	-1513.5	-455.78	-475.21	-47.749	**301.4**	-178.87
54	-1013.6	-1172.8	-882.53	-1132	-364.58	-471.72	98.381	-607.08	**189.06**
55	-390.09	-985.32	-260.79	135.03	432.21	**542.75**	247.55	197.98	130.55
56	-673.65	-568.69	-607.53	-1021.6	113.28	91.742	**304.71**	227.28	281.42
57	-915.98	-930	-663.07	-877.93	-19.369	16.421	175.97	**229.39**	142.01
58	-1144.6	-1171.5	-842.93	-825.01	-109.72	17.26	**285.09**	149.93	272.55
59	-1433.3	-1278.7	-864.9	-1353.3	-423.65	-287.02	98.586	**380.69**	15.712
60	-1112.3	-1219.7	-871.57	-888.53	-167.24	-82.437	**258.79**	-12.182	238.88

Table C-3 Log-likelihood results from the passage time based method (N=3).

Condition Numbers as in Table 3.2.	Reference Condition Numbers								
	1	7	13	46	47	55	45	53	54
		Slug			Finely Dispersed Bubble			Churn	
1	**37.828**	-1110.2	-366.69	-1345.5	-1004.1	-1955.9	-714.51	-2871.8	-638.37
2	**-448.21**	-1154.5	-459.43	-2822.8	-1778.4	-3228.2	-1292	-3431.4	-1219.4
3	-866.93	-1371.7	**-410.4**	-3942	-2413.4	-4205.3	-1688.6	-3632.2	-1708.9
4	-1852.7	**-452.3**	-1235	-7310.5	-3050.6	-6056.7	-2328.9	-2774.1	-2550.2
5	-1059.8	-1518.1	**-332.84**	-3870.9	-2261.1	-4015.8	-1587	-3125	-1733.1
6	-1650.3	**-413.84**	-1375.7	-6407.6	-2630.4	-5140.9	-2034.8	-2685	-2132.2
7	-1422.9	**-205.92**	-1250.3	-5439.5	-2194.3	-4481.7	-1739.4	-2470	-1861.4
8	-1303.2	**-326.45**	-1200.5	-5121.7	-1913	-3916.9	-1491.3	-2102.8	-1526.1
9	-1213.4	**-347.87**	-1052	-4449.9	-1692.9	-3673.3	-1354.3	-1946.6	-1474.5
10	**-255.8**	-1230.7	-399.55	-2307.4	-1786.1	-3178.2	-1233.8	-3981.3	-1092.7
11	-710.3	-1363.1	**-391.5**	-3987.2	-2522.8	-4408.6	-1717.7	-4199	-1712.1
12	-1003	-1562.7	**-375.04**	-4419.3	-2778.5	-4751.7	-1934	-4061.2	-1906.7
13	-994.63	-1457.4	**-246.04**	-3489.7	-2145.4	-3862.8	-1561.1	-3198.2	-1646
14	-1216.5	-1536.6	**-523.57**	-3502	-2017.5	-3359.7	-1396.5	-2622	-1450.3
15	-1052.1	-1372	**-392.57**	-2509.6	-1333	-2225	-979.36	-1797.3	-1083.9
16	-1151.3	**-581.44**	-1105.9	-3228	-1106.6	-2335.9	-773.23	-1332.7	-774.3
17	-1275.1	**-496.85**	-1194.7	-3835	-1387.2	-2912.2	-1027.6	-1663.1	-1026.8
18	-1129.2	-1246.5	**-599.7**	-2515.5	-1129.6	-2143	-800.94	-1307.2	-952.56
19	**-268.23**	-1250	-446.34	-2242.8	-1749.5	-3016.5	-1202.4	-4010.8	-1020.8
20	-582.84	-1323.6	**-388.08**	-3174.1	-2071.4	-3829.8	-1420.2	-3719.4	-1472.7
21	-1561.4	**-574.89**	-1150	-5374.5	-2087.6	-4164.2	-1586.1	-1821.5	-1689.8
22	-1524.3	**-471.03**	-1282.1	-4941.1	-1828.6	-3813.9	-1346.2	-1804.8	-1438
23	-898.96	-1449.4	**-452.19**	-1977.4	-1066.1	-1902.7	-791.63	-1746.2	-822
24	-922.44	-1403.5	**-463.57**	-1671.7	-782.81	-1484.4	-605.82	-1205.7	-766.64
25	-1154.1	-540.25	-1091.8	-2870.1	-888.96	-1982.1	**-533.89**	-1023.4	-613.85
26	-1031.7	-737.77	-961.5	-2019.7	-561.02	-1244.6	**-178.75**	-791.63	-233.63
27	-1247.7	-1103.2	-777.93	-2579.1	-967.47	-1756	**-685.78**	-767.18	-798.68
28	**-182.7**	-1137.2	-468.99	-1441.8	-1232.1	-2110.6	-834.58	-3342.1	-656.45
29	-1707.1	**-429.28**	-1053.1	-6353.4	-2447	-4876.1	-1914.4	-1678.5	-2063.1
30	-1379.9	**-422.19**	-1078.7	-4368.8	-1545.3	-3079.2	-1262.5	-1321.2	-1279.1
31	-867.47	-1332.1	**-493.62**	-1554.2	-701.42	-1297.9	-513.92	-1182.6	-591.04
32	-770.25	-1217.5	-387.05	-1077.1	-412.93	-766.02	**-314.39**	-679.18	-455.65
33	-938.61	-1267.3	-490.36	-1242.8	-466.12	-802.07	**-385.92**	-555.51	-454.75
34	-976.39	-645.19	-1004.3	-1998.5	-442.19	-1098.1	**-90.806**	-489.95	-90.651
35	-1190.3	-1286	-709.01	-1514.8	-520.08	-1117.1	-363.87	**-112.47**	-573.2
36	-1040.1	-989.91	-873.73	-1619.1	-533.57	-1140.5	-160.65	-873.68	**-153.56**
37	**-85.982**	-1416.4	-233.56	-179.9	-456.84	-793.28	-346.8	-2026.3	-141.86
38	-241.79	-1065.1	-275.68	-475.21	**-171.07**	-514.72	-203.67	-1198.9	-207.07
39	-970.76	-357.04	-885.3	-2592.6	-505.52	-1419.8	-351.45	**-333.99**	-359.59
40	-750.37	-1174.7	-457.68	-535.67	-28.921	-224.09	**-27.372**	-103.31	-132.88
41	-1046.9	-734.09	-894.3	-1579.2	-230.68	-718.75	**138.12**	-130.41	106.51
42	-1135	-959.71	-897.97	-1184	-146.82	-369.73	**297.26**	26.887	274.99
43	-1130.5	-1214.3	-699	-1214.9	-275.42	-479.25	-62.031	**152.51**	-164.3
44	-1065.1	-981.32	-927.89	-1195.1	-193.78	-530.98	**224.66**	-243.77	184.66
45	-1011	-1220.1	-873.73	-1016.4	-379.85	-601.92	**118.91**	-561.86	-15.985
46	-205.25	-1572.5	-120.63	**532.74**	94.842	77.658	-81.307	-913.2	150.44
47	-253.99	-949.68	-250.03	49.653	**439.35**	219.28	124.51	-180.33	63.059
48	-760.17	-587.65	-662.4	-1260.1	-29.548	-406.54	**81.645**	11.73	13.329
49	-940.66	-904.01	-771.31	-983.29	-31.721	-249.15	**254.19**	106.88	199.81
50	-1154.5	-1040.2	-933.43	-1102.3	-140.88	-303.99	**321.66**	121.88	271.14
51	-1171.7	-1123.8	-940.16	-976.19	-129.29	-230.1	**345.34**	56.935	293.72
52	-1087.9	-1143.3	-911.46	-954.19	-146.3	-227.64	**306.02**	15.869	302.22
53	-1363.8	-1273	-876.31	-1445.1	-393.39	-624.99	-59.327	**370.31**	-168.68
54	-1055.3	-1232.3	-949.66	-1068	-344.29	-615.53	102.34	-592.18	**240.19**
55	-417.44	-994.66	-281.35	155.84	421.28	**584.79**	225.71	202.19	142.81
56	-731.39	-637.39	-674.94	-914.13	152.39	-65.898	**306.66**	223.29	289.41
57	-943.94	-1042.1	-724.27	-781.62	5.4214	-119.13	159.76	**272.94**	151.71
58	-1208.6	-1248.8	-893.53	-777.63	-82.569	-103.02	**321.28**	163.33	281.46
59	-1495.5	-1398.3	-960.81	-1339.4	-364.36	-400.25	106.4	**379.58**	29.122
60	-1148.9	-1285	-920.91	-834.35	-154.32	-222.64	**280.37**	16.072	270.88

Table C-4 Log-likelihood results from the passage time based method (N=5).

Condition Numbers as in Table 3.2.	Reference Condition Numbers								
	1	7	13	46	47	55	45	53	54
	Slug			Finely Dispersed Bubble			Churn		
1	**162.79**	-1271.4	-388.64	-1210.6	-1165.1	-2054.1	-1128.6	-2905.8	-887
2	-520.55	-1539.3	**-470.65**	-2413.8	-2120.1	-3315.4	-1913.5	-3806.1	-1436.9
3	-975.14	-1712.4	**-434.24**	-3281.5	-2952.3	-4240.2	-2325.9	-4050.2	-1802
4	-2143.6	**-469.74**	-1423.6	-6138.5	-3884.2	-6202.9	-2938.7	-3277	-3416.4
5	-1227.5	-1722.5	**-358.63**	-3263.2	-2669.3	-4067.5	-2172.8	-3470.5	-1827.7
6	-1898.1	**-467.18**	-1533.4	-5441.8	-3391.9	-5491.4	-2469.7	-3142.4	-2912.8
7	-1714.7	**-104.89**	-1361.5	-4793.5	-2853.5	-4827.4	-2133.4	-2876.3	-2530.9
8	-1521.1	**-356.32**	-1323.2	-4392.8	-2509.5	-4186.3	-1764.3	-2476.5	-2109.4
9	-1421.1	**-371.52**	-1170.9	-3935.9	-2228.2	-3975	-1626.5	-2289.4	-1896
10	**-314.45**	-1527.2	-424.74	-2034.3	-2094.1	-3238.6	-1898.8	-4257.7	-1264.6
11	-773.1	-1668.3	**-485.79**	-3303	-3013.1	-4524.7	-2512.3	-4677.2	-1873.3
12	-1127.1	-1939.1	**-403.98**	-3719.1	-3300.5	-4789.3	-2670	-4555.9	-2098.9
13	-1196.3	-1741.5	**-148.44**	-3053.1	-2510.4	-3917.9	-2142.7	-3544.2	-1741.1
14	-1484.6	-1698.8	**-540.06**	-3058.9	-2369.6	-3372.8	-1820.4	-2879.3	-1620.2
15	-1237.3	-1437.3	**-437.5**	-2231	-1527	-2259.1	-1256.9	-1927.6	-1157.3
16	-1310.8	**-513.27**	-1244.6	-2970.8	-1500.7	-2555	-877.31	-1519.2	-1037.5
17	-1503.5	**-476.5**	-1323.1	-3537	-1885.5	-3098.6	-1186.1	-1917.2	-1441.9
18	-1338.5	-1247.9	**-679.2**	-2281.4	-1302.9	-2098.4	-956.85	-1338.2	-1089.4
19	**-330.72**	-1538.1	-468.38	-2006	-2078.1	-3065.5	-1826.8	-4241.1	-1219.6
20	-651.24	-1592.3	**-421.08**	-2735.7	-2394.3	-3917.3	-2065.7	-4071.4	-1643.8
21	-1821.2	**-579.06**	-1325	-4655.6	-2739.4	-4233.3	-1835.8	-2185.6	-2180.2
22	-1733.5	**-453.95**	-1416.4	-4366.6	-2434.1	-3997.5	-1568.1	-2063.2	-1891.1
23	-1050	-1450.5	**-480.9**	-1845.3	-1172.2	-1910.5	-1038	-1762.3	-993.63
24	-1123.8	-1353.1	**-521.36**	-1624.5	-763.51	-1506.3	-793.97	-1216.7	-822.22
25	-1273.8	**-487.82**	-1241.9	-2700.1	-1238.5	-2178.4	-598.47	-1168.3	-782.27
26	-1149.4	-692.9	-1100.3	-1997.3	-769.45	-1320	**-202.23**	-851.5	-304.26
27	-1471	-1030.3	-888.52	-2352.6	-1214.2	-1854.4	**-772.6**	-859.87	-892.92
28	**-218.58**	-1428.7	-482.45	-1321.5	-1414.3	-2238.4	-1258.5	-3309.9	-909.41
29	-2061.4	**-459.18**	-1304.9	-5345.4	-3277.7	-4956.4	-2252.9	-2142.9	-2845.6
30	-1546.9	**-431.51**	-1210	-3855.5	-2128.7	-3295.5	-1499.5	-1603.8	-1646.9
31	-1048.4	-1287.9	**-563.49**	-1504.3	-823.3	-1308.9	-659.12	-1162	-659.23
32	-925.86	-1158.2	-430.48	-1070.3	-444.56	-844.67	**-420.12**	-645.17	-457.27
33	-1085.1	-1216.9	-553.73	-1222.8	-541.21	-839.72	-518.07	-586.42	**-496.15**
34	-1137.7	-589.77	-1174.4	-2001.6	-669.13	-1223.8	**-103.31**	-579.34	-143.6
35	-1419.1	-1175.3	-824.55	-1600.7	-583.33	-1043.8	-436.35	**-144.71**	-640.51
36	-1193.6	-897.26	-1031.2	-1685.9	-742.33	-1221	-223.53	-922.18	**-212.74**
37	**-138.79**	-1577.1	-276.41	-213.6	-495.32	-896.82	-600.76	-2035.9	-311.93
38	-360.26	-1086.7	-285.69	-490.03	**-220.71**	-599.64	-372.99	-1142.5	-344.23
39	-1077.5	**-292.77**	-1000	-2344.4	-829.93	-1587.8	-375.33	-462.25	-462.76
40	-879.56	-1064.1	-547.74	-654.01	**-84.1**	-285.25	-94.817	-112.36	-190.9
41	-1181.4	-607.58	-1070.7	-1651.9	-424.36	-726.02	**124.34**	-186.54	79.396
42	-1215	-808.19	-1087.1	-1311.1	-329.6	-466.31	**298.68**	-19.199	280.74
43	-1286.1	-1037.9	-818.5	-1285.5	-384.5	-563.71	-86.433	**119.65**	-191.17
44	-1178.3	-867.87	-1096.5	-1377	-345.03	-598.19	**199.32**	-259.19	150.28
45	-1156	-1139.2	-1007.5	-1127.7	-517.63	-704.22	**189.34**	-580.22	-54.324
46	-283.47	-1655.4	-133.61	**580.51**	86.843	-13.207	-218.03	-964.28	49.474
47	-362.12	-878	-285.16	-2.6874	**522.22**	157.12	83.751	-185.8	-29.461
48	-877.01	-469.6	-777.07	-1271.6	-206.57	-476.28	**76.347**	-54.891	17.19
49	-1056.7	-728.23	-936.46	-1126.6	-155.79	-283.5	**251.03**	77.88	186.23
50	-1264.6	-859.69	-1091.5	-1338	-303.87	-332.49	**319.38**	58.057	283.42
51	-1316.6	-952.32	-1146.8	-1201.9	-297.78	-337.82	**350.79**	34.68	304.38
52	-1264.4	-982.77	-1108.7	-1166.7	-277.95	-254.81	**297.72**	-12.89	276.58
53	-1544.6	-1104.6	-1003.5	-1541.2	-594.28	-703.73	-44.108	**412**	-193.08
54	-1256.2	-1154	-1114.7	-1258.1	-478.89	-692.57	65.93	-620.51	**313.88**
55	-514.66	-891.59	-360.21	74.634	363.59	**639.87**	220.2	189.9	93.035
56	-837.28	-499.45	-818.98	-1011.3	59.55	-68.502	**313.98**	153.13	287.48
57	-1166.9	-866.01	-854.1	-964.91	-94.889	-171.86	171.2	**257.16**	127.43
58	-1367.2	-1061.8	-1068	-1012.2	-202.35	-202.31	**320.42**	141.97	291.9
59	-1660.1	-1181.4	-1097.1	-1456.7	-565.36	-436.24	116.17	**330.19**	29.588
60	-1334	-1159.3	-1111.5	-1072.2	-245.23	-284.57	**275.29**	-14.442	248.22

Table C-5 Log-likelihood results from the passage time based method (N=7).

Condition Numbers as in Table 3.2.	Reference Condition Numbers								
	1	7	13	46	47	55	45	53	54
	Slug			Finely Dispersed Bubble			Churn		
1	**268.33**	-1604.9	-654.82	-1692.3	-1672.8	-2588.6	-1348.8	-2749.9	-1225.8
2	**-686.95**	-1876.6	-909.78	-3179	-2803.1	-4015.4	-2222.6	-4246.6	-1902.4
3	-1133.3	-2193.9	**-746.65**	-4225.8	-3761.9	-4921	-2877.4	-4797	-2444.3
4	-2618	**-616.37**	-2007.2	-8869.9	-5638	-7167.7	-3604.6	-3957.6	-3783.5
5	-1369.1	-2053.1	**-479.07**	-3968.9	-3298.2	-4617.7	-2624.2	-4119.1	-2440.7
6	-2481.5	**-516.76**	-2100.3	-7952.7	-5004.3	-6167.5	-3036.9	-3745.3	-3054.3
7	-2185.2	**8.8725**	-1887.3	-7058.6	-4180.1	-5435.3	-2585.4	-3400.9	-2766.7
8	-1916.1	**-400.76**	-1802.1	-6472.2	-3781.8	-4748.2	-2104	-2925.9	-2340.7
9	-1819	**-458.95**	-1553.3	-5798.4	-3440.9	-4429	-2008.5	-2708.3	-2112
10	**-453.74**	-1904.1	-776.67	-2681.6	-2818	-4040.5	-2221.1	-4260.3	-1845.5
11	-904.01	-2032.9	**-829.71**	-4226.8	-3912.7	-5362.1	-2979.9	-5436.4	-2492.3
12	-1195.6	-2303.8	**-545.9**	-4626.9	-4142.8	-5741.2	-3205.8	-5372.7	-2775.5
13	-1329.8	-2065.2	**-9.4618**	-3829	-3064.6	-4660.1	-2555	-4155.7	-2462.8
14	-1552.2	-2089.1	**-732.55**	-3667.4	-2868.2	-4030.8	-2227.1	-3344.1	-2157.7
15	-1364.6	-1752.4	**-543.9**	-2721.2	-1803.4	-2580.6	-1474.8	-2317.1	-1511.4
16	-1733.6	**-600.97**	-1603.6	-4504.7	-2372.6	-2874.8	-1024.3	-1823	-1198.4
17	-1884.3	**-606.43**	-1701.9	-5161.3	-2936	-3460.7	-1381.1	-2315.4	-1722.4
18	-1534.5	-1490.9	**-836.1**	-2881.4	-1657.1	-2463.1	-1152.5	-1670.2	-1287.5
19	**-466.84**	-1887.9	-845.46	-2633.2	-2753.4	-3818.7	-2087.3	-4196.9	-1697.9
20	-764.5	-1930.8	**-678.76**	-3400.3	-3215.9	-4645.2	-2515.6	-4684.5	-2243.2
21	-2346.2	**-733.86**	-1752.4	-6664.3	-3872.6	-4849	-2209.9	-2609.9	-2505.6
22	-2234.9	**-482.85**	-1926.1	-6340.3	-3653.9	-4415.3	-1881.4	-2486.5	-2116.1
23	-1268.1	-1746	**-601.77**	-2225.4	-1459.6	-2248.4	-1217.8	-2028.9	-1196.6
24	-1325	-1650.8	**-606.65**	-1974.6	-962.86	-1702.1	-960.79	-1464.9	-1057.3
25	-1645.4	**-578.99**	-1516.9	-4130.1	-2073.3	-2379.9	-742.35	-1431.8	-1033.3
26	-1495.6	-867.07	-1283.6	-3007.2	-1345.2	-1502.6	**-240.07**	-984.26	-500.64
27	-1780.3	-1230.8	-1003	-3181.3	-1506.9	-2159.6	**-901.57**	-1111.2	-1125
28	**-350.3**	-1715.2	-820.81	-1819.9	-1932.9	-2784.5	-1511.4	-3122.8	-1343.2
29	-2555.5	**-664.81**	-1738.5	-7681.2	-4610	-5719.1	-2776.2	-2608.1	-2990.5
30	-2015.2	**-609.46**	-1656.9	-5631.1	-3009.9	-3801.4	-1666.2	-1935.2	-1861.2
31	-1221.2	-1553.1	**-550.61**	-1852	-1056.9	-1553.6	-824.88	-1411.9	-919.34
32	-1120	-1422.6	**-479.44**	-1277.6	-545.08	-943.83	-505.7	-779.56	-625.26
33	-1367.3	-1493.3	-623.17	-1570.5	-679.22	-959.72	**-598.75**	-696.62	-633.83
34	-1466.8	-712.86	-1325.3	-3106.4	-1292.6	-1365.5	**-152.31**	-708.21	-243.68
35	-1735.4	-1467.9	-963.53	-2110.2	-833.17	-1312.5	-494.55	**-257.92**	-694.11
36	-1516.4	-1074.8	-1161.4	-2480.6	-1287.6	-1415.9	**-243.8**	-1048.7	-331.56
37	**-289.53**	-1879.6	-443.9	-416.41	-666.54	-1241.1	-726.11	-1589.6	-547.02
38	-535.76	-1370	-437.22	-798.99	**-325.87**	-752.65	-482.75	-1061.5	-578.73
39	-1409.9	**-358.07**	-1264	-3755.3	-1430.9	-1746.8	-413.66	-684.98	-565.83
40	-1161.4	-1355.8	-527.98	-923.32	-212.82	-412.77	-114.56	**-101.93**	-290.01
41	-1506.4	-706.44	-1164.2	-2566.9	-945.23	-928.85	**124.72**	-319.79	-1.5261
42	-1546.5	-911.18	-1124.4	-2084.6	-810.32	-521.15	**269.13**	-134.98	229.54
43	-1609.7	-1221.4	-892.9	-1809.2	-585.5	-734.68	-107.39	**105.85**	-250.36
44	-1475.2	-1027.3	-1175.6	-2098.8	-839.39	-706.22	**183.41**	-402.2	57.637
45	-1506.9	-1366.2	-1124	-1769.4	-933.46	-832.49	**256.02**	-642.49	-170.91
46	-438.73	-2045.8	-249.47	**652.91**	94.889	-174.09	-283.3	-501.28	-97.277
47	-627.68	-1144.1	-373.72	-258.72	**583.52**	33.9	20.619	-41.605	-174.29
48	-1214.9	-588.56	-910.03	-2131.1	-535.36	-584.78	**45.671**	-203.56	-78.277
49	-1377.7	-789.99	-979.14	-1836.8	-521.27	-381.2	**250.03**	-62.943	170.71
50	-1593.3	-968.1	-1153.3	-2042.7	-777.85	-491.37	**303.41**	-31.186	244.95
51	-1658	-988.97	-1177.5	-1819.9	-690.99	-406.9	**351.89**	-44.006	230.07
52	-1597.7	-1069.4	-1154.7	-1748.5	-685.74	-442.49	**283.11**	-58.524	205.99
53	-1932.1	-1252.8	-1096	-2189.8	-873.89	-798.16	-70.103	**514.24**	-207.56
54	-1584.6	-1313.7	-1205.9	-1932.8	-891.55	-839.9	45.392	-658.27	**377.93**
55	-790.58	-1137.3	-390.46	-145.47	328.61	**699.97**	197.67	287.02	26.054
56	-1152	-552.59	-880.69	-1740.7	-301.02	-187.27	**303.78**	68.415	227.88
57	-1508.4	-919.41	-925.28	-1382.8	-359.3	-230.61	164.13	**227.06**	46.878
58	-1737.6	-1159.4	-1081.8	-1572.2	-535.52	-262.1	**316.91**	105.6	251.45
59	-2040.1	-1251.1	-1163.5	-2117.7	-869.35	-563.75	122.21	**287.22**	42.291
60	-1695	-1288.5	-1145.1	-1648.9	-582.15	-375.57	**281.07**	-32.751	215.12

Table C-6 Log-likelihood results from the passage time based method, using different reference conditions (N=3).

Condition Numbers as in Table 3.2.	Reference Condition Numbers								
	1	2	10	46	47	55	52	53	60
	Slug			Finely Dispersed Bubble			Churn		
1	**37.828**	-166.4	-316.02	-1345.5	-1004.1	-1955.9	-1500.1	-2871.8	-1594.1
2	-448.21	**-119.47**	-342.86	-2822.8	-1778.4	-3228.2	-2513.9	-3431.4	-2736.8
3	-866.93	**-362.89**	-530.06	-3942	-2413.4	-4205.3	-3230.1	-3632.2	-3516.3
4	-1852.7	**-1425.6**	-1730.1	-7310.5	-3050.6	-6056.7	-4805	-2774.1	-5474.1
5	-1059.8	**-540.19**	-793.11	-3870.9	-2261.1	-4015.8	-3120.8	-3125	-3457.4
6	-1650.3	**-1462.2**	-1818.6	-6407.6	-2630.4	-5140.9	-3990.2	-2685	-4768.5
7	**-1422.9**	-1526.5	-1657.3	-5439.5	-2194.3	-4481.7	-3641	-2470	-4070.4
8	**-1303.2**	-1472.5	-1727.9	-5121.7	-1913	-3916.9	-3029.2	-2102.8	-3563.3
9	**-1213.4**	-1400.2	-1661.9	-4449.9	-1692.9	-3673.3	-2855.6	-1946.6	-3166
10	-255.8	-169.34	**17.002**	-2307.4	-1786.1	-3178.2	-2440.5	-3981.3	-2480
11	-710.3	**-334.8**	-367.86	-3987.2	-2522.8	-4408.6	-3488.6	-4199	-3728.8
12	-1003	**-451.54**	-639.18	-4419.3	-2778.5	-4751.7	-3581.8	-4061.2	-4030.2
13	-994.63	**-604.56**	-843.68	-3489.7	-2145.4	-3862.8	-2962.8	-3198.2	-3252.3
14	-1216.5	**-844.23**	-1174.6	-3502	-2017.5	-3359.7	-2502.2	-2622	-2880.5
15	-1052.1	**-797.53**	-1182	-2509.6	-1333	-2225	-1787.7	-1797.3	-2091.2
16	-1151.3	-1593.7	-1957.6	-3228	**-1106.6**	-2335.9	-1537.3	-1332.7	-1859.3
17	**-1275.1**	-1667.3	-1959.3	-3835	-1387.2	-2912.2	-2050.8	-1663.1	-2333.4
18	-1129.2	**-1058**	-1504.2	-2515.5	-1129.6	-2143	-1604.7	-1307.2	-1813
19	-268.23	**-204.51**	-221.67	-2242.8	-1749.5	-3016.5	-2252.6	-4010.8	-2420.7
20	-582.84	**-331.38**	-394.28	-3174.1	-2071.4	-3829.8	-2891	-3719.4	-3068
21	-1561.4	**-1519.8**	-1871.9	-5374.5	-2087.6	-4164.2	-2963.1	-1821.5	-3565
22	**-1524.3**	-1659.6	-1977.3	-4941.1	-1828.6	-3813.9	-2631.3	-1804.8	-3066.3
23	-898.96	**-803.51**	-1215.1	-1977.4	-1066.1	-1902.7	-1438.2	-1746.2	-1782.4
24	-922.44	-981.51	-1357.6	-1671.7	**-782.81**	-1484.4	-1245.1	-1205.7	-1332.7
25	-1154.1	-1740.9	-2078.8	-2870.1	**-888.96**	-1982.1	-1151.3	-1023.4	-1388.1
26	-1031.7	-1731.7	-2135.6	-2019.7	**-561.02**	-1244.6	-604.04	-791.63	-632.94
27	-1247.7	-1363	-1857.5	-2579.1	-967.47	-1756	-1198.9	**-767.18**	-1420
28	**-182.7**	-292.94	-360.06	-1441.8	-1232.1	-2110.6	-1597.8	-3342.1	-1646.1
29	-1707.1	**-1425.6**	-1793.7	-6353.4	-2447	-4876.1	-3393.5	-1678.5	-4199.7
30	-1379.9	-1525.4	-1882.3	-4368.8	-1545.3	-3079.2	-2304.8	**-1321.2**	-2872
31	-867.47	-1005.3	-1387.4	-1554.2	**-701.42**	-1297.9	-985.71	-1182.6	-1127.5
32	-770.25	-964.19	-1333.6	-1077.1	**-412.93**	-766.02	-664.75	-679.18	-805.54
33	-938.61	-1076.3	-1515.4	-1242.8	**-466.12**	-802.07	-665.3	-555.51	-860.04
34	-976.39	-1801.1	-2194.1	-1998.5	-442.19	-1098.1	**-371.17**	-489.95	-447.87
35	-1190.3	-1454.7	-1985.1	-1514.8	-520.08	-1117.1	-684.57	**-112.47**	-722.75
36	-1040.1	-1679.1	-2067.3	-1619.1	**-533.57**	-1140.5	-573.65	-873.68	-559.44
37	**-85.982**	-256.97	-312.53	-179.9	-456.84	-793.28	-728.11	-2026.3	-710.9
38	-241.79	-500.65	-746.58	-475.21	**-171.07**	-514.72	-603.28	-1198.9	-619.24
39	-970.76	-1528.7	-1878.5	-2592.6	-505.52	-1419.8	-637.47	**-333.99**	-871.95
40	-750.37	-1159.4	-1574.5	-535.67	**-28.921**	-224.09	-194.56	-103.31	-226.9
41	-1046.9	-1870.6	-2271.6	-1579.2	-230.68	-718.75	**-32.575**	-130.41	-125.17
42	-1135	-1927.1	-2474.1	-1184	-146.82	-369.73	**180.42**	26.887	156.19
43	-1130.5	-1570.1	-2076.9	-1214.9	-275.42	-479.25	-124.7	**152.51**	-244.83
44	-1065.1	-1876.4	-2372	-1195.1	-193.78	-530.98	81.284	-243.77	**88.561**
45	-1011	-1693	-2175.7	-1016.4	-379.85	-601.92	-152.57	-561.86	**-127.31**
46	-205.25	-355.25	-490.87	**532.74**	94.842	77.658	-133.84	-913.2	-69.254
47	-253.99	-643.9	-979.08	49.653	**439.35**	219.28	-50.291	-180.33	-0.6138
48	-760.17	-1398.3	-1792.4	-1260.1	-29.548	-406.54	-15.466	**11.73**	-130.3
49	-940.66	-1725.8	-2196.9	-983.29	-31.721	-249.15	**181.87**	106.88	147.07
50	-1154.5	-1961.1	-2555.3	-1102.3	-140.88	-303.99	241.39	121.88	**244.63**
51	-1171.7	-2065.9	-2600.4	-976.19	-129.29	-230.1	273.86	56.935	**292.86**
52	-1087.9	-1950.3	-2462.1	-954.19	-146.3	-227.64	**393.6**	15.869	285.5
53	-1363.8	-1828.4	-2425.2	-1445.1	-393.39	-624.99	-79.194	**370.31**	-170.68
54	-1055.3	-1878.8	-2253.5	-1068	-344.29	-615.53	**-19.102**	-592.18	-57.94
55	-417.44	-888.23	-1242.4	155.84	421.28	**584.79**	202.95	202.19	243.66
56	-731.39	-1553	-1997.6	-914.13	152.39	-65.898	**306.86**	223.29	197.23
57	-943.94	-1667.3	-2104.5	-781.62	5.4214	-119.13	173.84	**272.94**	79.705
58	-1208.6	-2009	-2579.4	-777.63	-82.569	-103.02	268.61	163.33	**321.44**
59	-1495.5	-2099.3	-2717.4	-1339.4	-364.36	-400.25	108.4	**379.58**	35.03
60	-1148.9	-1996.4	-2532.4	-834.35	-154.32	-222.64	248.62	16.072	**413.13**

Table C-7 Numerical likelihood values and confidence difference values for passage time (N=3).

Condition Numbers as in Table 3.2.	Reference Condition Numbers			Confidence Difference
	1, 2, 10	46, 47, 55	45, 53, 54	
	Slug	F. D. Bubble	Churn	
1	-1439.062	-4305.5	-4224.68	2785.618
2	-2062.14	-7829.4	-5942.8	3880.66
3	-2649.03	-10560.7	-7029.7	4380.67
4	-3540	-16417.8	-7653.2	4113.2
5	-2910.74	-10147.8	-6445.1	3534.36
6	-3439.84	-14178.9	-6852	3412.16
7	-2879.12	-12115.5	-6070.8	3191.68
8	-2830.15	-10951.6	-5120.2	2290.05
9	-2613.27	-9816.1	-4775.4	2162.13
10	-1886.05	-7271.7	-6307.8	4421.75
11	-2464.9	-10918.6	-7628.8	5163.9
12	-2940.74	-11949.5	-7901.9	4961.16
13	-2698.07	-9497.9	-6405.3	3707.23
14	-3276.67	-8879.2	-5468.8	2192.13
15	-2816.67	-6067.6	-3860.56	1043.89
16	-2838.64	-6670.5	-2880.23	41.59
17	-2966.65	-8134.4	-3717.5	750.85
18	-2975.4	-5788.1	-3060.7	85.3
19	-1964.57	-7008.8	-6234	4269.43
20	-2294.52	-9075.3	-6612.3	4317.78
21	-3286.29	-11626.3	-5097.4	1811.11
22	-3277.43	-10583.6	-4589	1311.57
23	-2800.55	-4946.2	-3359.83	559.28
24	-2789.51	-3938.91	-2578.16	211.35
25	-2786.15	-5741.16	-2171.14	615.01
26	-2730.97	-3825.32	-1204.01	1526.96
27	-3128.83	-5302.57	-2251.64	877.19
28	-1788.89	-4784.5	-4833.13	2995.61
29	-3189.48	-13676.5	-5656	2466.52
30	-2880.79	-8993.3	-3862.8	982.01
31	-2693.19	-3553.52	-2287.56	405.63
32	-2374.8	-2256.05	-1449.22	806.83
33	-2696.27	-2510.99	-1396.18	1114.81
34	-2625.88	-3538.79	-671.407	1954.473
35	-3185.31	-3151.98	-1049.54	2102.44
36	-2903.74	-3293.17	-1187.89	1715.85
37	-1735.942	-1430.02	-2514.96	305.922
38	-1582.57	-1161	-1609.64	421.57
39	-2213.1	-4517.92	-1045.03	1168.07
40	-2382.75	-788.681	-263.562	525.119
41	-2675.29	-2528.63	114.22	2642.85
42	-2992.68	-1700.55	599.137	2299.687
43	-3043.8	-1969.57	-73.821	1895.749
44	-2974.31	-1919.86	165.55	2085.41
45	-3104.83	-1998.17	-458.935	1539.235
46	-1898.38	705.24	-844.067	1549.307
47	-1453.7	708.283	7.239	701.044
48	-2010.22	-1696.188	106.704	1802.892
49	-2615.98	-1264.161	560.88	1825.041
50	-3128.13	-1547.17	714.68	2261.85
51	-3235.66	-1335.58	695.995	2031.575
52	-3142.66	-1328.13	624.109	1952.239
53	-3513.11	-2463.48	142.303	2605.783
54	-3237.26	-2027.82	-249.65	1778.17
55	-1693.45	1161.91	570.71	591.2
56	-2043.72	-827.638	819.36	1646.998
57	-2710.31	-895.3286	584.41	1479.7386
58	-3350.93	-963.219	766.07	1729.289
59	-3854.61	-2104.01	515.102	2619.112
60	-3354.81	-1211.31	567.322	1778.632